Formulation of Lipid Nanoparticles with Viral Subunit Antigens for Vaccination.

by

Joseph Daniel Bazzill

A dissertation submitted in partial fulfillment
of the requirements for the degree of
Doctor of Philosophy
(Pharmaceutical Sciences)
in the University of Michigan
2018

Doctoral Committee:

Associate Professor James J. Moon, chair
Associate Professor Wei Cheng
Adjunct Professor Susan Ciotti
Professor Alice Telesnitsky

Joseph D. Bazzill
jbazzill@med.umich.edu

ORCID iD: 0000-0001-9779-6524

Dedication

This dissertation is dedicated to my late grandfather Carroll Oliver Penberthy, who's suffering from Alzheimer's disease sparked within me a passion to contribute towards easing the suffering of others.

Acknowledgements

First and foremost, I am thankful to my parents, Danette and Kevin Carpenter. I could not have achieved what I have over these many years without their continued support and motivation to not stop until I achieved what I desired.

Second, I am deeply thankful to my committee members. To my mentor, Dr. James Moon, I thank for allowing me to join his lab, providing a project that proved challenging yet rewarding, supporting my research goals, providing insight, and tolerating my…spirited personality. To Dr. Wei Cheng, Dr. Susan Ciotti, and Dr. Alice Telesnitsky, I thank for their patience, guidance, and thoughtful critiques. Your presence and input have been invaluable to me and my research.

This work could not have been completed without financial supported in part by NIH (R01AI127070, R01EB022563, and R01HL125555) and the Defense Threat Reduction Agency (DTRACB3947, C.L.C) J.J.M. is a Young Investigator supported by the Melanoma Research Alliance (348774), DoD/CDMRP Peer Reviewed Cancer Research Program (W81XWH-16-1-0369), Emerald Foundation, and NSF CAREER Award (1553831). Opinions, interpretations, conclusions, and recommendations are those of the authors and are not necessarily endorsed by the US Department of the Army or the US Department of Defense. J.J.M. is an inventor on patents related to the ICMV technology, and these patents have been licensed to Vedantra Pharmaceuticals, Inc. I also want to thank the members of the Moon lab for any assistance and input they have provided over the past five years. In particular, Dr. Łukasz Ochyl has been integral

in the progression of my research, a valuable sounding board for ideas, and when needed a cold splash of reality. To the remaining lab members, thank you for tolerating my loud music, dancing, singing, and occasional grumpy attitude.

My research would not have been possible without the support of collaborators at the United States Army Medical Research Institute of Infectious Diseases, The Scripps Research Institute, and Cornell University. I thank everyone for their contributions to my research, be it reagents, experiments, critiques, or manuscript contributions. Notably, I want to thank Dr. Christopher C. Cooper, Dr. Sina Bavari, Sabrina M. Stronsky, Laura C. Kalinyak, Jess T. Steffens, and Sean A. van Tongeren from USAMRIID for their contributions to the Ebola virus project including providing the recombinant Ebola virus antigen and antigen-specific antibodies, conducting the *in vivo* studies and downstream analyses, providing expert knowledge and editing the manuscript drafts, and valuable input during our many teleconferences. To the same effect I thank Dr. Mansun Law, and Erick Giang, Shaun Castillo from The Scripps Research Institute for their contributions to the HCV project including providing the recombinant HCV antigens and antigen-specific antibodies, analyses of the vaccination sera, their additions in writing the manuscript, and valuable input. Additionally, I thank Dr. John Moore and Albert Cupo from Cornell University for providing the recombinant HIV antigens, and the International AIDS Vaccine Initiative for providing monoclonal antibodies used for characterization purposes. I would also like to thank Yuchen Fan for his contributions to the pilot HCV *in vivo* studies. Lastly, I thank Dr. Lukasz Ochyl for adapting and developing the NanoFACS protocol for use in the Moon lab, for his help with many of the larger scale immunofluorescence assays and later NanoFACS analysis (all projects), and for his contributions to the HCV *in vivo* study presented here.

I cannot forget the impact my family and friends have had before and during my time as a graduate student. They have provided support with my personal issues, sanctuary from my research, and most important, a boat-load of good memories. I thank my siblings: Melissa, Matt, and Rebecca; my sister-in-law, Dina; my nieces, Violet and Willa; and my friends: Ryan Andrews, Chris Fowler, Natalie Hillmann, Zack Yaw, Dr. Megan Beaird, Raquel Vargas-Ramírez, Dr. Zryan Shwani, Piero Protti, Dr. Patrick Grogan, Dr. Colleen Carpenter, Dr. Kristen Schimert, Marcos Núñez, Joe Nguyen, Dr. Karthik Pisupati, and many, many more that I have not mentioned.

One of the most significant friendships I have had the luck to form during my time at Michigan has been with Dr. Łukasz Ochyl. Not only was he a stellar lab mate, but a supreme friend and confidante, who helped me through countless issues and dilemmas. I genuinely count myself lucky to call him a friend.

Finally, my time at Michigan would not have been the same without Dr. Molly Kozminsky. Her support, motivation, and companionship kept me going, made me a better person, and brightened my time at Michigan. She was a part of my best days here and she helped me through my worst.

Table of Contents

List of Figures

List of Tables

Abstract

Vaccination provides significant advantages over post-infection treatment such as long-lasting protection, prevention of co-morbidities, and a reduction in the dissemination of pathogens. While vaccination has tempered many once virulent pathogens, others remain without effective vaccines. Moreover, the emergence of previously unknown or isolated pathogens is presenting a significant threat to human health. Overpopulation, increased urbanization, and international travel provide continuous sources of naïve hosts, permitting the persistence and spread of pathogens along with an increased potential of pandemics. Here, three projects are presented describing the development and characterization of viral subunit loaded vaccine nanoparticles for the generation of protective humoral immune responses against hepatitis C virus, Ebola virus, and human immunodeficiency virus.

In the first project, lipid-based nanoparticles, called interbilayer-crosslinked multilamellar vesicles (ICMVs), were produced with hepatitis C virus (HCV) recombinant antigens E2.661 or E2c.661, displayed average antigen loading efficiencies were 54% and 50%, respectively, and average nanoparticle dimeters between 115-132 nm. The preservation of surface displayed antigens was confirmed by indirect immunofluorescence staining with antigen-specific antibodies, and *in vivo* vaccination of mice with ICMV formulations generated ~10-fold higher antigen-specific serum IgG titers compared with control vaccine formulations. Immune sera were tested for their neutralization capacities by an *in vitro* assay, and both ICMV formulations exhibited neutralization of autologous and heterologous HCV virus like particles, with E2c.661 ICMVs

displaying a balanced neutralization profile compared to E2.661 ICMVs, indicating E2c.661 as a candidate antigen for a broadly effective vaccine formulation.

In a second application, recombinant Ebola envelope glycoprotein (rGP) was formulated with ICMVs or a variant (NTA ICMVs) for concerted display of rGP on ICMV surfaces. Loading efficiencies varied between formulations (15 and 33%), with the addition of NTA approximately doubling rGP loading. The large rGP complex and epitope conformations were preserved throughout nanoparticle synthesis, and both formulations displayed distinct antibody binding profiles. Regardless of the surface antigen display, both nanoparticle formulations generated marked titers of class switched antigen-specific antibodies in mice after vaccination compared to the vehicle or rGP control groups. Four weeks after immunization, mice were challenged with a lethal dose of murine adapted Ebola virus and 100% survival was observed for mice vaccinated with either ICMV formulation as well as the adjuvanted control formulation. While these data demonstrated short-term protection in three of the tested groups, further research is needed to evaluate long-term protection and the epitope specificity of the generated antibodies.

Lastly, a new ICMV nanoparticle design was developed for formulation with the recombinant human immunodeficiency virus envelope glycoprotein (SOSIP). The new nanoparticle, called ICMV-NHS, display ~25% loading efficiency of SOSIP, and a mean diameter of ~300 nm. Preliminary studies indicate preservation of the SOSIP protein complex and conformational epitopes, which are necessary to produce protective and broadly neutralizing humoral responses. However, further optimization and characterization of the nanoparticle are needed to enhance antigen loading and evaluate antigen display prior to *in vivo* immunogenicity studies.

The data reported here highlights the complexity of formulating subunit-loaded vaccine nanoparticles. Many factors including antigen design, display, and antigen-nanoparticle interfaces are important considerations and can contribute significantly to strength and specificity of the generated immune response. To bridge this gap of knowledge, in-depth characterization of nanoparticles, like those reported here, can aid in elucidating and correlating *in vitro* properties of vaccine nanoparticles with *in vivo* performance.

Chapter 1

Introduction

1.1 Overview of infectious diseases

Infectious diseases accounted for approximately 15% of worldwide deaths in 2016, [1] with a disproportionately high incidence in low income countries. Historically, some of the most significant losses of life were attributed to outbreaks of infectious diseases. Two well-known examples were the Black Death (circa mid-1300s), which is estimated to have killed between 75-200 million people (~16-44% of the global population); and the 1918 Spanish flu, which resulted in 50-100 million deaths in the span of about a year.[2-4] The spread and persistence of infectious pathogens are affected by factors like population density, travel, and public health measures (e.g. sanitation and access to medication).[2, 5, 6] As the global population grows and urbanization and global travel increase, any outbreak of infectious disease has a very a real and growing chance of producing a global concern.

In developed countries, pandemics like the Black Death or the 1918 Spanish flu have not been seen in approximately 100 years, owing in part to the development and application of sanitation, along with the discovery and development of vaccines and chemo-therapeutics. The mid-20th century saw an enormous increase in the development and use of vaccines and antibiotics

against numerous pathogens, reducing the impact and incidence of diseases which were previously a significant concern. However, in recent decades many pathogens have developed resistance to chemotherapeutics, prompting new strategies for effective treatment. Additionally, as the human population grows and expands, contact with previously isolated or unknown pathogens have presented new threats to public health. This dissertation will focus on three pathogens, hepatitis C virus, Ebola virus, and human immunodeficiency virus, all of which are currently global concerns.

1.2 Hepatitis C virus

Hepatitis C virus (HCV) was identified in 1989 as the causative agent of hepatitis C.[7] Currently, an estimated 71 million people are infected with chronic hepatitis C.[8] Transmission of HCV occurs mainly by parenteral routes with common modes being contaminated needles, blood transfusions, organ transplants, tattoos, and piercings.[9] Less frequent routes include sexual contact or mother-to-child transmission. Most HCV infections (~70%) are asymptomatic, thus unreported, undiagnosed, and progress to chronic hepatitis C which can persist unnoticed for years, increasing the chance of transmission. Chronic hepatitis C primarily affects the liver, and the main morbidity is liver fibrosis.[9] Approximately 15-30% of patients with liver fibrosis will progress to liver cirrhosis, potentially requiring a liver transplant. Additionally, a fraction of patients with liver cirrhosis will develop hepatocellular carcinoma, and hepatitis C is a leading risk factor in the United States.[10]

HCV is a genetically diverse virus grouped into seven genotypes (~35 % genetic diversity) with varied prevalence across the globe.[11, 12] Each genotype is divided into subtypes (<15% genetic diversity), and each virus mutates while residing in the host, giving rise to "quasi-

species."[12, 13] The random mutability and subsequent genetic diversity affords HCV an advantage to evade host immune responses by natural selection, which play a role in the persistence of chronic HCV infections. In a small fraction of cases, chronic hepatitis C can be cleared by the host immune system, even after years of residence and immune evasion. The spontaneous generation of neutralizing antibodies in chronically infected individuals has provided a template for the design of a HCV vaccine. Extensive research of HCV neutralizing antibodies has determined that the E2 subunit of the HCV envelope glycoprotein the main target of neutralizing responses. Furthermore, some antibodies produced have demonstrated the ability to neutralize HCV genotypes different than those residing in the host, suggesting that a pan-genotype HCV vaccine may be possible to produce. However, many of the mutations sites that result in the HCV genotypes and immune evasion are a part of the E2 antigen. These regions of high variability are highly antigenic and serve as decoys to the immune response, detracting from generation of cross-genotype neutralizing antibodies.[14, 15]

Unlike a HCV vaccine, therapeutics for hepatitis C have existed for decades; however, the earliest medications, interferon and ribavirin, are non-specific antiviral medications and are prone to severe side-effects thus limiting their effective use.[11, 16, 17] In 2011 direct acting antivirals (DAAs) were introduced against HCV, but when used as a monotherapy, viral resistance was observed in patients.[16] To combat the rise of antiviral resistant HCV strains, DAAs were used in conjunction with PEGylated interferon and ribavirin, leading to improved treatment efficacy, though side-effects caused by PEGylated interferon and ribavirin limited the widespread use of the combination therapy.[11, 16] Newer, second generation DAAs have tolerable side-effects, do not need co-administration of interferon and ribavirin, and successfully cure ~90% of hepatitis C when administered.[9, 11, 12] Though the treatment of HCV has increased dramatically in efficacy, the

regimen is lengthy, lasting between 2-6 months, and requires daily dosing leading to concerns of spread during the course of treatment and patient compliance.[11] Moreover, the genotypes of hepatitis C virus (HCV) are not universally affected by DAAs but require individualized therapies to maximize their efficacy. Lastly, the mutability of HCV poses the potential to generate DAA resistant strains, which have been observed against some DAAs, and require strict adherence to the therapy regimen.[11, 16] Currently, a pan-genotype DAA that is well tolerated has not been discovered, prompting a strategic and rational use of the limited number of available DAAs as well as the continued research of producing a widely effective HCV vaccine.

1.3 Ebola virus

Ebola virus disease (also called Ebola hemorrhagic fever) came to attention as a human pathogen in 1976 after separate outbreaks in the countries of Sudan and the Democratic Republic of Congo (formerly Zaire), which claimed the lives of 431 lives with a mortality rate of 72%.[18] Outbreaks of similar magnitude have occurred since then, and five strains have been identified: the eponymous Ebola virus (EBOV), Bundibugyo virus, Sudan virus, Tai Forest virus, and Reston virus. All strains save the Reston virus can infect humans, and the remaining strains displaying a range of disease severity and mortality rates with Ebola virus as the most virulent. The 2014 outbreaks in Sierra Leone, Liberia, and Guinea were caused by Ebola virus, and resulted in approximately 28,600 cases with a mortality rate of approximately 40% in the two years of the epidemic.[18]

Transmission of Ebola virus occurs via direct contact of mucosal membranes, open wounds, or lesions by infected people, bodily fluids, body parts, or contaminated items.[18]

Symptoms develop after 2-21 days and include fever, body aches, joint pain, nausea, diarrhea, and progress rapidly to multiple organ failure, internal and external bleeding, and systemic shock.[18, 19] In fatal cases, death occurs 6-16 days after symptoms begin. The cellular targets of Ebola are still being elucidated, but in the early stages after transmission, monocytes and macrophages are the primary targets.[20] After the incubation period, the virions spread systemically in an apparently non-discriminant fashion to infect hepatic, adrenocortical, and endothelial cells, among others.[19] Recent research has revealed that immune privileged sites such as the gonads, inner-eye, and placentas can retain Ebola virus after an infection has been resolved.[18, 19, 21]

Many details of EBOV pathogenesis remain uncertain including which host immune responses are necessary for protection and viral clearance. The role of cellular immune responses in protection is hotly debated, and EVD progression can induce lymphopenia (loss of CD4+ and CD8+ T cells) which may impact other immune responses.[22, 23] However, it is generally accepted humoral immune responses necessary, as fast and potent humoral responses are positively correlated with survival from EVD.[22, 23] Additionally, neutralizing antibodies have been discovered from EBOV inoculated animals, and can provide passive protection in animal models and are being developed as post-exposure therapies for humans.[24, 25] Unfortunately, EBOV evades host immune responses due to a number of factors. Among these factors is how the early-stage of infection primarily targets antigen presenting cells (APCs) such as dendritic cells, monocytes, and macrophages. APCs disseminate to local and systemic tissues and are thought to aid in spreading EBOV to other cell populations while concurrently destroying the APC population, which is important for both innate and adaptive immune responses.[19, 22]

The production of adaptive humoral responses are targeted against the only surface antigen of EBOV, the envelope glycoprotein (GP).[26, 27] Full length GP is translated as a heterodimer

composed of the subunits GP_1 and GP_2 which are covalently bound by a disulfide bond. Three GP heterodimers associate into a trimer which is expressed on the virion surface and functions to bind and facilitate entry into target cells.[28] While the GP trimer is a large and can have antibodies targeted against many regions, not all antibodies will neutralize the antigen. GP contains a large domain that is heavily glycosylated, called the mucin like domain, which is non-functional, highly antigenic, and can serve as an immune decoy from functional domains and promote the production of non-neutralizing antibodies.[29] Additionally, EBOV produces a non-functional, truncated variant of GP, called secreted GP (sGP),[28, 29] that is produced as a dimer and secreted from infected cells. sGP is transcribed approximately four times that of full length GP, and the disproportionally high amount and secreted nature of sGP is thought to also serve as an immune decoy against GP specific antibodies.[29-31] Notably, despite the high level of sequence similarities between sGP and GP, antibodies have been discovered that are selective against GP but not sGP, providing rational to the viability of an EBOV vaccine.[29]

Currently, many vaccine candidates have been produced for EBOV and a number of which are in clinical trials. The furthest advanced candidate is a recombinant virus where GP is expressed on the surface of vesicular stomatitis virus (rVSV-EBOV), a zoonotic virus, to produce a replication competent hybrid virus.[32] Clinical trials to assess the safety of rVSV-EBOV in healthy adults revealed the vaccine candidate was mostly well tolerated with some instances of acute arthritis and skin lesions;[33, 34] however, safety has yet to be evaluated in young children and immunocompromised patients. Apart from rVSV-GP, non-replicating hybrid viruses are also being produced and evaluated, though concerns of pre-existing immunity are being addressed as they have been observed against some of the tested viral vectors.[35, 36]. Lastly, DNA and RNA based vaccines are also in development, and have demonstrated some promise in animal models

and clinical trials, but development of protective responses required large doses of vaccine and multiple administrations and raise concerns of feasibility and patient compliance.[37]

Similar to EOBV vaccines, there are currently no specific treatments for EVD. Infected or suspected infected patients are given supportive care including fluid replacement and oxygen, along with management of symptoms such as pain, nausea, inflammation, and diarrhea.[18, 20] New investigational compounds are being evaluated against EBOV including the RNA-dependent-RNA polymerase inhibitor, favipravir; and two nucleoside analogues, GS-5734 and BCX4430,[38] but further clinical trials are needed to assess safety and efficacy.

1.4 Human immunodeficiency virus

Human immunodeficiency virus (HIV) was isolated in 1983 and determined as the causative agent of acquired immunodeficiency syndrome (AIDS).[39, 40] As of 2016, approximately 37 million people were infected with HIV worldwide, and 1 million deaths occurred as a result of AIDS.[41] The origins of HIV were traced to a similar virus found in primates, called simian immunodeficiency virus (SIV), which emerged as a human pathogen due to the genetic similarities between human and primates.[42] Separate events of HIV emergence have occurred and resulted in two broad categories off HIV; HIV-1, the more virulent virus from multiple chimpanzee (and potentially gorilla) origins;[43-45] and HIV-2, a less virulent virus originating from sooty mangabeys. HIV-1 is further divided into the four main groups: M, N, O, and P. Each group represents a single cross-species transmission event, and group M accounts for approximately 99% of infections, and is further divided into nine subtypes.

HIV transmission occurs through contact of infected bodily fluids (i.e. blood, seminal and pre-seminal fluids, rectal and vaginal fluids, and breast milk).[46] Most instances of HIV transmission occur form sexual contact and contaminated needles. Immediately after infection, the host's body responds to HIV as it would any other acute infection.[47] Transmitted virions are taken up by antigen presenting cells (APCs), like macrophages and dendritic cells, to initiate the immune response. However, while some virions are taken up by APCs, others bind to the cells and are transported to secondary lymphoid organs where there is a rich source of CD4+ T cells, which HIV selectively target.[48] These sites become the primary residence of HIV, and while many of the infected cells will be discovered and destroyed, some will persist as reservoirs of HIV.[49] This subset of T cells, called latently infected T cells, harbor HIV at a low replication stats that express little to no viral proteins. At some later time, stimulation of latently infected cells induces a surge of viral replication, and continues the chronic infection and dissemination of HIV.

During the initial infection when HIV virions are prevalent, antibodies are generated against the surface bound envelope glycoprotein (Env), and initially control the infection.[47] However, after latently infected T cells are established, selective pressure results in the survival of virions that are not recognized by circulating antibodies allowing for immune evasion and the persistence of chronic HIV infection. Three major immune evasion mechanisms of Env are: one, error prone replication that result in in phenotypic alterations on Env; two, extensive glycosylation of gp120 and gp41; and three, conformational masking of conserved epitopes.[50, 51] Mutations that arise during replication produce a diverse population of Env that respond to the selective pressures of the host immune system, and produce Env variants poorly recognized by the generated antibodies. Glycosylation of gp120 and gp41 serve as immune decoys, distracting the immune

response from functional sites, and also mask buried epitopes that are conserved between Env variants.

In 20-30% of chronically infected individuals, antibodies against conserved regions can be generated, and neutralize Env from multiple groups.[52, 53] These antibodies are called broadly neutralizing antibodies (bNAbs) and in a small subset of individuals they have been shown to naturally control HIV replication (called elite neutralizers). The unique and uncommon characteristics associated with HIV bNAbs are slowly generated over approximately two to three years of chronic infection, and typically do not afford any protection to host. However, they do provide valuable insight towards the production of an effective vaccine for HIV.

The many steps of the HIV infection cycle and transmission have presented multiple targets for antiretroviral compounds (ARTs), and can be grouped based on the steps they inhibit including: fusion/entry inhibitors, reverse transcriptase inhibitors, integrase inhibitors, and protease inhibitors.[54, 55] Unfortunately, the initial use of single ARTs (monotherapy) gave rise to ART resistant HIV strains due to poor infiltration sites of HIV reservoir, producing sub-therapeutic concentrations that allowed for continual survival and adaptation of HIV against the therapeutic. Updated regimens using combination therapy, administering medications that span at least two different mechanisms of action, are highly effective at limiting the reproductive capability of HIV and are the initial therapy for many patients. Due to the resistance HIV has gained against many available ARTs, standardized therapies are used to prevent resistance against all ARTs, in addition to limiting toxicity associated with some ARTs.[56]

Current ART regimens and guidelines are highly effective at reducing the presence of virions in patients to a point where viral RNA is undetectable, but ARTs are unable to cure patients of HIV.[55, 57] When ART therapy is paused or ended, HIV levels resurge in patients, thus requiring

life-long ART administration to prevent HIV replication and high serum levels.[55] The inability of ARTs to eliminate HIV has been linked to poor diffusion and sub-therapeutic levels of ARTs at sites of latently infected cells resulting in ineffective inhibition and clearance of HIV.[49, 58, 59]

1.5 Vaccines

1.5.1 Concept and history

Vaccination traces back to a common practice called variolation, or inoculation, in which patients would be administered, or inoculated, with matter from an infected person to induce an immune response that would confer protection in the naïve patient.[60, 61] One of the most extensive and widespread applications of variolation was for smallpox in the early 18th century at the peak of the smallpox epidemic in Europe, which had a mortality rate of 20-60%.[61] Smallpox variolation proved effective but had three major drawbacks. First, there was a chance of death after variolation, though it was approximately 10-fold less than natural smallpox infections.[60, 61] Second, inoculation of matter from infected people inadvertently spread other carried diseases such as tuberculosis.[61] Lastly, after variolation the patients were contagious as the pathogen was not weakened by any means and risked new outbreaks, as evidenced by smallpox epidemics in the 1960s and '70s.[60, 61]

Vaccination, on the other hand, functions on the premise that ill-adapted or weakened pathogens can confer protection against the virulent, native pathogen while reducing side-effects and avoiding new epidemics. The discovery of vaccination is credited to Edward Jenner, who was first to test and prove the theory that inoculation of cowpox (*vaccinia*), a similar but less virulent disease to smallpox, can provide immunity against smallpox..[60, 61] Jenner validated his theory by

inoculating a young boy (James Phipps) with the cowpox virus, which he termed vaccination. The child developed the symptoms of cowpox, and when they subsided he was inoculated with smallpox, but did not develop the disease, thus proving that cowpox vaccination can protect against smallpox infection. Use of Jenner's method curbed the smallpox epidemic and paved the way for its eradication.

The determination and use of cowpox as a viable substitution for smallpox was a fortuitous and quite unique event given the antigenic similarities between the two viruses, which were unknown at the time. However, those vaccinated against smallpox were observed to contract the disease years later, therefore requiring periodic re-vaccination to maintain protective immunity. Later, Louis Pasteur developed less-virulent pathogens for a variety of diseases by serial inoculation of host species that were weakly susceptible to the pathogens. This method weakened, or "attenuated," the pathogens to their natural hosts and produced replication competent vaccines with mild side effects and ushered in a new era of vaccination.

1.5.2 Types and components of vaccine formulations

Conventional vaccines are comprised of attenuated vaccines, inactivated ("killed") vaccines, and subunit vaccines. Attenuated vaccines are highly effective due to their ability to replicate, which provides a continual source of the pathogen along with other components called pathogen-associated molecular patterns (PAMPs) that are recognized by the host immune system as exogenous matter and results in an intensification of the host immune response.[62] Due to these two factors, attenuated vaccines usually require only one administration to provide long-term, or life-long, immunity. Inactivated vaccines are rendered non-replicative by heat, chemicals, or radiation, and while they possess the same components of attenuated vaccines the lack of replication requires booster vaccinations to produce protective and long term immune responses.

Additionally, the methods used for inactivation can degrade or alter the pathogen in a way that contributes to less protective immunity.

Both attenuated and inactivated conventional vaccines consist of the whole pathogen, and carry inherent risks that have been historically observed.[63, 64] Since attenuated viruses can replicate their use in people with weakened immune systems may produce severe side effects. Also, attenuated vaccines can potentially revert to a virulent state after vaccination, thus producing the natural disease in the patient along with potentially spreading the virulent pathogen. However, modern techniques utilizing genetic alteration of pathogens can remove or modify genetic components that contribute to virulence, which have helped to reduce the potential of vaccine reversion. For inactivated vaccines there is a potential of incomplete inactivation, resulting in inoculation of virulent pathogens into patients. These factors along with others have limited the use of whole-pathogen vaccines for pathogens that are highly virulent.

Subunit vaccines utilize only the component(s) of a pathogen that immune responses are generated against (called antigens), thereby minimizing the risk of infecting inoculated patients. Though subunit vaccinations are safer than whole pathogen vaccines, they are poorly immunogenic and require additional formulation. Notably, subunit vaccines do not replicate and may not contain PAMPs, and require booster administration and incorporation of immunostimulatory compounds (called adjuvants), respectively, to improve immunogenicity.

1.5.3 Modern vaccines

Methods and technologies beginning in the 1950's have led to a new generation of vaccines along with enhancing conventional vaccines. Some notable examples will be briefly mentioned. Virus like particles (VLPs) are non-replicating nanoparticles produced from structural components

of viruses, and can be considered a type of subunit vaccine as they contain only a fraction of the viral components.[65] The presented antigens are displayed in a native-fashion on VLP surfaces, thus mimicking the natural pathogen and enhancing immunogenicity. However, VLPs are unique to viruses, but recent advances in recombinant technologies permitted antigens of other pathogens to be combined with VLPs for expression on VLP surfaces.[66]

Similar to VLPs are the use of viral vectors to administer antigens for heterologous pathogens. Antigen from the pathogen of interest are recombinant added to viral vectors that display little or no pathogenicity to humans. The recombinant viral vectors are replication competent and contain endogenous PAMPs. An example is rVSV-EBOV, where the Ebola virus envelope glycoprotein was recombinant added and expressed on vesicular stomatitis virus, a zoonotic virus. [33, 34]. Other viruses used as vectors include many type of adenovirus and modified vaccinia Ankara virus.[33, 34, 37, 67] While recombinant viral vectors are effective at eliciting immune responses without boost vaccinations, there are concerns of their safety in patients with compromised immune systems. Additionally, reports of anti-vector immunity has led to the removal of some viral vector candidates as well as foreshadowing future issues with long-term immunity and efficacy.

DNA and RNA based vaccines are also popular alternatives vaccine formats in which DNA or RNA encoding the antigen(s) of interest is administered and taken up by cells, and the encoded antigens is produced and expressed by the host cell.[68, 69] The advantages of this system is that short the antigen is produced for a time, providing a renewable source for the immune response. Additionally the genetic material can be delivered to cells without the accompanying pathogen, avoiding issues seen with whole pathogen vaccines. However, soluble DNA and RNA are not efficiency taken up by cells and when done, they can be degraded. A common practice to enhance

delivery to target cells is to formulate the DNA/RNA with nanoparticles, such as lipid-based or polymeric nanoparticles, or VLPs.[68, 69]

1.5.4 Adjuvant incorporation

To produce an immune response that is comparable to those of attenuated vaccines, immunostimulatory compounds (or adjuvants) are included in subunit vaccine formulations.[70] Adjuvants are used to mimic the effect a pathogen has on innate immunity, which helps to produce a stronger adaptive response.

In the United States two adjuvants are approved for general use in vaccinations: aluminum salts (alum) and monophosphoryl lipid A (MPLA). Alum is known for producing strong Th_2 responses and has been incorporated into many vaccines since the 1930's.[71] This adjuvant is believed to function by acting as a depot for slow release of antigen once administered. MPLA is a derivative of lipopolysaccharide, a component of gram-negative bacteria, and is an activator of the Toll-like Receptor 4 (TLR 4) PRR.[72] Experiments using MPLA in soluble antigen formulations induce strong Th_1 responses, yet when incorporated into particles it has been reported to induce more balanced Th_1/Th_2 response.[73]

The discovery and development of new adjuvants is a growing area of research. One experimental adjuvant that is currently in phase 2 trials is ISCOMATRIX®. This adjuvant is a combination of cholesterol, phospholipid, and ISCOPREP saponin, and when combined form a cage-like structure.[74] When admixed with antigens, ISCOMATRIX® serves a delivery vehicle to draining lymph nodes and promotes uptake by antigen presenting cells. The saponin component of ISCOMATRIX® is also an immunostimulatory agent top induce cytokine release and promote the adaptive immune response; however, the direct mechanism of action is not known.

1.6 Interbilayer-crosslinked multilamellar vesicles (ICMVs)

1.6.1 Concept and development

Delivery of antigens to immunological sites is a continued area of research. The antigen must not only be delivered to these areas but it must be done so at amounts that can produce an effective response. Adjuvants that are incorporated into vaccines must also be delivered to the same sites as the antigen. Significant improvements in responses are seen between antigen only, co-administered antigen and adjuvant, and co-delivery of antigen and adjuvant.[75] For soluble vaccine strategies, the simultaneous delivery of vaccine components is not assured due to differences in pharmacokinetic parameters. Different permeability and distribution properties can greatly affect where and to what degree vaccine components disseminate in the host. However, nanoparticles are designed to contain each of the vaccine components in a dense package.

ICMVs are multilayered liposomes that contain covalent bonds between functionalized lipid head groups. The rationale behind this design is to increase the stability of the particle *in vivo*. Other designs such as liposomes or multi-lamellar vesicles (MLVs) that are not cross-linked are quickly degraded once administered.[76] The use of a phospholipid bilayer design allows ICMVs to retain both hydrophobic and hydrophilic compounds. Lipophilic compounds are generally contained in the lipid bilayer; whereas, hydrophobic compounds are either in nanoparticle core, between bilayers, or adsorbed onto the particle surface. Therefore, widely varying compounds can be packaged into a single unit to be co-delivered to immune sites.

ICMVs are produced by rehydration of a phospholipid film that is partially comprised of a phospholipid with a maleimide-functionalized head group (MPB).[76]. Rehydration results in a

heterogeneous population of multi-layered vesicles which are sonicated to produce simple liposomes of a more uniform size. Addition of calcium chloride induces fusion of the liposomes into a stratified particle that is approximately 250 nm in diameter. Cross-linking is achieved by the addition of dithiothreitol (DTT), a membrane permeable reducing agent that reacts with the maleimide head groups of opposing bilayers to form interbilayer covalent bonds. The ICMV is washed to remove any excess calcium and unbound DTT, and unreacted maleimide on the surface of the ICMV can be conjugated to PEG-thiol to promote longer circulation *in vivo*.

IMCVs have previously been tested as a vaccine formulation in mice using a model antigen and resulted in a 1000 fold increase in antibody titers compared to simple liposomes and around a 10 fold increase compared to MLVs.[76] Another vaccination strategy using a malarial antigen incorporated into ICMVs produced immune responses compared to soluble antigen admixed with alum.[73] Additionally, these ICMV formulations provided a more balanced cellular and humoral response despite using MPLA, which is known to generate strong Th_1 responses.

ICMVs have also been used in prior vaccination attempts with recombinant Env displayed on the particle surface.[77] The study resulted in enhanced antibody titers compared to the levels produced in response to the soluble antigen. However this study did not utilize the interior surfaces of ICMVs to retain antigen, a major advantage of ICMVs.

1.6.2 Components of ICMVs

ICMV components can be divided into three different groups: lipid bilayer components, crosslinking compounds, and fusion inducers. Depending on the characteristics desired for the ICMV structure or what is needed to support the antigen type, any of these groups can be modified.

Typically ICMVs are produced using a 1:1 molar ratio of the phospholipids DOPC and maleimide functionalized DOPE (MPB).[76] Both of these lipids have a net negative charge which is conferred to the ICMV once produced and the unsaturated dioleoyl acyl chains have melting temperatures well below room temperature. Modification to either of these properties can be achieved by addition or replacement with other phospholipids, such as those with the saturated distearoyl acyl chain or with neutral or positively charged lipids (e.g. DOPE or DOTAP, respectively). Lipophilic compounds can also be added to this group for various functions, such as cholesterol to increase membrane rigidity or lipophilic fluorophores for ICMV visualization. Other functionalized lipids can be added for distinct functionalization of the particles such as the use of lipids conjugated with NTA, a chelating agent that is used to retain compounds containing polyhistidine tags.[78]

Thiol containing compounds are required for the maleimide-thiol conjugation reaction that crosslinks bilayers into a stable structure.[76] DTT is the preferred thiol containing agent in ICMV synthesis due to its strong reducing potential and efficient reaction with maleimide. The short length of DTT produces a consistent distance between bilayers of roughly the length as DTT. This presents a dilemma for encapsulation of compounds of larger size in the interbilayer space. The reducing ability of DTT also has the potential to react with cysteines present on proteins and peptides. Though this may bind and retain antigens it can also affect their presentation.

Divalent metal ions are the choice fusion inducers with calcium ions producing the best results.[73] Other fusion inducers are currently being tested, and include the use of ionic polymers that serve as the sources of both the fusion inducer and the thiol groups for crosslinking of bilayers.

Chapter 2

Towards elicitation of broadly neutralizing antibody responses against hepatitis C virus with vaccine nanoparticles presenting E2 antigen

2.1 Abstract

Hepatitis C remains a global epidemic despite the global distribution and administration of antiviral therapeutics. An estimated 1% of the global population has contracted hepatitis C, and ~80% of those infections are asymptomatic and progress to chronic infection that increases the risk of liver fibrosis in those infected and transmission to others. Currently, a vaccine against hepatitis C virus (HCV) does not exist due to the extreme diversity and adaptability of the virus that leads to immune evasion. Here, we report the generation of autologous and heterologous neutralizing antibodies using two recombinant HCV antigens, E2.661 and E2c.661, loaded into lipid-based nanoparticles called, interbilayer-crosslinked multilamellar vesicles (ICMVs). Specifically, after three rounds of vaccination in mice, ICMVs loaded with E2.661 and E2c.661 generated autologous neutralizing antibodies in 100% and 86% of mice, respectively, whereas, measureable heterologous neutralization was observed with serum from 43% and 86% of mice. Further investigation of the immunization sera revealed that 100% and 43% of sera from E2c.661 ICMV and E2.661 ICMV vaccinated mice bound to the conserved and broadly neutralizing HCV1 epitope, suggesting its contribution to the heterologous responses. These data indicate ICMVs

loaded with E2c.661, but not E2.661, as a candidate vaccine for further investigation to generate cross-genotype protective humoral responses against HCV.

2.2 Introduction

As of 2015, approximately 71 million people were living with chronic hepatitis C worldwide, with an estimated 1.75 million new cases that year.[8] Chronic HCV infection can lead to liver fibrosis and cirrhosis, and is a leading contributor to hepatocellular carcinoma.[79] Despite the advances of direct acting antivirals (DAAs) against the hepatitis C infection, the treatment is lengthy (lasting 2-6 months), and requires daily dosing that is tailored to the diverse genotypes of HCV.[11] Furthermore, the escalating crisis of opioid epidemics and injecting drug use in the US and elsewhere fuel the spreading of HCV.[80] An HCV vaccine that can prevent HCV transmission or the development of chronic HCV infection will be an important tool for the elimination of this devastating human pathogen.

Analyses of monoclonal antibodies (mAbs) from chronically infected patients have identified cross-genotype neutralizing antibodies recognizing the E2 subunit of the HCV envelope glycoprotein complex,[15, 81-84] with many of these antibodies recognizing epitopes within the CD81 binding site (CD81bs) of E2.[14, 15, 82] Recently, we demonstrated that three antibodies against this epitope protected chimeric liver mice of HCV after passive immunization.[85] Additionally, in a previous report, immunization of humanized mice with a recombinant E2 antigen generated cross-genotype targeting antibodies; however, an extensive dosing schedule was required, and only two mAbs were identified from a pool of 51 inoculated mice.[86] Generation of cross-neutralizing antibodies has remained a challenge, partially because the three variable regions (VRs) of E2 are highly mutagenic and antigenic, thus skewing humoral immune responses away from crucial

conserved epitopes.[87-89] Extensive research from us and others has led to the development of a engineered E2 subunit that retains its conformation and immunogenicity,[90-93] and we have recently determined the E2 core structure (E2c), devoid of the highly variable region 1 (HVR1) and variable region 2 (VR2), while preserving key epitopes, including the important CD81bs on the E2 neutralizing face.[94, 95]

In this report, we have developed synthetic vaccine nanoparticles loaded with soluble recombinant antigens of E2 and E2c truncated to residue 661 (E2.661 and E2c.661, respectively) and evaluated for their antigenicity and immunogenicity. As soluble antigens, E2.661 and E2c.661 lack the multivalent display, concerted orientation, and presence of immunostimulatory danger signals as HCV virions. We have previously demonstrated that subunit antigens loaded into lipid-based nanoparticles, called interbilayer-crosslinked multilamellar vesicles (ICMVs), can significantly improve immune responses to protein antigens.[73, 76]

Here we sought to test the immunogenicity of ICMVs loaded with E2.661 or E2c.661, and evaluate the display of the antigens on ICMV surfaces. ICMVs were analyzed by immunofluorescence staining and evaluated both as bulk formulations and individual nanoparticles. Notably, the CD81bs-targeting broadly neutralizing antibody HCV1 selectively bound to E2c.661 ICMVs, compared with E2.661 ICMVs. Vaccination with ICMV formulations generated log-fold increases in antigen-specific serum IgG titers, compared with soluble controls. Neutralization of HCV pseudotype-like particles (HCVpp) were more frequent and of a greater capacity by serum collected form ICMV immunized mice compared to soluble controls. Specifically, immune sera from the E2.661 ICMV group preferentially neutralized autologous HCVpp in 7 of 7 mice with high potency. In contrast, immune sera from 6 of 7 animals immunized with E2c.661 ICMVs exhibited neutralizing-capacity against autologous HCVpp (albeit at

moderate level) as well as heterologous HCVpp, thus demonstrating broadening and cross-genotype activity of humoral immune responses.

2.3 Materials and Methods

Generation of soluble E2 constructs for protein expression and purification.

We have previously reported the cloning and purification of the recombinant antigens of the HCV E2 glycoprotein.[94] Here, E2.661 and E2c.661 recombinant antigens of the E2 glycoprotein from the prototypic HCV strain H77 were both C terminally truncated to amino acid residue 661 for comparison of the effect of VR deletion on E2. Spaete *et al.* showed previously that E2 truncated at amino acid 661 can be expressed as folded, soluble recombinant protein despite the presence of odd number of cysteine residues in the protein.[90] E2c.661 has the additional modifications: 1) N-terminal truncation to residue 412; 2) replacement of amino acids 460-485 with a gly-ser-ser-gly linker; and 3) removal of the N-linked glycosylation sites at residues 448 and 576. Antigens were co-transfected with pAdvantage (Promega) into FreeStyle 293-F mammalian cells (Invitrogen) supplemented with 7.5 μM kifunensine and incubated for 72 hours at 37°C. The proteins were purified over an AR3A antibody affinity column (AR3A chemically conjugated to protein A (GE) using DMP (Thermo Fisher Pierce)), eluted with 0.2 M glycine buffer pH 2.2.

Antibody production and purification.

We have previously reported the production of the HCV-specific antibodies AR1B, AR2A, AR3A, and HCV1.[14, 83] Briefly, variable and constant antibody fragments were cloned into pDR12 vectors and pIgG1 vectors, respectively, then co-transfected into CHO (Chinese hamster

ovarian) cells. The expressed antibodies were collected and purified via a protein A-agarose column (GE Healthcare).

ICMV synthesis.

ICMVs were synthesized with slight modifications from our previous report.[76] Briefly, solutions of 1,2-dioleoyl-sn-glycero-3-phosphocholine (DOPC) and 1,2-dioleoyl-sn-glycero-3-phosphoethanolamine-N-[4-(p-maleimidophenyl)butyramide] sodium salt (MPB) (Avanti Polar Lipids) in chloroform were mixed in equal molar ratios and dried to produce thin lipid films. Stock antigens were diluted in 10 mM bis-tris propane (BTP) (Fisher Scientific) at pH 7 for a final concentration of 250 μg/mL. These solutions were used to rehydrate the dried films. The resulting suspensions were sonicated by probe tip (QSonica Q125) to produce small unilamellar vesicles that were subsequently $CaCl_2$ and DTT (Fisher), which were added to fuse and crosslink interbilayer maleimides, respectively, to produce ICMVs. The resulting particles were incubated for one hour in at 37 °C and centrifuged (Eppendorf 5430R) at 14,000 r.c.f. for 4 minutes at 4 °C to remove unloaded antigen. The pelleted ICMVs were washed with DNA grade water (Fisher), and this process was repeated once more before a final suspension 200 μL of sterile filtered phosphate buffered saline (Gibco). For the immunostaining assays, ICMVs were produced as above with the addition of a lipophilic fluorophore, 1,1'-Dioctadecyl-3,3,3',3'-Tetramethylindodicarbocyanine, 4-Chlorobenzenesulfonate Salt (DiD) (Thermo Scientific), at less than 0.2 molar percent to the lipid films. ICMVs used for inoculation were produced as those above with the addition of the Toll-like receptor-4 agonist, monophosphoryl lipid A (MPLA, Avanti Polar Lipids) to the initial phospholipid mixture, similar to a previous report.[76]

Antigen loading.

Loading of E2.661 or E2c.661 into ICMVs was evaluated by sodium dodecyl-sulfate polyacrylamide gel electrophoresis (SDS-PAGE) under reducing conditions on Bolt™ 8% Bis-Tris Plus gels (Invitrogen). Gels were run using MOPS SDS running buffer (Invitrogen) for 45 minutes at 200V. Following protein migration, the gels were stained with Coomassie Brilliant Blue R-250 (Fisher), and after sufficient rounds of destaining, the gels were visualized with a FluorChemM digital imager (ProteinSimple) and analyzed via ImageJ software.

ICMV size analysis.

The diameter of ICMVs was measured by DLS using ZetaSizer Nano ZSP (Malvern) and by nanoparticle tracking analysis via NanoSight NS300 (Malvern) equipped with a 405nm or 488nm laser. The zeta potential of ICMVs was measured using a ZetaSizer NanoZSP. For size analysis, the formulations were diluted in 0.22μm filtered water, whereas, formulations used of zeta potential measurements were diluted in 0.22μm filtered water or 0.22μm filtered phosphate buffered saline (PBS).

Evaluation of surface-displayed antigens.

Antigen-loaded ICMVs containing DiD were diluted 1:2 in FACS buffer (1% BSA (Fisher) in PBS) and briefly water-bath sonicated to disrupt nanoparticle aggregates. The samples were further diluted two-fold with FACS buffer containing either antigen specific primary antibodies AR1B, AR2A, AR3A, and HCV1,[14, 83, 86] or isotype control human IgG1 kappa antibody (Sigma-Aldrich) at a working concentration of 0.018 mg/mL. An additional control group consisting of FACS buffer alone was also included, termed “Processed Control”. All samples were incubated overnight at 4°C and then centrifuged at 20000 r.c.f. for 45 minutes at 4°C to remove unbound

antibodies. The pellets were washed with FACS buffer and centrifuged again. All processed samples were suspended in 100 µL phycoerythrin (PE) conjugated goat anti-human IgG (eBioscience) secondary antibody at a 1:50 dilution and incubated for one hour at room temperature away from light. Unbound secondary antibodies were removed by two rounds of configuration and washing as above, and the particles were suspended in FACS buffer and plated into a black opaque 96-well plate (Costar). The emission/excitation signals of DiD and PE were measured at 644/670 and 488/578, respectively. For NanoFACS analysis, the above samples were transferred after the plate-based measurements into FACS tubes and diluted approximately two-fold with FACS buffer. The samples were placed on ice analysis on a Beckman Coulter MoFlo Astrios fitted with M1 and M2 masks. Data gathered by NanoFACS was analyzed using FloJo software.

In vivo vaccination studies.

Female, 5- to 8-week old, C57/BL-6 mice (Envigo) were vaccinated on days 0, 21, and 42 by subcutaneous injection (100 µL) divided equally on either side of the tail base. Four vaccine formulations were evaluated, consisting of either soluble antigen (E2.661 or E2c.661) plus MPLA or antigen loaded ICMVs (E2.661 or E2c.661) plus MPLA. Initial vaccinations administered 10 µg of indicated antigens along with approximately 1 µg MPLA. Subsequent vaccinations contained 5 µg of indicated antigens and approximately 0.5 µg MPLA. Serum samples collected for ELISAs and *in vitro* pseudo-virus neutralization assays were collected via submandibular punctures on day -1, 20, 41, 62, 104, 142, and 176. Sera were collected into Microvette® 500 Z-gel tubes (Sarstedt) and processed according to the manufacturer's instructions. Serum samples were removed and stored at -80°C until used.

Enzyme linked immunosorbent assays.

Endpoint titers of E2-specific IgG from immune sera were determined by ELISA similar to a previous report.[96] In summary, ELISA microwells were pre-coated with 5 μg/ml *Galanthus nivalis* lectin (Vector Labs) overnight at 4°C. Microwells were washed with 1X PBS/0.05% Tween20 and blocked with 4% non-fat milk (Bio-Rad) for 1 hour at room temperature (R.T.). H77 E1E2 antigens were captured from the cell lysate of 293T cells with an expression plasmid for 1 hour at R.T. Serially diluted serum from immunized animals were added, and incubated for 1 hour at R.T. Antibodies bound to the antigen were detected by peroxidase (HRP)-conjugated goat anti-mouse IgG Fc antibody (1/2000) (Jackson ImmunoResearch) and TMB substrate (Pierce). Endpoint titers were measured as the highest dilution of serum producing a signal 3-fold greater than the background signal. For the recognition of linear peptide epitopes by serum antibodies, the HCV H77 corresponding HVR1 peptide (amino acids 384-411; sequence ETHVTGGNAGRTTAGLVGLLTPGAKQNI) (Genscript) or a long peptide (amino acids 407-424; sequence AKQNIQLINTNGSWHINS) (NIH) containing the HCV1 epitope (residues 412-423) were coated onto wells at 5 μg/mL overnight at 4 °C for binding of immune sera.

In vitro pseudotype-virus particle neutralization assay.

The production of HCV pseudotype-virus particles (HCVpp) and the in vitro neutralization assay have been described previously.[83] Briefly, HCVpp expressing firefly luciferase and E1E2 from either H77 (genotype 1a), UKN1b12.6 (genotype 1b), or J6 (genotype 2b) were collected from the supernatants of cultured 293T cells. Immune sera at 1:50 dilutions were combined with the HCVpp containing supernatants and incubated for 1 hour and 37°C. The antibody-virus mixtures were added to microwells seeded with Huh7 cells the day prior and incubated at 37°C. After 4-6 hours incubation the mixtures were replaced with fresh culture medium and incubated for an additional 72 hours. The firefly luciferase signal from HCVpp infected cells was determined

using Bright-Glo™ Luciferase Assay System (Promega) according to the manufacturer's instructions. HCVpp neutralization was calculated as a percent of the residual virus infectivity divided by infectivity without sera after background subtraction. Pseudotype virus particles transfected with pNL4-3.lucR−E only was used to determine the background infectivity, while pseudotype virus particles expressing the envelope glycoprotein from lymphocytic choriomeningitis virus (LCMVpp) were used as a negative control.

Statistical analysis.

Determination of statistical significance was performed using Prism 7.0.3. One-way or two-way ANOVA significance tests with Tukey's or Sidak's post-hoc multiple comparison test were used for group-wise analysis as indicated in the figure legends. Statistical significance is indicated as: n.s. $p > 0.05$, *$p < 0.05$, **$p < 0.01$, ***$p < 0.001$, and ****$p < 0.0001$.

2.4 Results

Antigen design.

The recombinant antigens used in this study were derived from the E2 envelope glycoprotein of the prototypic HCV strain H77 (**Figure 2-1A**).[93, 94] Both antigens were truncated to remove part of the stalk and the entire transmembrane regions to improve solubility.[90] Additional modifications to the E2c.661 include removal of N-linked glycans and two variable regions while retaining a native-like conformation.[94] Previous research has suggested that the VRs are immunogenic decoys and contributing factors of immune evasion by HCV.[97, 98]

Characterization of antigen-loaded ICMVs.

Antigen-loaded ICMVs were produced following the standard protocol by thin film rehydration using buffer containing 50 µg of E2.661 or E2c.661. After removal of unloaded antigens, ICMVs were analyzed by dynamic light scattering (DLS) to determine their diameter and zeta potential **(Figure 2-1B)**. Measurement of the bulk samples by DLS reported an average

A.

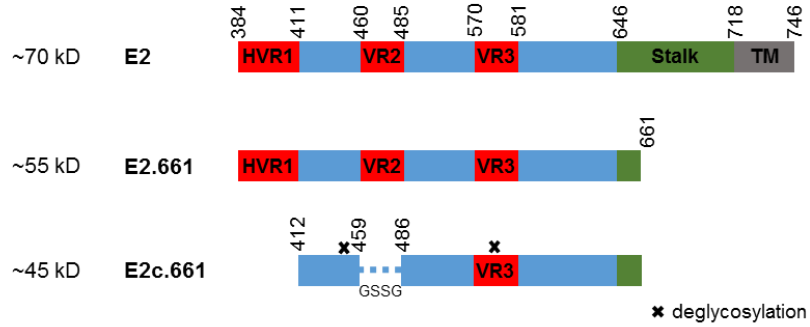

B.

	Z-Avg. (nm) by DLS	PDI	ZP (mV) in PBS	ZP (mV) in water	Size (nm) by NTA	LE%
E2.661 ICMV	132 ± 16	0.23 ± 0.02	-23 ± 2	-35 ± 7	115 ± 12	54 ± 8
E2c.661 ICMV	123 ± 2	0.21 ± 0.02	-24 ± 1	-30 ± 16	121 ± 14	50 ± 7

C.

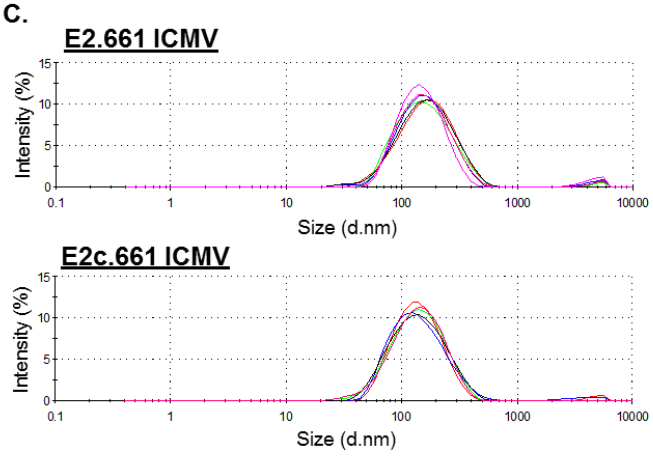

D.

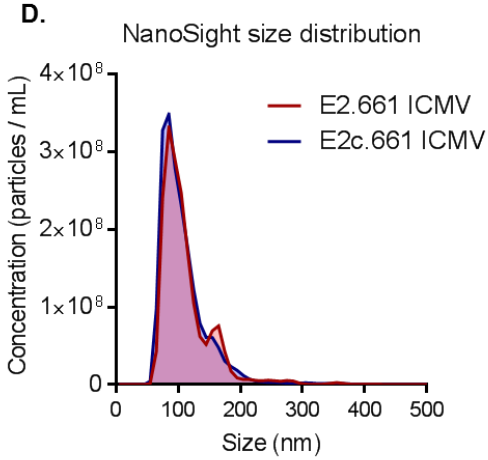

Figure 2-1. Schematic representations of antigen constructs and characterization of antigen-loaded ICMVs. **A)** Native HCV E2 is represented with conserved regions (blue) interspersed with 3 variable regions (VRs). E2.661 and E2c.661 are truncated at amino acid 661 to remove most of the stalk region and the entire transmembrane domain (TM). Additional alterations in E2c.661 are the removal of the hypervariable region 1 (HVR1) and VR2 (replaced with a gly-ser-ser-gly linker), and removal of N-linked glycans at residues 448 and 576. **B)** Table of percent loading efficiencies of initial antigen (LE %), average diameters by DLS or NTA, polydispersity indices (PDI), and zeta potentials (ZP) of ICMVs. **C**) Intensity-based Zetasizer distributions of E2.661 and E2c.661 ICMVs. **D)** NanoSight size distributions (number-based) of E2.661 and E2c.661 ICMVs. Measurements reported as mean ± SD.

diameter of 132 ± 16 nm and 123 ± 2 nm for ICMVs loaded with E2.661 and E2c.661, respectively **(Figure 2-1B),** and both formulations demonstrated largely homogeneous size distributions, indicated by polydispersity indices of 0.23 ± 0.02 and 0.21 ± 0.02 and size distribution peaks focused around 130 nm **(Figure 2-1B, C)**. The zeta potentials were relatively conserved between the ICMV formulations, at -35 ± 7 mV and -30 ± 16 mV for ICMVs and NTA ICMVs diluted in

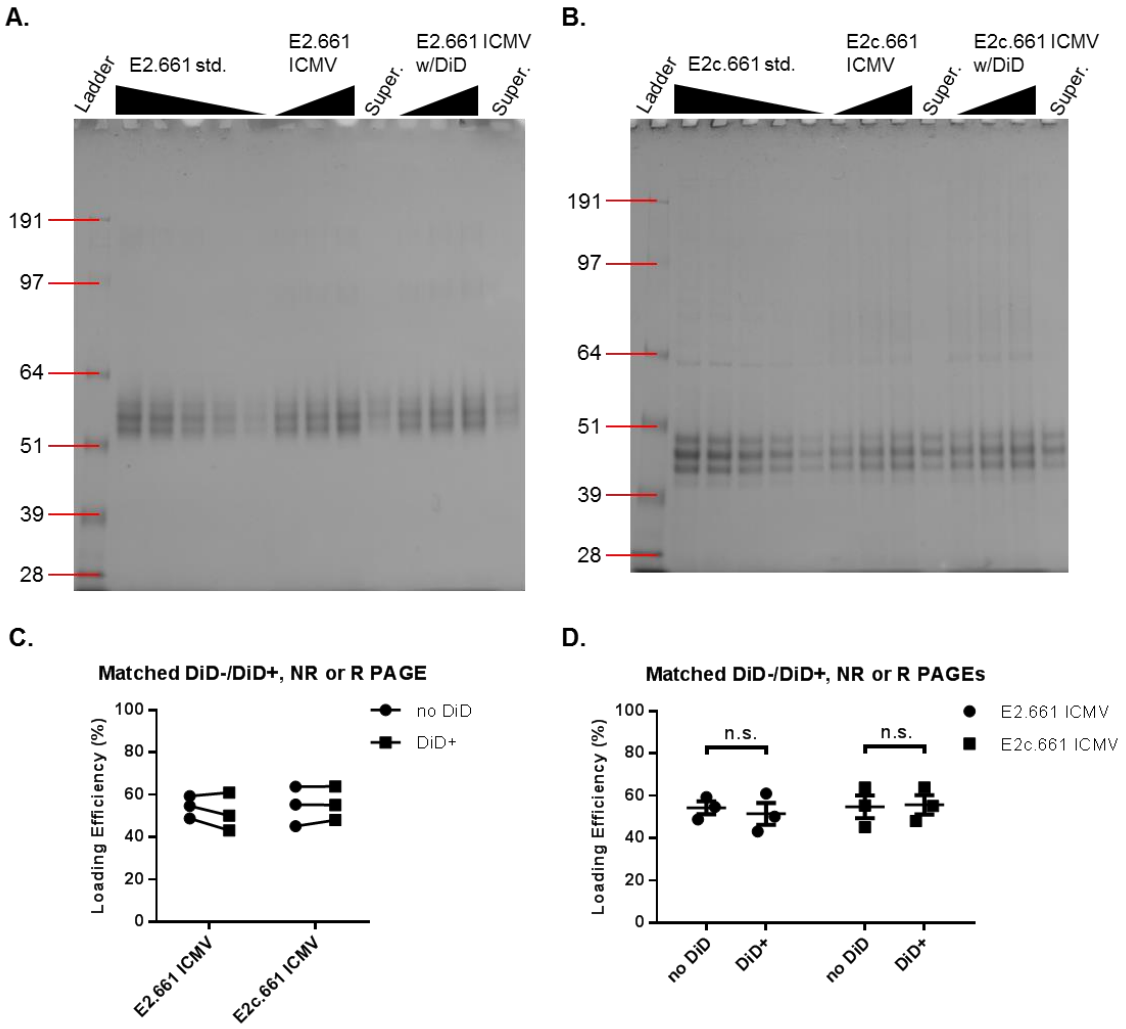

Figure 2-2. Analysis of antigen loading efficiencies in ICMVs. **A, B)** Reducing SDS PAGEs of E2.661 and E2c.661 ICMVs (with or without DiD) to determine loading efficiency (super. = supernatant of first centrifugation after ICMV production). Note: the multiple adjacent bands represent the different glycoforms of recombinant E2. **C)** Loading efficiencies of three independent DiD- and DiD+ ICMV pairs. **D)** Average loading efficiencies of production matched ICMVs. Measurements reported as mean ± SEM. Statistical analysis performed by two-way ANOVA of matched pairs, followed by Sidak's multiple comparisons test. n.s. $p > 0.05$.

water, respectively, confirming that the antigens did not affect the anionic charge of ICMVs. Individual nanoparticle sizes as measured by nanoparticle tracking analysis (NTA) were 115 ± 12 nm and 121 ± 14 nm in diameter for E2.661 and E2c.661 ICMVs, respectively, with main distribution peaks around 100 nm (**Figure 2-1B, D**). The antigen content of ICMVs loaded with either E2.661 or E2c.661 was determined by SDS PAGE under reducing conditions, followed by Coomassie staining **(Figure 2-2A, B)**. We observed loading efficiencies of 54 ± 8% and 50 ± 7% for E2.661 ICMVs and E2c.661 ICMVs, respectively, with no significant difference between the two ICMV formulations ($p > 0.05$, **Figure 2-1B**).

Interrogation of surface-displayed antigen on ICMVs.

To assess display of surface-bound antigens and antibody-mediated recognition of epitopes on ICMVs, we performed an indirect immunofluorescence assay on ICMVs using a microplate-based whole population approach[73] as well as NanoFACS-based interrogation of individual nanoparticles (see below) **(Figure 2-3A)**. For both approaches, ICMVs were incubated with primary antibodies directed against E2 epitopes, followed by incubation with phycoerythrin (PE)-conjugated secondary antibodies **(Figure 2-3A)**. To account for particle loss from the immunofluorescence process, we included a small amount (< 0.2 molar %) of a lipophilic fluorophore, DiD, during the ICMV synthesis as a non-discriminate marker of nanoparticles. We evaluated the loading efficiencies of antigens in DiD+ and DiD- ICMVs and observed similar antigen loading between the formulations **(Figure 2-2A-D)**. Next, we incubated DiD+ E2.661 or E2c.661 ICMVs with antigen-specific antibodies, AR1B, AR2A, AR3A, or HCV1, which recognize four different antigenic sites on E2.[14, 15] Control groups included an isotype control antibody to assess non-specific antibody binding and FACS buffer alone as a negative control. To evaluate nanoparticle recovery, the DiD signals of the processed samples (those that were

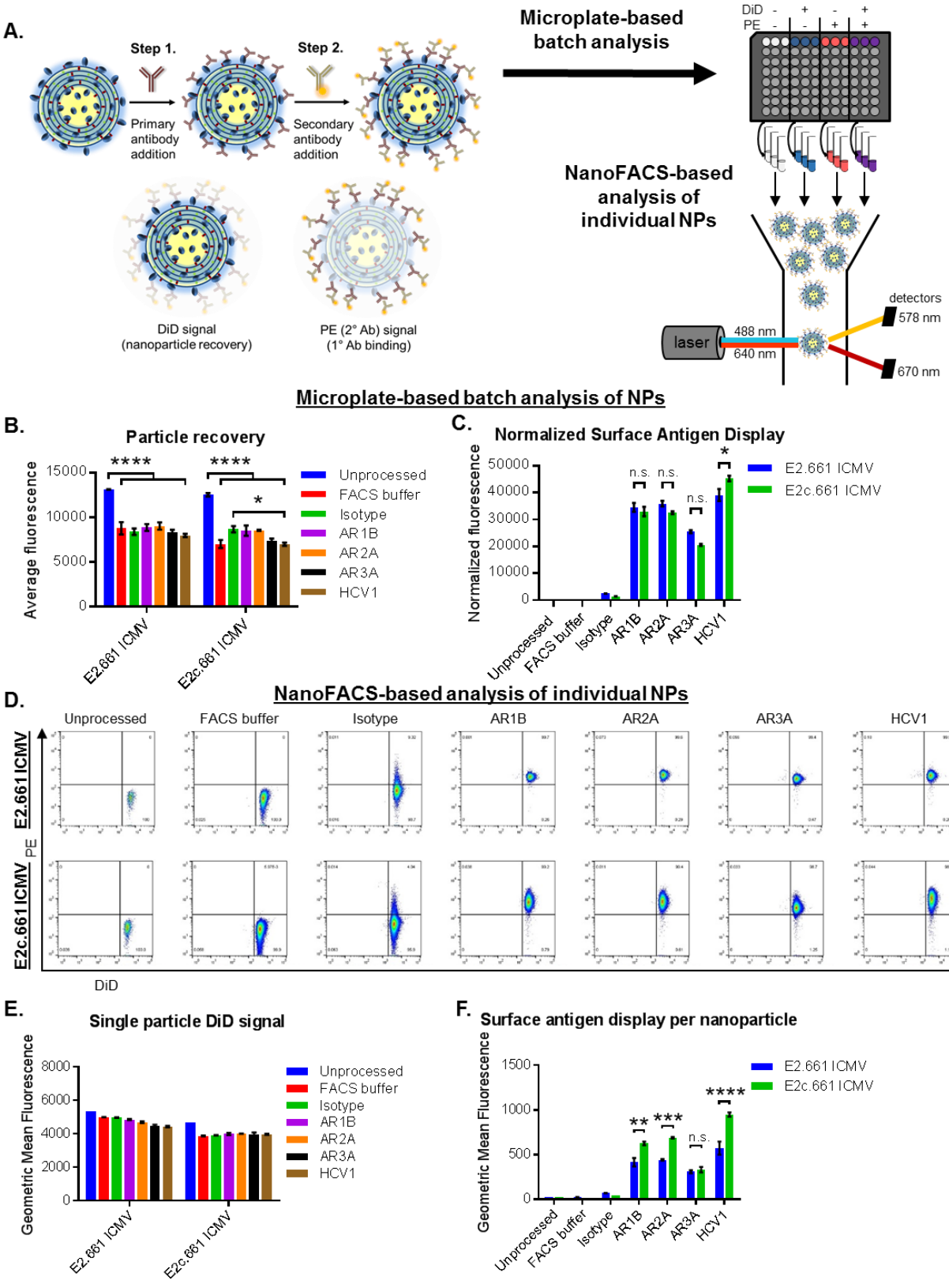
A.
Step 1.
Primary antibody addition
Step 2.
Secondary antibody addition
DiD signal (nanoparticle recovery)
PE (2° Ab) signal (1° Ab binding)
Microplate-based batch analysis
DiD
PE
NanoFACS-based analysis of individual NPs
laser
488 nm
640 nm
detectors
578 nm
670 nm
Microplate-based batch analysis of NPs
B.
Particle recovery
Average fluorescence
Unprocessed
FACS buffer
Isotype
AR1B
AR2A
AR3A
HCV1
E2.661 ICMV
E2c.661 ICMV
C.
Normalized Surface Antigen Display
Normalized fluorescence
n.s.
E2.661 ICMV
E2c.661 ICMV
D.
NanoFACS-based analysis of individual NPs
Unprocessed
FACS buffer
Isotype
AR1B
AR2A
AR3A
HCV1
E2.661 ICMV
E2c.661 ICMV
PE
DiD
E.
Single particle DiD signal
Geometric Mean Fluorescence
F.
Surface antigen display per nanoparticle

Figure 2-3. Analysis of surface antigen conformation and display. **A)** Schematic of the immunofluorescence staining process. Step 1, ICMVs labeled with DiD (blue glow) are incubated with primary antibodies (or FACS buffer). Step 2, after washing the samples are incubated with PE-labeled secondary antibodies (or FACS buffer). DiD fluorescence is used to assess particle loss during processing, while PE fluorescence corresponds to bound primary antibodies. Immunofluorescence staining is first measured on a batch basis then each sample is recollected and analyzed on an individual nanoparticle basis using flow cytometry. **B)** DiD fluorescence signal of processed and unprocessed (DiD control) samples. **C)** Secondary antibody signal normalized to DiD loss. **D)** Representative NanoFACS plots from each group tested. **E)** DiD fluorescence of immunofluorescence stained ICMVs measured by NanoFACS. **F)** NanoFACS signal of bound secondary antibody after incubation with designated ICMVs. Measurements reported as mean ± SEM. Statistical analysis performed by two-way ANOVA, followed by Tukey's multiple comparisons test. *$p < 0.05$, **$p < 0.01$, ***$p < 0.001$, ****$p < 0.0001$.

incubated with antibodies and washed) were compared against the unprocessed ICMVs (those that were not incubated with any antibody).

The microplate-based assessment of the whole ICMV population revealed the average particle recovery rate of 65 ± 5% and 67 ± 4% for E2.661 ICMVs and E2c.661 ICMVs, respectively **(Figure 2-3B)**. We then measured the PE signals from antibody-bound ICMVs and normalized the values by the particle recovery rates (**Figure 2-3C**). Both ICMV formulations were recognized and bound by antibodies specific to various epitopes across E2, demonstrating maintenance of antigenicity in ICMVs. Notably, the signal for the E2c.661 ICMVs was significantly greater than that of E2.661 ICMVs for HCV1 antibody ($p < 0.5$, **Figure 2-3C**).

Immunofluorescence staining is a useful tool for discerning antigen display profiles on ICMVs; however, analysis of bulk samples, as above, does not provide insights into antigen display on individual particles. To address this issue, we have employed a flow cytometry-based analysis method, termed NanoFACS, which we adopted from previous reports.[99-103] The same samples used in the plate-based method were analyzed by NanoFACS. After gating on individual ICMVs, the DiD signal and PE-antibody signal were plotted **(Figure 2-3D)**. The DiD signal on the X-axis indicates individual ICMVs, while the PE-antibody signal on the Y-axis shows the extent of antibodies binding to individual ICMVs. Notably, that there was some loss of DiD during

the immunofluorescence process, as reflected by the slight decrease in the DiD signal between the unprocessed and processed samples **(Figure 2-3E)**. Consistent with the microplate-based method, we observed strong binding of various E2 epitope-specific antibodies on the surfaces of both E2.661 ICMVs and E2c.661 ICMVs **(Figure 2-3F)**. Importantly, there were notable differences in the PE-antibody signals obtained by the microplate- and NanoFACS-based methods. Compared with E2.661 ICMVs, E2c.661 ICMVs exhibited significantly elevated binding of AR1B, AR2A, and HCV1 antibodies ($p < 0.01$, $p < 0.001$, and $p < 0.0001$, respectively, **Figure 2-3F)**, suggesting enhanced presentation of E2 epitopes on E2c.661 ICMVs.

E2c.661 ICMVs generate neutralizing antibodies against autologous and heterologous E1E2.

We next sought to determine whether the differences in the antigen design and epitope display on the surfaces of ICMVs have any impact on the immunogenicity of ICMVs *in vivo*. To bolster the immune responses, we incorporated an immunostimulatory adjuvant, MPLA (a Toll-like receptor 4 agonist) in all of the vaccine formulations. Mice were vaccinated subcutaneously at the tail base with the prime dose of 10 μg antigen plus 1 μg MPLA and two boost doses of 5 μg antigen and 0.5 μg MPLA with a three-week interval between immunizations **(Figure 2-4A)**. We collected serum samples spanning day -1 to 176 and analyzed them for IgG titers against the native E1E2 antigen by sandwich ELISA. Both ICMV formulations demonstrated a rapid increase in antigen-specific IgG titers after the first vaccination, whereas seroconversion of the soluble groups was observed after the second vaccination **(Figures 2-4B and Figure 2-5)**. Regardless of the antigen used, E2-serum IgG titers from the ICMV vaccine groups were similar in magnitude throughout the vaccination study, and were consistently greater than their respective soluble controls, with at least 6 and 20-fold increases for E2.661 ICMV and E2c.661 ICMV groups, respectively **(Figure 2-4B)**.

A.

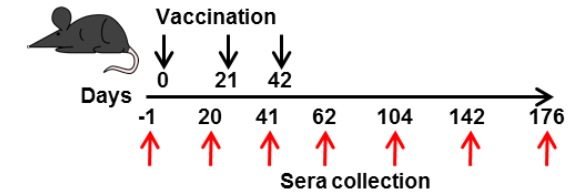

B.

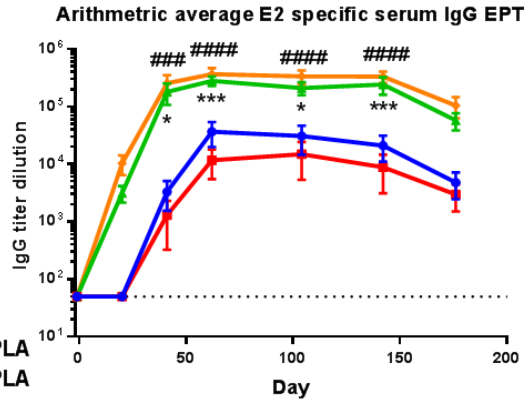

C.

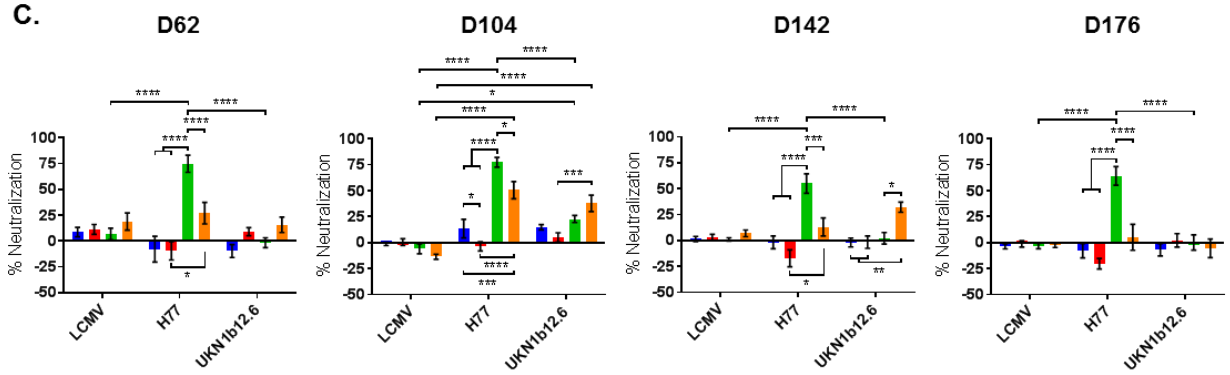

D

Formulation	Mouse ID	Day 62 % Neutralization			Day 104 % Neutralization						Day 142 % Neutralization			Day 176 % Neutralization		
		LCMV	H77 (GT1a)	UKN1b12.6 (GT1b)	LCMV	H77		UKN1b12.6		J6	LCMV	H77	UKN1b12.6	LCMV	H77	UKN1b12.6
E2.661 + MPLA	1	-11	-69	-32	-3	-24		11			-4	-15	13	-18	-41	-35
	2	-1	4	-10	-3	40		17			0	14	9	-4	11	-8
	3	28	-34	-20	4	-1		18			6	-16	-8	6	-21	-9
	4	10	-25	-9	-2	9		20			6	-27	-7	-1	-16	-1
	5	4	-21	-24	-10	3		11			-6	-12	-22	-2	3	-5
	6	9	28	-3	1	49		19			-7	16	1	0	18	11
	7	25	24	26	0	-4		0			12	13	10	-4	-18	17
	8	5	30	-5	3	36		23			6	13	-11	-5	2	-25
E2c.661 + MPLA	9	23	25	21	-2	-7	-34	3	-32	-35	9	11	17	-6	-51	-23
	10	26	34	20	-10	18	24	7	-2	-5	0	3	-22	-14	-4	-8
	11	-10	-35	18	-6	-23	-11	21	-7	-13	-8	-59	-27	-12	-24	-22
	12	-3	-21	-3	-5	-7	-12	-1	1	-7	3	-33	0	3	-20	7
	13	11	-25	10	12	-3	-18	12	1	-12	20	2	22	7	-9	22
	14	3	-26	-9	8	-12	-38	-21	-22	-11	1	-14	3	7	-23	24
	15	16	-14	4	14	9	-10	15	16	-5	-3	-22	-6	-1	-11	10
	16	24	-13	12	-7	-4	-27	4	-6	-26	2	-25	1	7	-21	8
E2.661 ICMV + MPLA	17	24	58	17	3	69		30			1	57	11	1	73	30
	18	17	88	7	-1	89		29			4	63	-11	0	66	15
	19	12	60	-10	13	58		18			3	19	-14	-2	38	-25
	20	-15	98	-20	-4	85		18			-7	66	-9	-12	80	-17
	21	-10	94	-6	-25	88		16			6	79	13	-14	91	-11
	22	3	85	-7	-14	85		12			0	79	1	2	76	-1
	23	17	41	8	-13	68		36			1	22	25	3	26	10
E2c.661 ICMV + MPLA	24	-6	42	17	-10	63	63	49	46	-7	5	36	38	-2	38	0
	25	4	10	15	-12	8	-33	-4	-26	-35	20	-6	26	-1	17	16
	26	3	80	55	-22	79	67	58	59	29	12	49	52	-10	57	31
	27	10	14	0	-21	50	30	43	33	25	12	-10	20	-8	-24	-22
	28	26	18	-8	-8	44	16	31	5	10	2	-6	20	-4	-8	-39
	29	51	-4	13	-17	55	25	52	20	7	-7	8	24	1	-32	-15
	30	44	29	18	-5	55	53	36	4	-1	5	21	45	6	-12	-9

<25% | 26-50% | 51-75% | >75%

Figure 2-4. Vaccination study in C57BL/6 mice. **A)** Vaccination scheme indicating days of subcutaneous vaccinations (black arrows) and serum collection (red arrows). **B)** Arithmetric average E2 specific IgG titers from serum collections. Endpoint antibody titers of mouse samples were determined by calculating the highest serum dilution producing an absorbance value 3-fold above background. Measurements reported as mean ± SEM. Statistical analysis was performed on groups with similar antigens (e.g. E2.661 + MPLA vs. E2.661 ICMV + MPLA) using two-way ANOVA with matched pairs followed by Tukey's multiple comparisons test. Statistical significance levels are denoted by asterisks (*) for E2 antigen formulations and pound signs (#) for E2c antigen formulations. (#/*) $p < 0.05$, (##/**) $p < 0.01$, (###/***) $p < 0.001$, (####/****) $p < 0.0001$. **C)** Average *in vitro* pseudotype-virus particle neutralization various by diluted vaccination serum collected at various time points. Measurements reported as mean ± SEM. Statistical analysis was performed by two-way ANOVA using matched pairs followed by Tukey's multiple comparisons test. *$p < 0.05$, **$p < 0.01$, ***$p < 0.001$, ****$p < 0.0001$. **D)** Individual *in vitro* serum neutralization titers. LCMV (Lymphocytic Choriomeningitis Virus, negative control), HCV H77 (autologous HCV), and HCV UKN1b12.6 and J6 (heterologous strains from genotype 1b and 2a, respectively).

We evaluated the antigen specificity and neutralization capacity of the immune sera by *in vitro* neutralization assay against HCV pseudotype-virus particles (HCVpp) expressing E1E2 glycoproteins from autologous (H77) or heterologous (UKN1b12.6 and J6) HCV strains, or the envelope glycoprotein from lymphocytic choriomeningitis virus (LCMV) as a negative control. Serum samples from day 62 demonstrated autologous HCVpp neutralization in 7 of 7 and 3 of 7 serum samples from E2.661 and E2c.661 ICMV groups, respectively, compared to 2 of 7 and 1 of 7 for their respective control groups. At this time point only two serum samples possessed heterologous HCVpp neutralizing capacity, one from the E2.661 control group and the other from the E2c.661 ICMV group. At day 104, autologous responses were sustained for the E2.661 ICMV group, but interestingly expanded to 6 of 7 mice from the E2c.661 ICMV group, and in both groups heterologous neutralization also increased to 3 of 7 and 6 of 7 mice (**Figure 2-4C, D**).

Vaccination with E2.661 ICMVs generated immune sera with strong neutralizing activity against autologous HCVpp, with 6 out of 7 mice exhibiting > 30% neutralization at day 176; however, they exhibited weak and short-lived neutralizing capacity against heterologous HCVpp **(Figure 2-4C, D)**. In stark contrast, immune sera from the E2c.661 ICMV group exhibited neutralizing capacity against both autologous (albeit at a lower capacity) and heterologous HCVpp

in 6 out of 7 mice by day 104 ($p < 0.001$, compared with the soluble control, **Figure 2-4C, D**). We confirmed these data by retesting serum from both E2c.661 vaccination groups and included a cross-genotype (2a) HCVpp, J6. We again observed neutralization against H77 and UKN1b12.6 HCVpp as well as one cross-genotype neutralizing sample **(Figure 2-4D)**. On day 142, the neutralizing responses from the E2c.661 ICMV group began to wane, but 3 of 7 samples still exhibited heterologous HCVpp neutralization, and an average neutralization capacity significantly higher than the E2.661 ICMV or soluble control groups ($p < 0.05$ and $p < 0.01$, respectively **Figure 2-4C, D**).Given these data, the ICMV formulations incited potent antigen-specific antibody responses with neutralizing capacity against autologous and heterologous viruses, whereas the soluble groups were less antigenic and immunogenic.

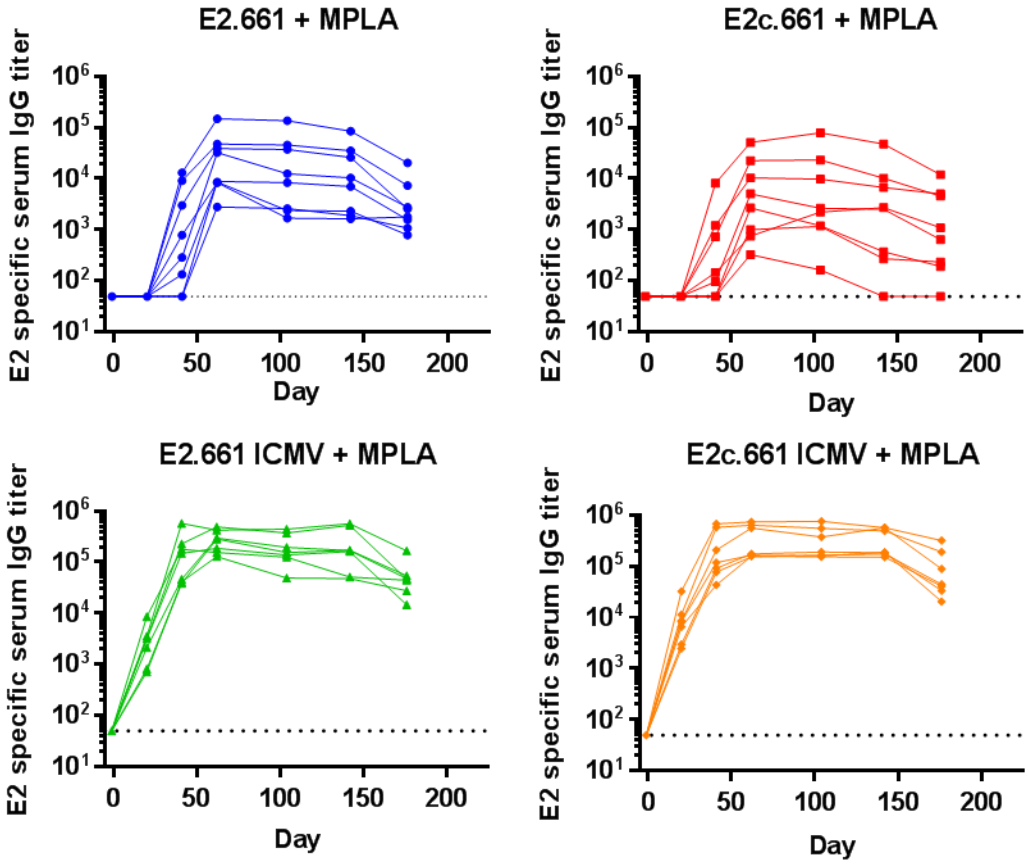

Figure 2-5. E2 specific serum IgG titers of individual mice. Endpoint serum antibody titers were determined by calculating the highest serum dilution that produced an absorbance signal 3-fold above background.

Epitope recognition of immune serum.

Lastly, we evaluated the specificity of the serum antibodies against linear epitopes most affected by the recombinant alterations of E2, HVR1 and AS412 (the epitope of HCV1). Based on the neutralization data **(Figure 2-4C, D)**, we selected serum samples from day 104 to analyze IgG-binding against either peptide (**Figure 2-6**). As a control, day -1 collected serum samples were tested for antigen specificity, and no peptide-specific IgG were observed at any of the tested

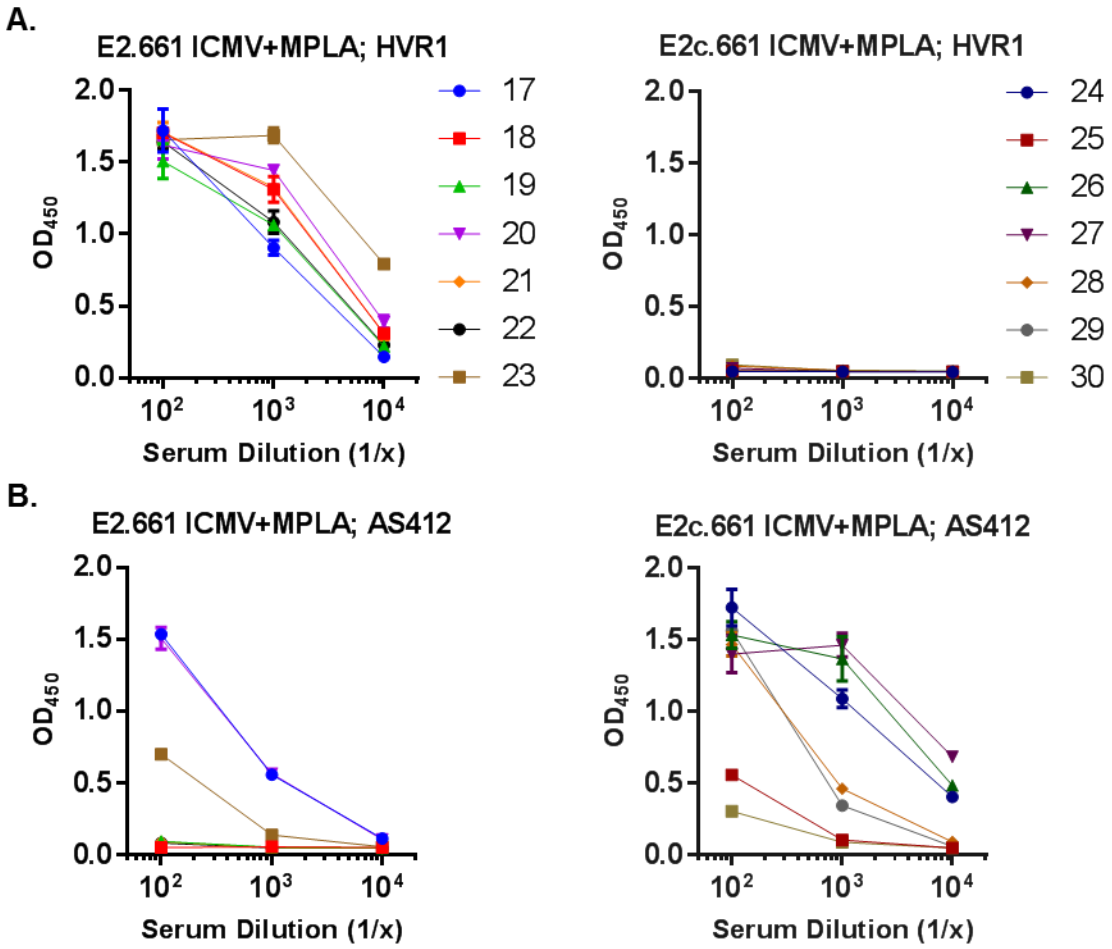

Figure 2-6. Specificity of immune sera to HVR1 and HCV1-epitope peptides. **A)** Optical densities (O.D) of log-fold serum samples after incubation on HVR1 coated ELISA plates. Shown are day 104 immune sera from mice vaccinated with E2.661 ICMVs and E2c.661 ICMVs. **B)** Optical densities of log-fold serum samples after incubation on ELISA plates coated with AS412 containing long peptide. Individual serum samples are color matched between **A)** and **B).**

dilutions **(Figure 2-7)**. On the other hand, all day 104 serum samples from the E2.661 ICMV + MPLA group bound to the HVR1 peptide **(Figure 2-6A)**. As expected, positive responses were absent from serum samples of the E2c.661 ICMV group since HVR1 is deleted in E2c.661 **(Figures 2-1A and 2-6A)**. However, removal of the highly antigenic HVR1 region appeared to increase antibody production to the adjacent HCV1 epitope region. All serum samples (7 of 7) from the E2c.661 ICMV group possessed HCV1 long-peptide targeting antibodies, compared to 3 of 7 samples from the E2.661 ICMV group **(Figure 2-6B)**. Interestingly, when we plotted the peptide binding ELISA data for HVR1 against the autologous HCVpp neutralization percentage, there was a positive correlation trend for E2.661 ICMV + MPLA (r = 0.58), and a negative trend

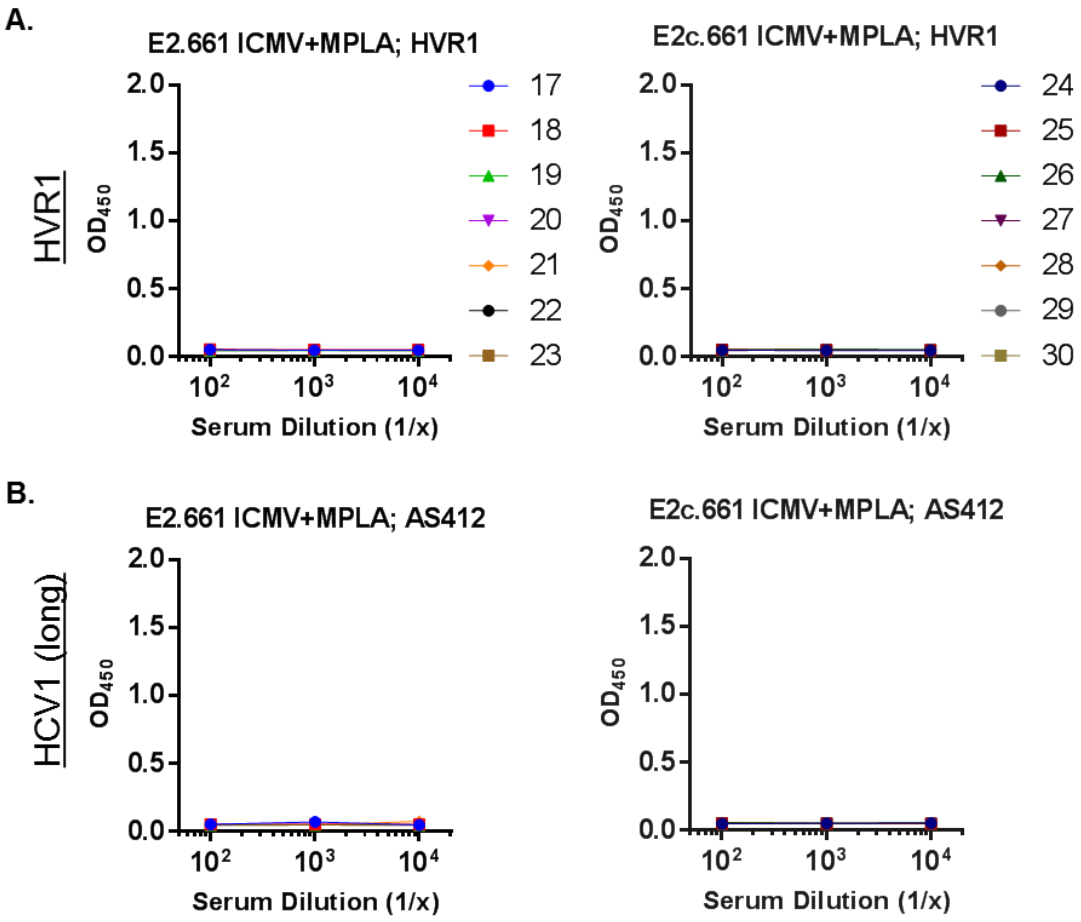

Figure 2-7. E2.661 ICMV and E2c.661 ICMV day -1 vaccination serum specificity to HVR1 and HCV1 peptides. **A)** Optical densities of log-fold serum samples after incubation with HVR1 coated ELISA plates. B) Optical densities of log-fold serum samples after incubation with HCV1 long peptide coated ELISA plates. Individual serum samples are color matched between A and B.

for the E2c.661 ICMV + MPLA samples (r = -0.06), suggesting a correlation between the presence of HVR1 and H77 neutralization **(Figure 2-8A)**. A similar analysis of the HCV1 long-peptide ELISA data compared to the corresponding heterologous neutralization demonstrated positive trends for both nanoparticle formulations, with the E2c.661 ICMV + MPLA group exhibiting a greater correlation between the two factors (r = 0.66), compared to the E2.661 ICMV + MPLA group (r = 0.32) **(Figure 2-8B)**. Taken together, these data suggest that the presence of HVR1 may have a positive effect on autologous neutralization, but may not be required. Additionally, antibody response to the HCV1 epitope region may positively impact heterologous neutralization, although other epitopes may also contribute.

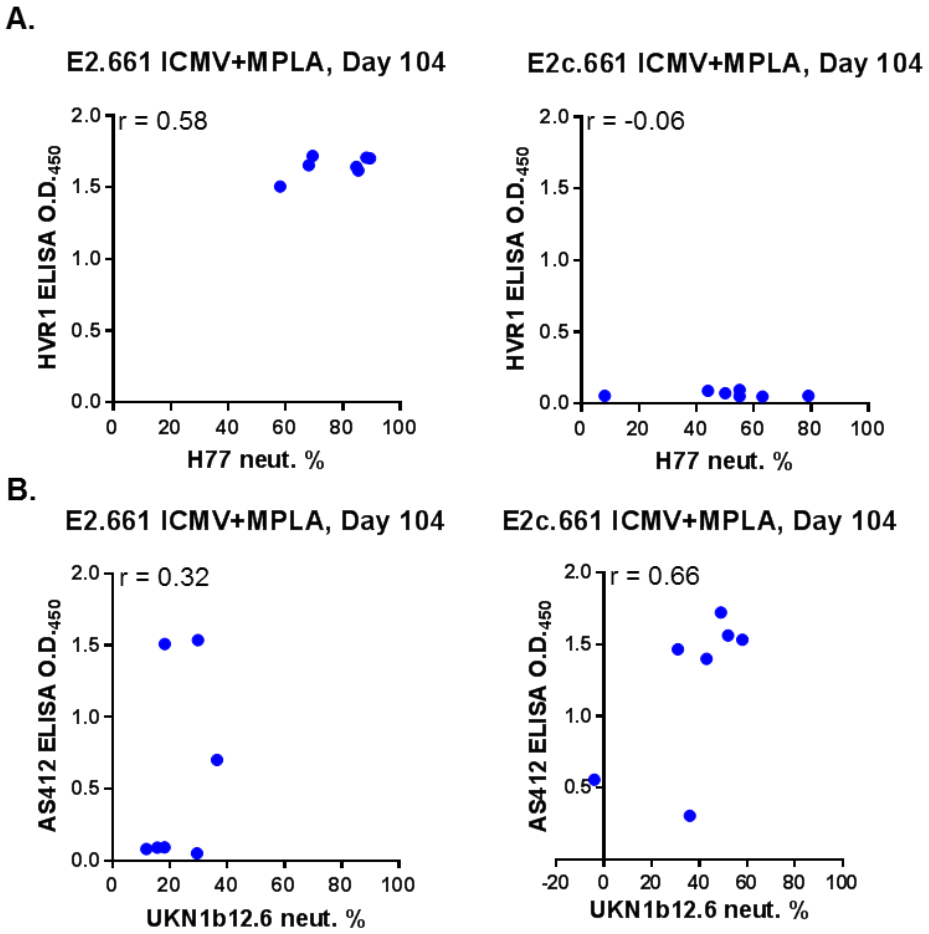

Figure 2-8. Correlation of day 104 peptide specific ELISA O.D. to *in vitro* neutralization. **A)** HVR1 ELISA O.D. values from 1:100 diluted serum plotted against *in vitro* neutralization percentage of H77 HCVpp. **B)** AS412 ELISA O.D. values from 1:100 diluted serum plotted against *in vitro* neutralization percentage of UKN1b12.6 HCVpp. Pearson correlation coefficient is indicated for each plot.

2.5 Discussion

We have developed ICMVs loaded with recombinant HCV E2 antigens and interrogated antigen display and orientation on the surfaces of ICMVs using both whole population- and single particle-based analyses of antibody-antigen interactions. Our work demonstrates that *in vitro* assessment of conformational antigen display on nanoparticles can aid in selection of vaccine formulations that may elicit broadly neutralizing antibody responses *in vivo*. In particular, antigen loaded ICMVs elicited greater E2-specific IgG titers with superior neutralizing capacities than their respective soluble controls **(Figure 2-4)**. When compared directly, immune sera from the E2.661 ICMV group displayed a selectivity for autologous neutralization, whereas, immune sera from the E2c.661 ICMV group exhibited both autologous and heterologous neutralization (**Figure 2-4C, D**). These data aligned with our *in vitro* analysis in which the broadly neutralizing antibody HCV1 bound with a greater extent to E2c.661 ICMVs **(Figure 2-3C, F)**, suggesting a contribution of the HCV1 epitope in generating heterologous neutralization. Detailed analysis of epitope recognition by immune sera revealed that all mice administered E2.661 ICMVs generated HVR1-specific antibodies, whereas only 3 of 7 mice elicited antibodies to the HCV1 epitope region (**Figure 2-6A, B**). In stark contrast, all mice administered with ICMVs carrying E2c.661 (HVR1 removed) skewed antibody responses to the HCV1 epitope region (**Figure 2-6B**). These data suggest the importance of screening for proper antigen display on nanoparticle vaccines, as different orientations may impact the breadth and potency of immune responses *in vivo*.

Our initial characterization of antigen loading and particle sizes showed comparable results for both E2.661 ICMVs and E2c.661 ICMVs **(Figure 2-1)**; however, these metrics do not provide insights on antigen conformation or orientation on nanoparticle surfaces. To evaluate these properties, we employed an indirect immunofluorescence staining assay using E2-specific

antibodies recognizing spatially distinct antigenic sites **(Figure 2-3)**. Additionally, we examined the homogeneity of antigen display by comparing a microplate-based analysis of bulk samples to a flow-based analysis of individual nanoparticles **(Figure 2-3A)**. Notably, while the microplate-based assay showed similar binding for all but one of the E2-recognizing antibodies (**Figure 2-3C**), analysis of individual nanoparticles by NanoFACS revealed significantly enhanced binding of AR1B, AR2A, and HCV1 antibodies on E2c.661 ICMVs, in comparison to E2.661 ICMVs **(Figure 2-3F)**. This discrepancy highlights a limitation of the population-based assessment of the vaccine nanoparticles. As antigen-displaying nanoparticles may aggregate with incubation of antibodies during the immunofluorescence staining process, a more sensitive approach, such as NanoFACS, is needed to probe antigen display on individual nanoparticles.

The *in vitro* antibody binding profiles **(Figure 2-3C, F)** allowed us to hypothesize on how the antigen constructs are presented on ICMV surfaces. Most apparent is the difference in AR3A and HCV1 binding, both of which recognize epitopes on the neutralizing face of E2. AR3A signals were the lowest of all antigen-specific antibodies, despite its high affinity, suggesting that this epitope may be partially occluded or in an unfavorable position for AR3A recognition. The orientation of the E2 constructs was likely influenced by either 1) the presence of free thiols which could bind with maleimides present on the lipid bilayers, or 2) electrostatic interactions with the ICMV surface. Initially we suspected that the sole free cysteine (C652) of the antigens [94, 104] reacted with MPB on ICMV surfaces and anchor the antigen to the nanoparticle. However, the C652 residue is located on an exposed stretch of amino acids near the C terminus (back layer) which is on the opposite face of the CD81bs.[94] In this presentation, where the back layer interacts with the ICMV surface, the CD81bs would likely be presented outwardly on ICMVs and should not inhibit AR3A binding. Furthermore, the back layer contains the AR2A epitope,[105] which was

readily bound by AR2A **(Figure 2-3C, F)**, suggesting the back layer is not in contact with the ICMV surface. Alternatively, a region of basic amino acids is present on the E2 core near the neutralizing face and in the vicinity of the flexible VR2 region.[94, 105, 106] If these basic residues interacted with the anionic surface of ICMVs, then the neutralizing face would likely not be presented outwardly and may be in a position that affects antibody binding. Previous research indicates the VR2 region is disordered and flexible,[94, 105] suggesting some exposure of the basic region is possible on E2.661. Similarly, the removal of VR2 in E2c.661 can greatly expose this basic region to interface with ICMVs, and in tandem with the lack of VR2 may alter the orientation of the antigen.[94]

The presentation of antigens on ICMVs was a major aspect of this work, focusing on both the orientation on ICMVs and the conformation of neutralizing epitopes. For the later aspect, our data indicate that neither the mechanical nor chemical (i.e. DTT) stresses of ICMV synthesis affected the three antigenic sites of E2 **(Figure 2-3C, F)**. In particular, we were concerned with the reduction of disulfide bonds by the crosslinking agent DTT (a mild reducing agent), which is typically detrimental to the structure and function of proteins. Yet, Fenouillet et al. reported that partial reduction of an E2 fusion protein did not abolish binding to CD81, and, when administered to mice, increased vaccine antigenicity and the neutralization capacity of the immune serum.[107] In this study, the redox status of the antigens loaded into ICMVs was not assessed, but may have contributed to the observed increase in immune responses between ICMVs and the soluble control groups, suggesting a non-canonical role for partial reduction of antigens in vaccination strategies.

While the results reported here are promising, the collected data was limited to two heterologous strains of HCV, one of which was the same genotype as the autologous strain. Additional research is needed to assess the breadth of the observed immunogenicity against the

other HCV genotypes, and to determine what properties of the antigen loaded ICMV can be used to enhance both the breadth and potency of immune responses.

2.6 Individual contributions

J. Bazzill, M. Law and J.J. Moon designed the experiments. J. Bazzill, L.J. Ochyl., E. Giang, and S. Castillo performed the experiments. J. Bazzill., E. Giang, M. Law and J.J. Moon analyzed the data and wrote the manuscript.

Chapter 3

Vaccine nanoparticles displaying recombinant Ebola virus glycoprotein for induction of potent antibody and polyfunctional T cell responses

3.1 Abstract

The 2014 outbreak of *Ebolavirus* (EBOV) in West Africa led to unprecedented cases of Ebola virus disease that resulted in ~11,000 deaths, and there is a recent outbreak in Congo as of the time of this writing. While several viral vector-based vaccine candidates have progressed to clinical trials for vaccination against EBOV, there are still concerns about their efficacy due to anti-vector immunity as well as their side effects, especially among infants and immunocompromised individuals. Here, we aimed to develop synthetic nanoparticles as a safe and highly immunogenic platform for vaccination against EBOV. Here, we report that a large recombinant EBOV GP (rGP) can be successfully incorporated into lipid-based nanoparticles, termed interbilayer-crosslinked multilamellar vesicles (ICMVs), while preserving its epitope configuration and orientation. Briefly, we encapsulated rGP in two different variants of ICMVs with or without nickel nitrilotriacetic acid (NTA)-functionalized lipids. The quaternary structure of rGP was properly maintained on the surfaces of both formulations of ICMVs, and when administered together with monophosphoryl lipid A (MPLA, a Toll-like receptor-4 agonist) in

mice, both forms of rGP-ICMVs elicited potent humoral and cellular immune responses. Notably, the rGP-ICMV group without the NTA-lipids enhanced formation of germinal center (GC) B cells and polyfunctional T cells and elicited immune sera with improved neutralizing-capacity against rVSV-GP across the most dilutions. When mice were challenged with a lethal dose of murine adapted EBOV, 100% survival was observed by those vaccinated with nanoparticles as well as one soluble antigen group. This study suggests the potential of vaccine nanoparticles as a safe and immunogenic platform for configurational, multivalent display of large subunit antigens and elicitation of neutralizing antibody and polyfunctional T cell responses.

3.2 Introduction

Since the emergence of EBOV in 1976, approximately 13,000 lives have been lost to Ebola virus disease, with mortality rates of 25-90% among infected individuals. [108] The 2014 outbreak of EBOV in West Africa led to unprecedented cases of Ebola virus disease (EVD) resulting in ~11,000 deaths, approximately 7-fold greater than all previous incidents combined [108]. This outbreak also marked the first inter-continental cases of EVD, prompting a worldwide response to the endemic. Therefore, there is an urgent need to develop an effective vaccine against EBOV.

To that end, several vaccine candidates for EBOV have progressed to clinical trials, most of which are so far based on recombinant viral constructs expressing the EBOV envelope glycoprotein (GP). As the only surface-expressed EBOV antigen, GP is naturally presented as a trimer with an apparent fully glycosylated molecular weight of ~670 kDa and contains motifs for both target cell binding and viral membrane fusion making it a valuable target to inhibit EBOV infection [28, 109, 110]. While the recombinant vesicular stomatitis virus vaccine candidate (rVSV-

EBOV) has been shown to induce potent immune responses after a single dose in clinical trials, numerous side effects have been reported among healthy adults, including acute arthritis and skin lesions [32-34]. Additionally, the potential for toxic side effects in infants and immunocompromised individuals remain as major concerns [32]. Alternatively, non-replicating recombinant adenovirus vectors co-expressing GP are a safer alternative, but issues with potency require booster vaccinations, and in many cases pre-existing or post exposure anti-vector immunity may affect vaccine efficacy [35, 36].

In contrast, EBOV subunit vaccines may offer a safer alternative while maximizing immune responses at the antigen of interest, and a resurgence of EBOV subunit vaccines have been reported, many of which utilize non-mammalian cells and/or fusion proteins to enhance GP production and purification [111-114]. However, subunit vaccines generally suffer from weak and transient immune responses, and to elicit potent immune responses, high antigen doses, multiple vaccinations, or formulation with adjuvants were required [111-113]. Additionally, off target effects from fusion proteins can substantially contribute to the antigenic responses, as observed by Rios-Huerta et al. [114]. Similarly, adjuvant incorporation and selection can produce varied results, as demonstrated by Kondoro et al., where protection in mice was induced using 100 µg doses sans adjuvant [115]. A follow up study in guinea pigs highlighted the variability in adjuvant selection in immunogenicity and protection [112]. Adjuvant incorporation is a common method to enhance overall immune response to vaccines, but for humoral responses specifically, vaccines are typically formulated with a multivalent antigen display. A recent report evaluated a solid-protein core nanoparticle, consisting only of multivalent displayed full length EBOV GP [116]. When administered to mice along with the adjuvant Matrix M, protective responses were observed in all mice two weeks after final vaccination.

Outside of DNA or RNA based vaccines, to the best of our knowledge there has been one previous instance where a synthetic nanoparticle was used for EBOV vaccination. In that research irradiated EBOV virions were encapsulated into liposomes and used to vaccinate mice with successful protection against challenge; however, later trials in non-human primates failed to protect from lethal viral challenge [117, 118]. While many laboratories, including ours, have focused on engineering vaccine delivery platforms that can improve immunogenicity of subunit antigens [116-120], it remains unclear how *in vivo* performance of subunit vaccination is dictated by configurational orientation of antigens and their multivalent display on vaccine delivery vehicles, especially for large subunit antigens as in the case of the EBOV GP trimer. Our goals for this project were to develop synthetic nanoparticles as a safe and highly immunogenic platform for vaccination against EBOV and to examine how antigen orientation impacts T cell and B cell immune responses *in vivo*. We have previously reported the development of lipid-based nanoparticles, called interbilayer-crosslinked multilamellar vesicles (ICMVs) [76]. We have shown that ICMVs can elicit potent T cell and B cell immune responses with a variety of antigens, including peptides and recombinant proteins [73, 76, 121]. While the potential of ICMVs to display a large recombinant HIV Env protein has been recently demonstrated using chemical fixation or post-modification of particles with Env protein [77], it remains to be seen how to preserve the epitope configuration and orientation of large recombinant proteins while maintaining their immunogenicity *in vivo*.

Here, we report that a recombinant EBOV GP (rGP) with minimal recombinant alterations and no chemical cross-linking can be successfully incorporated into ICMVs while preserving its epitope configuration and orientation. Specifically, we tested rGP encapsulated in two different ICMV variants, either the traditional ICMVs or ICMVs containing nickel nitrilotriacetic acid-

functionalized lipids (NTA ICMVs). Introduction of NTA-lipid is thought to allow binding of poly-histidine tagged rGP on the surfaces of NTA ICMVs. We then performed detailed immunofluorescence analyses with monoclonal antibodies specific for linear and configurational rGP epitopes on a population and single nanoparticle level. Our results indicated that the quaternary structure of rGP was properly maintained on the surfaces of both nanoparticle formulations. Mice vaccinated with both forms of rGP nanoparticles carrying an immunostimulatory adjuvant, MPLA (a Toll-like receptor-4 agonist) increased humoral and cellular immune responses, compared with the soluble control. In particular, the rGP ICMV + MPLA group induced formation of germinal center B cells and polyfunctional T cells and generated immune sera with enhanced neutralizing-capacity

3.3 Materials and Methods

Animals.

Female 8-12-weeks-old C57BL/6 mice were obtained from Charles River. Research was conducted under an IACUC approved protocol in compliance with the Animal Welfare Act, PHS Policy, and other Federal statutes and regulations. The United States Army Medical Research Institute of Infectious Diseases (USAMRIID) IACUC committee approved this protocol, and experiments were conducted at an Association for Assessment and Accreditation of Laboratory Animal Care, International accredited facility. Animal status following viral infection was evaluated according to an Intervention Scoresheet approved by USAMRIID IACUC. Animals were monitored at least once daily and increased to at least two times daily at the onset of disease.

Euthanasia was performed by CO2 inhalation followed by confirmatory cervical dislocation. All surviving animals were euthanized on day 14 post infection.

Vaccinations and Viral Infections.

Mice were prime-boost vaccinated at a three-week interval using bi-lateral subcutaneous injections at the tail base. Antigen and adjuvant amounts were administered at 3 μg and 2.5 μg, respectively, for both vaccinations. Four weeks post final vaccination mice were inoculated by intraperitoneal injection with a target dose of 1,000 plaque forming units (p.f.u.) of mouse-adapted Ebola virus/H.sapiens-tc/COD/1976/Yambuku-Mayinga (Ma-EBOV) in biosafety level 4 containment. Clinical observations were recorded starting after virus inoculation. Moribund mice were euthanized based on institution-approved clinical scoring.

Protein production and purification.

Recombinant Ebola virus glycoprotein (rGP) was constructed starting from a full-length EBOV Mayinga (GenBank) GP coding sequence. To generate a soluble variant of EBOV GP, the transmembrane (TM) domain (amino acids 651-676) was deleted and replaced with a 6-histidine protein purification tag. The resulting coding sequence was cloned into the pDisplay mammalian expression vector (Thermo), and transfected into human embryonic kidney suspension cell-line 293E (Thermo) using lipofectamine 3000 (Life Technologies) following manufacturer's recommended protocols. Cell supernatants were harvested after 72 hours of incubation at 37°C, and rGP was purified by affinity chromatography using a Nickel Sepharose High Performance column (GE Healthcare). Collected fractions were concentrated using Amicon Ultra filter with 50kDa cutoff (Millipore), and protein concentration was determined using Bradford assay and

quantitative ELISA. Molecular weight and epitope preservation were analyzed by SDS-PAGE and Western blot, respectively.

Interbilayer-crosslinked multilamellar vesicle synthesis and characterization.

ICMV formulations were synthesized similar to those reported previously, with some modifications [73, 76]. In brief, 1,2-dioleoyl-sn-glycero-3-phosphocholine (DOPC), 1,2-dioleoyl-sn-glycero-3-phosphoethanolamine-N-[4-(p-maleimidophenyl)butyramide] sodium salt (MPB), and 1,2-dioleoyl-sn-glycero-3-[(N-(5-amino-1-carboxypentyl)iminodiacetic acid)succinyl] nickel salt (DOGS NTA) (Avanti Polar Lipids), were mixed in either 50:50:0 or 48:50:2 molar ratios and dried to produce thin films. Hydration buffer containing rGP was added to the dried films and vortexed to produce large multilamellar vesicles (MLVs), and were probe tip sonicated (QSonica) at 40% amplitude for 5 minutes to produce unilamellar vesicles (ULVs). ICMVs were formed by adding CaCl2 and dithiothreitol (DTT) at working concentrations of 33mM and 1.24mM to ULV suspensions to induce nanoparticle fusion and crosslinking, respectively. ICMVs were centrifuged at 14,000 r.c.f. at 4 °C to remove unloaded rGP, washed with DNA grade water (Fisher), and suspended in 0.22 μm filtered PBS (Gibco).

ICMVs produced for immunostaining assays and NanoFACS analysis were produced as above with the addition of the lipophilic fluorophore 1,1'-Dioctadecyl-3,3,3',3'-Tetramethylindodicarbocyanine, 4-Chlorobenzenesulfonate Salt (DiD, Thermo Scientific) at less than 0.2 molar percent in dried films.

Monophosphoryl lipid A (MPLA) (Avanti Polar Lipids) was added to the initial phospholipid mixture for production of ICMVs for vaccination. MPLA retention was estimated using fluorescently labeled phospholipid 1,2-dioleoyl-sn-glycero-3-phosphoethanolamine-N-

(lissamine rhodamine B sulfonyl) (ammonium salt) (Liss-Rhod-PE, Avanti Polar lipids) as a surrogate marker. Briefly, Liss-Rhod-PE containing rGP MLV and ICMV formulations were produced and the fluorescence signal was measured at 560/593nm. Liss-Rhod-PE retention was determined as a percentage of ICMV fluorescence relative to the respective MLV, which was assumed to be fully retained. If necessary, additional MPLA (1 mg/mL in DMSO) was added for an injection amount of 2.5 µg MPLA. Unloaded ICMVs (vehicle control) were synthesized similarly to rGP ICMVs + MPLA, but with a working concentration of 2.46 mM DTT, and formulated for injection the same as the rGP ICMV + MPLA group.

Antigen loading was assessed by poly-acrylamide gel electrophoresis under non-reducing conditions (NR PAGE). Samples were prepared following manufacturer's instructions, loaded into Bolt 4-12% Bis-Tris Plus gels (Invitrogen), and ran for 35 minutes at 200V in MOPS running buffer (Novex). Protein content was assessed by Coomassie Brilliant Blue R-250 staining (Fisher), imaged with FluorChem M (Protein Simple), and quantified using ImageJ software.

Samples were prepared and ran on NativePAGE™ Novex® Bis-Tris gel system (Life Technologies) following manufacturer's protocols. Briefly, samples were diluted in Native PAGE sample buffer, bath sonicated to disrupt aggregates, and incubated with N-Dodecyl β-D-maltoside (DDM, Invitrogen) at a 1.11% working concentration for 30 minutes on ice. Immediately before loading onto gels (3-12% Bis-Tris), G-250 was added to samples containing DDM following manufacturer's instructions. Samples that were not detergent incubated were prepared in sample buffer and remained on ice until loaded. Gels ran at room temperature using dark blue cathode buffer for approximately 100 minutes. Gels were destained according to manufacturer's instructions, and protein migration was assessed by silver staining (Thermo Fisher).

Mass Spectrometry analysis.

LC-HRMS analysis of rGP content in the *in vivo* vaccine formulations was performed similarly as described previously [122]. Briefly, formulation aliquots were digested with trypsin/lys-C (Promega) in the presence of Protease Max™ (Promega). Prior to LC-HRMS injection the samples were combined with isotopically labelled AQUA Ultimate™ (Thermo Fisher) peptides as internal standards, and comprised of two GP-specific peptides as both fully cleaved and missed cleavage variants. The spiked samples were ran on an Ultimate 3000 HPLC (Thermo Fisher) with downstream Orbtrap Elite MS/MS (Thermo Fisher). The extracted ion chromatograms were obtained by XCalibur 2.0 (Thermo), and standard curves were generated after normalizing the heavy AQUA peptides to their light counterparts derived from the vaccine formulations. The rGP content was back calculated to determine the rGP content in the dosing formulations, production batches, and the nanoparticle loading efficiency. Particle diameter and zeta potential were measured by dynamic light scattering (DLS) using a Malvern ZetaSizer Nano ZSP. Samples were diluted in 0.22 μm filtered diluent for DLS analysis, recollected, and diluted further for individual particle sizing by nanoparticle tracking analysis via a NanoSight NS300 instrument (Malvern). Samples were diluted in DNA grade water for size determination, and in PBS for measuring zeta potentials.

Immunofluorescence stained nanoparticles were prepared by incubating equal volumes of ICMVs overnight at 4 °C in 0.04 mg/mL antigen specific primary monoclonal antibodies 6D8 or 13C6 (USAMRIID), or mouse IgG_1, κ isotype (BP Pharmingen) in FACS buffer (1% BSA in PBS), or in FACS buffer alone. Samples were washed by centrifuging at 20,817 r.c.f. for 45 minutes at 4 °C, discarding the supernatant, and suspending the pellets in FACS buffer. The wash step was repeated prior to incubation in 100 μL F(ab')2 α-mouse IgG-PE secondary antibody

(eBioscience) for one hour at room temperature. Unbound secondary antibody was removed by washing and the particles were plated, and fluorescence signal was measured at 488/578 and 644/670 nm for PE and DiD, respectively. After immunostaining assay, samples were transferred to FACS tubes, and analyzed on a Beckman Coulter MoFlo Astrios with M1 and M2 masks. NanoFACS data was analyzed via FloJo software.

Enzyme-linked Immunosorbent Assays.

Blood was collected into MiniCollect serum tubes (GBO) at day 35 via submandibular route, and recovered serum was stored at -80^{o}C until use. Serial serum dilutions were added to plates coated with 2 μg/ml rGP starting at 1:10 dilution for IgM or 1:100 dilution for IgG and subclasses and incubated for 1 hour at room temperature. Plates were then washed three times with PBS-T, and secondary antibody was incubated for 1 hr at a final concentration of 0.6 μg/ml. Secondary antibodies included goat anti-mouse IgG-HRP (Southern Biotech 1030–05), IgG1-HRP (Southern Biotech 1070-05), IgG2c-HRP (Southern Biotech 1079–05), and IgM-HRP (1030-05). Plates were subsequently washed three times with PBS-T, developed using Sure Blue TMB 1-component substrate and stop solutions (KPL) and optical density (O.D.) read at 450 nm on a SpectraMax M5 (Molecular Devices). Serum from unvaccinated animals was used to establish background. Pooled convalescent serum from previous EBOV vaccine studies was included in each assay as a positive control. End-point titers were defined as the background plus 0.2. O.D.

Germinal Center B-cell Analysis.

Ten days after the second vaccination the draining lymph nodes were harvested for B cell assays. Single-cell suspensions of draining lymph nodes were washed with FACS buffer (PBS, 0.5% BSA and 2 mM EDTA) and counter-stained. B cell staining included B220 (BD Clone RA3-

6B2), CD95 (Company?), CD138 (BD Clone 281-2), and T & B Cell Activation Antigen (BD Clone GL-7). All samples were Fc-blocked (anti- CD16/CD32, BD), and stained to evaluate viability (live/dead aqua, Invitrogen) prior to counterstaining. Samples were run on a BD FACS Canto II and analyzed using FlowJo.

Antigen specific T and B cell ELISpot Assays.

ELISpot plates were coated overnight with either IFNγ capture antibody (clone AN18) or rGP. Plates were washed and blocked per manufacturer's instructions. Splenocytes were isolated from vaccinated animals and red blood cells were lysed (Lonza). For T cell assays, splenocytes were suspended in complete medium (RPMI with 20 U/mL mouse recombinant IL2 (Life Technologies), 2 μg/mL mouse CD49d (BD), and 2 μg/mL mouse CD28 (BD)), and was plated at $2.5x10^5$ cells/well. To each well an additional 100 μL of complete media with either 4 μg/mL EBOV GP-specific peptide (WIPYFGPAAEGIYTE, Mimotopes), 4 μg/mL DMSO (Sigma) for negative controls, or 4 μg/mL cell stimulation cocktail (eBiosciences) for positive controls was added. For B cell assays, 100 uL aliquots of splenocyte suspensions in complete medium were directly seeded at $2.5x10^5$ cells/well into rGP coated ELISpot plates. Cells were then incubated for 16 h at 37°C prior to development per the manufacturer's instructions. All ELISpot plates were analyzed using a CTL ImmunoSpot instrument (Cellular Technology Limited).

Intracellular Cytokine T cell Assays.

Following red blood cell lysis, splenocytes were cultured at 10^6 cells/mL in complete media (90% RPMI 1640, 10% FBS, 20 mM Hepes, 1% Pen/strep, 0.05 mM BME) with 10 U/mL mouse recombinant IL2, 1 μg/mL mouse CD49d, 1 μg/mL mouse CD28, and 1X protein transport inhibitor cocktail (eBioscience). Cell suspensions were plated at 100 uL/well and stimulated with

either cell stimulation cocktail (eBioscience), DMSO, or EBOV GP-specific peptide WE15 at 2 μg/mL. Cells were stimulated for five hours then washed in PBS + 10% FBS. Live/Dead Aqua (Life Technologies) was used to detect viable cells by incubation for 10 min at 4°C; Fc Block (Miltenyi) was used to prevent non-specific antibody binding. After washing, surface antibodies CD3-V450 (BD), CD8-APC-H7 (BD), and CD4-FITC (BD) were incubated with samples for 20 min at 4°C. Cells were washed and fixed with 3.7% paraformaldehyde overnight. Cells were permeabilized with perm/wash buffer (eBioscience) and stained with IFNγ-PE-Cy7 (BD), IL2-APC (BD), and TNFα-PE (BD) antibodies. Samples were run on a BD FACSCanto II and analysis was conducted using FlowJo software (Tree Star, Inc.).

Neutralization Assay.

Percent neutralization of serum antibodies was assessed by enhanced green fluorescent protein (eGFP) fluorescence of residually infected Freestyle™ 293-F cells (ThermoFisher). Briefly, recombinant vesicular stomatitis virus expressing both Ebola virus glycoprotein and eGFP (rVSV-GP) (a kind grift from Kartik Chandran, Albert Einstein College of Medicine) were incubated with serial dilutions of vaccination serum and 5% v/v guinea pig complement (Cedarlane Laboratories) for 1 hour at 37 °C. The rVSV-GP/serum mixtures were added to 100uL suspensions of Freestyle™ 293-F cells at a concentration of $1x10^6$ cells/mL and incubated for 18–20 hours at 37°C. Percentage of infection, i.e. eGFP expression, was measured using a BD FACSCanto II, and, neutralization was calculated by normalizing the infection percentages to the ICMV + MPLA control group.

Statistical Analysis.

Determination of statistical significance was performed using Prism 7.0.3. One-way or two-way ANOVA significance tests with Tukey's post-hoc multiple comparison test was used for group-wise analysis as indicated in the figure legends.

3.4 Results

Recombinant GP and nanoparticle design.

EBOV GP viral spike is displayed as a trimer of GP_1/GP_2 heterodimers embedded in the viral surface by a transmembrane domain (TM) of GP_2 (**Figure 3-1A**). EBOV rGP used for ICMV

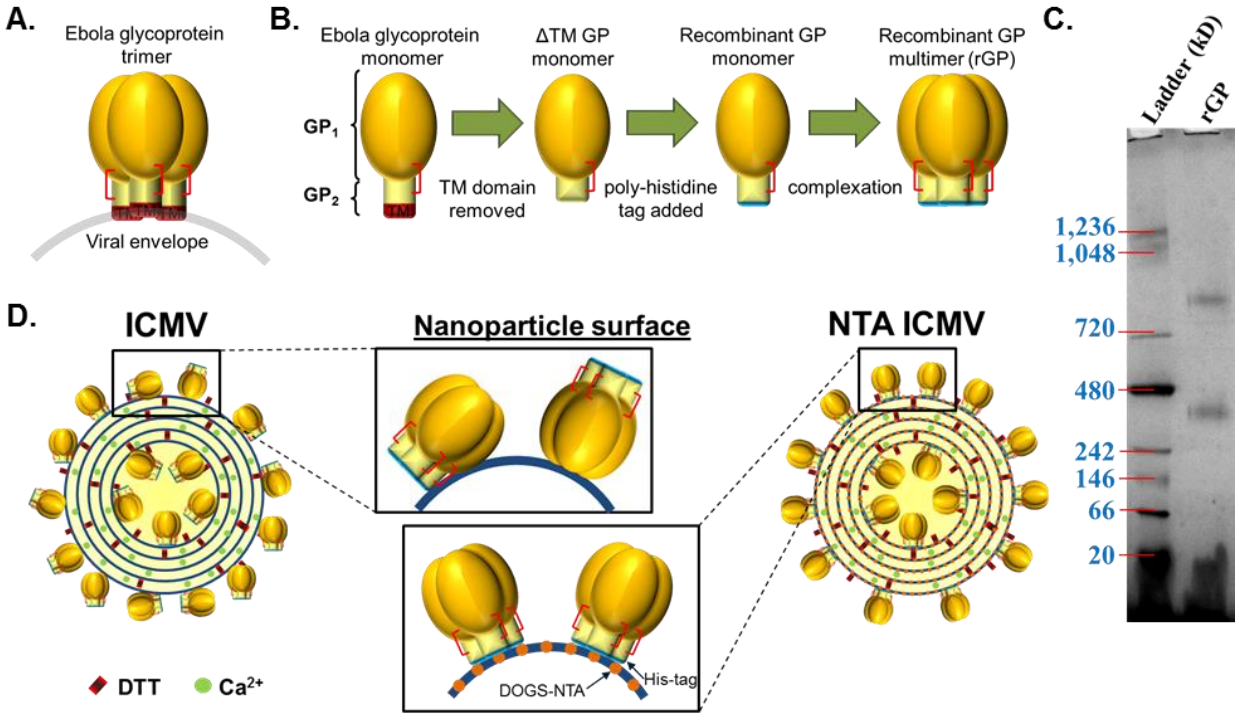

Figure 3-1. Antigen and nanoparticle design. (A) Illustration of ZEBOV envelope glycoprotein (GP) displayed on the viral envelope as a native trimer (red brackets indicate the GP1/GP2 disulfide bond). (B) Illustration recombinant modifications to produce rGP (TM, transmembrane domain). (C) Blue Native PAGE of rGP followed by Coomassie staining. (D) Diagram of expected rGP display on an ICMV or NTA ICMV (DTT, dithiolthreitol).

formulations was modified to generate a soluble form by removal of the transmembrane domain (TM) from the C terminus of GP_2 (**Figure 3-1B**). Additionally, a polyhistidine-tag (his-tag) was inserted at the C terminus of truncated GP_2 for purification, and the resulting antigen appears as two bands around 400 kDa and 800 kDa when migrated on non-denaturing and non-reducing Blue Native PAGE (**Figure 3-1C**). Production of ICMVs with rGP can lead to uncontrolled display of antigen, likely dictated by electrostatic interactions or free sulfhydryl groups (**Figure 3-1D**). On the other hand, we hypothesized that NTA ICMVs can selectively bind his-tags, thus allowing for concerted display of rGP.

Preservation of rGP in ICMVs.

ICMV synthesis may affect the tertiary and quaternary structure of rGP. Specifically, preservation of the GP_1/GP_2 disulfide bond is necessary to retain the protein complex and its immunogenic epitopes. We initially produced rGP ICMV formulations using the standard synthesis method with 2.46 mM of DTT used as a crosslinker of the opposing lipid layers within ICMVs, but this resulted in reduction of the GP_1/GP_2 disulfide bond (data not shown). We titrated down the concentration of DTT to 1.24 mM in order to remove excess thiols not required for interbilayer crosslinking. This led to preservation of the GP_1/GP_2 disulfide bond as demonstrated by NR-PAGE (**Figure 3-2A**). rGP formulated into either ICMVs or NTA ICMVs migrated at molecular weights similar to the original stock rGP without any fragmentation or reduction. In contrast, fully reduced rGP dissociated as separate GP_1 and GP_2 fragments (far right lane in **Figure 3-2A**).

We assessed whether the quaternary structure of rGP was maintained during the ICMV formulation by Blue Native PAGE. To analyze individual rGP complexes, we disrupted the ICMV formulations using a mild detergent, dodecyl β-D-maltoside (DDM). rGP from both traditional

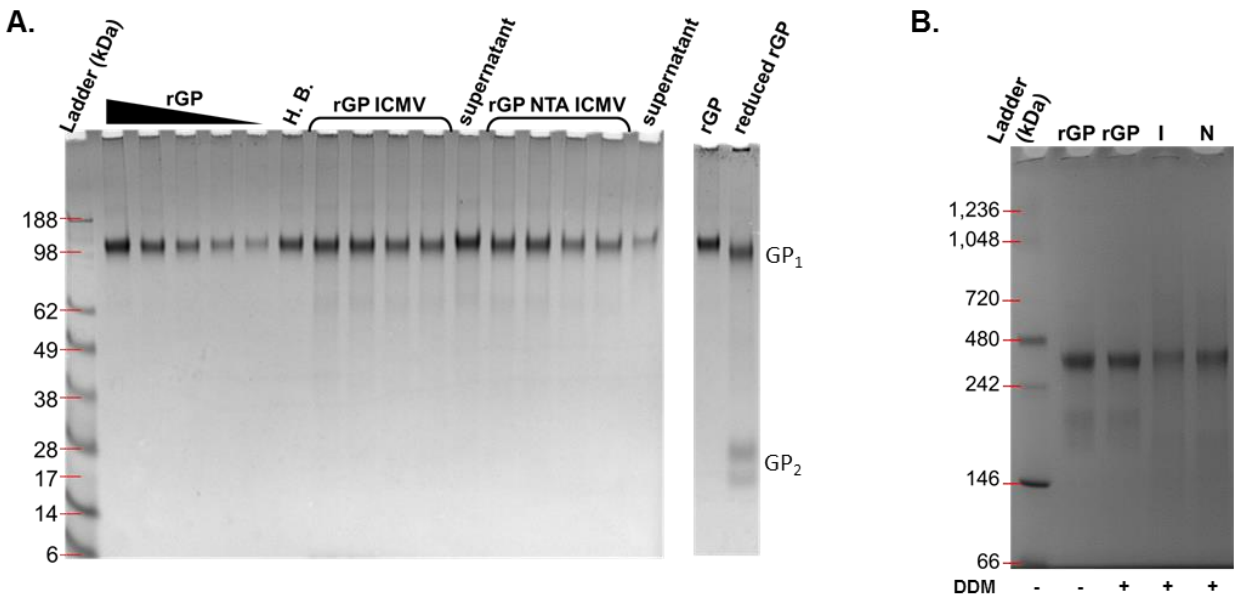

Figure 3-2. Preservation of rGP incorporated into ICMVs. (A) Non-reducing PAGE of rGP containing ICMVs and NTA ICMVs. Far right lane containing reduced rGP shows bands of GP1 and GP2. (B) BN PAGE of rGP, rGP ICMVs (I), and rGP NTA ICMVs (N). Samples incubated with DDM are indicated.

ICMVs or NTA-linked ICMVs appeared primarily around 400 kDa (**Figure 3-2B**). Interestingly, soluble rGP incubated with or without DDM had 400 kDa MW bands as well as prominent bands at lower MW, which were absent in the lanes for rGP ICMVs or rGP NTA ICMVs (**Figure 3-2B**). These results indicated that rGP was stably loaded in ICMVs and NTA ICMVs without any significant fragmentation or dissociation of the GP_1/GP_2 heterodimer.

Loading of rGP in ICMVs.

We tested the effect of the initial protein loading amount and the addition of DOGS-NTA on the loading efficiency of the EBOV rGP in ICMV formulations. Batches of ICMVs and NTA ICMVs were produced using 20 µg or 40 µg rGP, and incorporation of antigen was determined by NR-PAGE (**Figure 3-1 and Table 3-1**). While doubling the initial loading amount of rGP did not significantly alter the loading efficiencies (17.2 ± 8.4% and 15.0 ± 6.5% for ICMVs, and 26.1 ± 6.8% and 32.8 ± 5.1% for NTA ICMVs), the total amount of rGP incorporated into a batch of

	n	Loading Efficiency (%)	rGP per batch (µg)
20µg rGP ICMV	3	17.2 ± 8.4	3.4 ± 1.7
40µg rGP ICMV	5	15.0 ± 6.5	6.0 ± 2.6
20µg rGP NTA ICMV	4	26.1 ± 6.8	5.2 ± 1.4
40µg rGP NTA ICMV	4	32.8 ± 5.1	13.1 ± 2.1

n.s., n.s., n.s., **, n.s., ***, ***, **

Table 3-1. Antigen loading of rGP nanoparticles. Loading efficiencies are reported as percent of initial rGP used for production. Measurements reported as sample mean ± standard deviation. Statistical analysis performed by two-way ANOVA followed by Tukey's multiple comparisons test. n.s. (not significant), *p<0.05, **p<0.01, ***p<0.001.

ICMVs and NTA ICMVs increased by ~1.8 fold and ~2.5 fold, respectively **(Table 3-1)**. Addition of DOGS-NTA to ICMVs contributed to the loading efficiency and mass content, increasing either by ~1.5 and ~2.2-fold for particles produced with 20 µg and 40 µg rGP, respectively; however, the increase was only statistically significant for particle produced with 40 µg rGP ($p < 0.001$). Based on the increased antigen content, ICMVs and NTA ICMVs produced with 40 µg rGP were selected for further *in vitro* characterization and *in vivo* immunogenicity studies.

Characterization of ICMVs.

We utilized dynamic light scattering (DLS) to examine the size, zeta potential, and unilamellar vesicle (ULV) properties of traditional ICMVs or NTA ICMVs loaded with rGP. The average diameter of ULVs and NTA ULVs were 63.4 ± 6.9 nm and 57.9 ± 1.4 nm, respectively, which increased approximately by 55 nm after processing them into respective ICMVs (117.2 ± 10.1 nm and 117.5 ± 17.6 nm), consistent with previous reports [76] (**Figure 3-3A**). Both ICMVs and NTA IMCVs exhibited homogenous particle sizes, as evidenced by average polydispersity indices of 0.17 ± 0.02 and 0.18 ± 0.01, respectively, along with negative zeta potentials (-22.3 ± 1.4 mV and -21.7 ± 1.3 mV, **Figure 3-3A, B**). Because DLS measures bulk samples and may generate data skewed towards larger particle sizes, we validated our results with individual particle-based nanoparticle tracking analysis. The data indicated that the size distribution of ULVs

and NTA ULVs as well as their respective ICMV formulations correlated well with the DLS results (**Figure 3-3A, C**).

A.

	Z Avg. size (nm)	Poly-dispersity Index	Zeta Potential (mV)	Avg. diameter by NTA (nm)
rGP ULV	63.4 ± 6.9	0.22 ± 0.11	-20.0	73.1 ± 16.1
rGP NTA ULV	57.9 ± 1.4	0.19 ± 0.02	-27.9	71.7 ± 20.5
rGP ICMV	117.2 ± 10.1	0.17 ± 0.02	-22.3 ± 1.4	109.5 ± 34.2
rGP NTA ICMV	117.5 ± 17.6	0.18 ± 0.01	-21.7± 1.3	118.0 ± 41.9

Measurements reported as sample mean ± standard deviation.

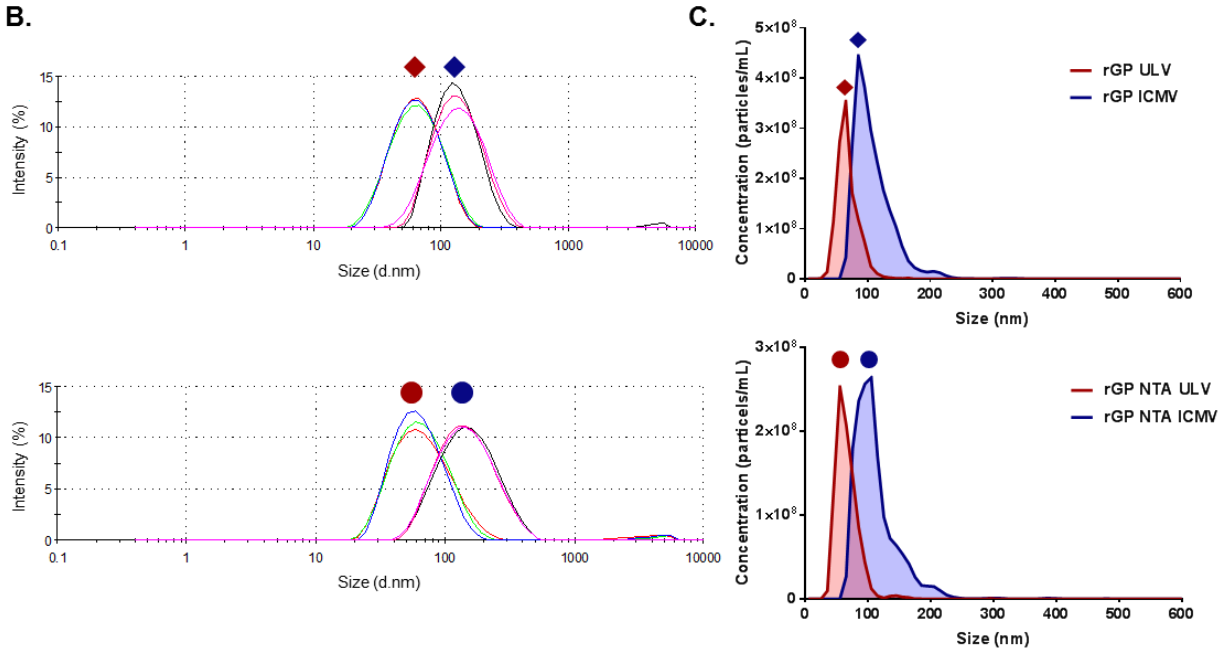

Figure 3-3. Size distributions of rGP ULV and ICMV formulations. (A) Table of intensity based nanoparticle sizes, and polydispersity indices and zeta potentials from Zetasizer measurements, along with number based nanoparticle diameters by nanoparticle tracking analysis. (B) Intensity based size distributions of antigen loaded ICMV formulations compared to respective ULVs. (C) Number based size distributions of antigen loaded ICMV formulations compared to respective ULVs.

Antigen conformation and display on nanoparticles.

Antigen loaded ICMVs and NTA ICMVs were evaluated by a plate-based indirect immunofluorescence staining assay [73] to examine display and preservation of rGP epitopes on the surfaces of nanoparticles. First, nanoparticle retention was determined by adding a trace amount of DiD, a lipophilic fluorophore, during the nanoparticle synthesis, followed by determining fluorescence signal of processed and unprocessed nanoparticles (**Figure 3-4A**). Processed ICMV and NTA ICMV samples exhibited an average retention of 44 ± 3% and 59 ± 2%, respectively, and similar retention rates were observed with or without the presence of antibodies.

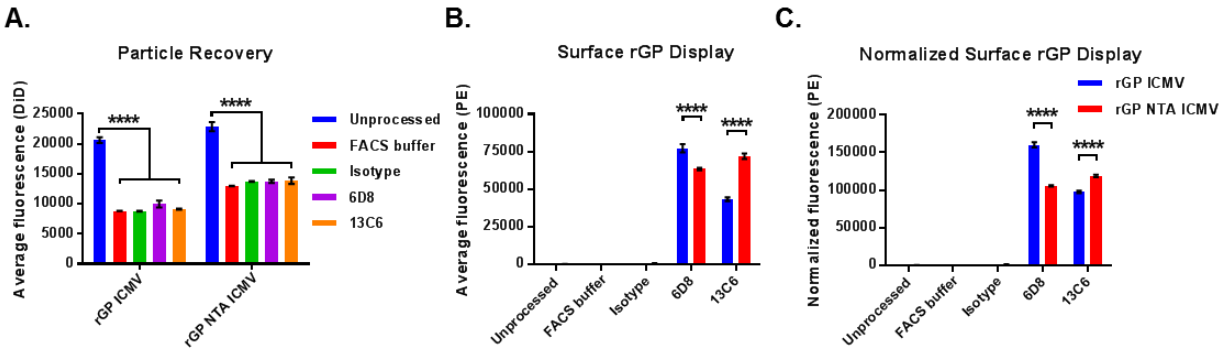

Figure 3-4. Bulk analysis of rGP display on nanoparticle surfaces. (A) Particle recovery after immunostaining process by retention of DiD signals in unprocessed and processed nanoparticles. (B) Fluorescence signals of PE-labeled secondary antibodies bound to nanoparticles incubated with the indicated primary antibodies. (C) Secondary antibody signals normalized to particle retention. (A-C) Measurements reported as mean ± SEM. Statistical analysis performed by two-way ANOVA followed by Tukey's multiple comparisons test. ***p<0.001.

We next evaluated ICMVs and NTA ICMVs for preservation of linear and conformational epitopes by indirect measurement of bound EBOV GP-specific mouse monoclonal IgG antibodies (mAb), 6D8 or 13C6 [26, 27], respectively. Signal cross-over of DiD and non-specific antibody binding produced nominal signals (FACS buffer and Isotype groups, respectively, **Figure 3-4B**). In contrast, we measured marked phycoerythrin (PE) signals from the linear and conformational antibody groups. Specifically, the PE signal associated with the linear antibody (6D8) was ~1.2-fold higher on ICMVs, compared with NTA ICMVs ($p < 0.0001$, **Figure 3-4B**). In contrast, the

fluorescence signal associated with the conformational antibody (13C6) was ~1.7-fold higher on NTA ICMVs than ICMVs ($p < 0.0001$, **Figure 3-4B**). The PE fluorescence signal normalized to the particle retention (as measured by the DiD recovery in **Figure 3-4A**) exhibited the similar trend of antibody binding (**Figure 3-4C**). The PE signal associated with 6D8 was ~1.5-fold higher on ICMVs than NTA ICMVs, while that for 13C6 was ~1.2-fold higher on NTA ICMVs than ICMVs ($p < 0.0001$, **Figure 3-4C**).

To further investigate display and preservation of rGP epitopes on a single particle level, we have adopted a flow cytometry-based assay that we termed NanoFACS [99-103]. Using this method, we were able to examine individual nanoparticle populations and quantify both DiD and PE fluorescence of each particle (**Figure 3-5A**). We first confirmed similar DiD content between

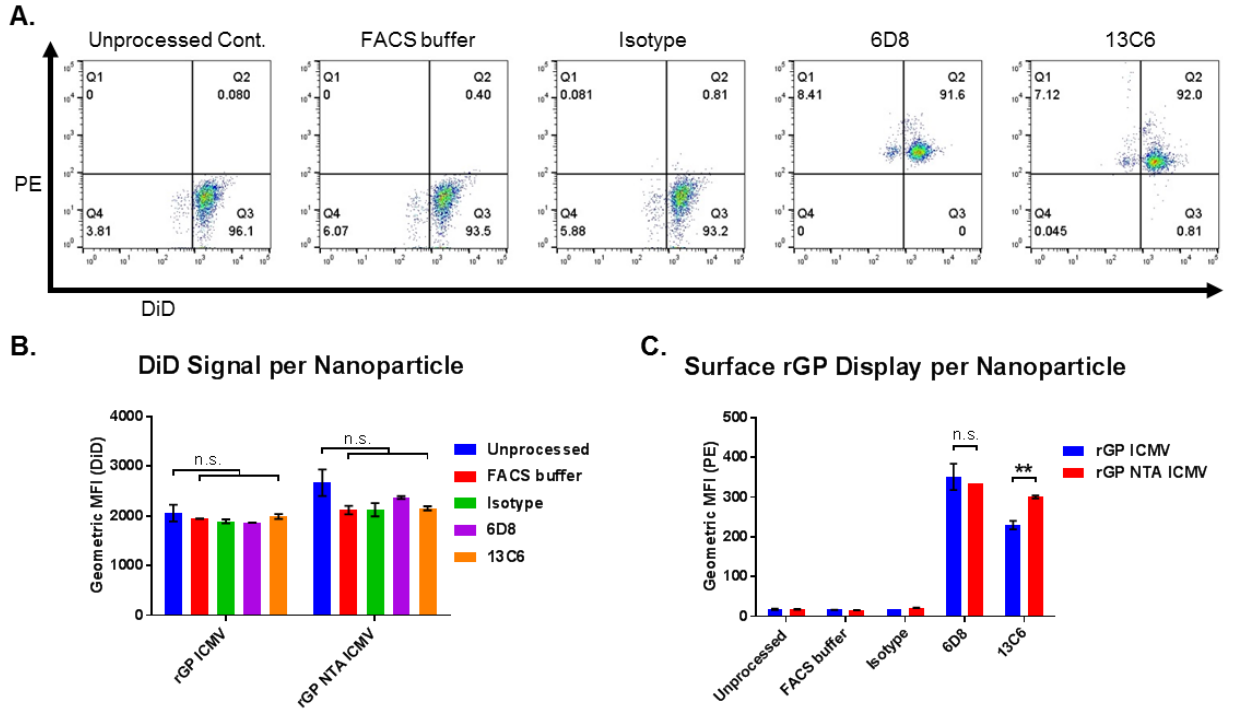

Figure 3-5. Display of rGP on single nanoparticles. (A) Representative flow cytometry plots of PE and DiD signals for immunostained rGP ICMVs. (B) DiD fluorescence of individual particles. (C) Fluorescence signal of PE-labeled secondary antibodies bound to single particles. (B-C) Measurements reported as geometric mean ± SEM. Statistical analysis performed by two-way ANOVA followed by Tukey's multiple comparisons test. n.s.>0.05, **p<0.01.

individual particles that were processed with different antibodies (**Figure 3-5B**). Interestingly, linear antibody binding was not significantly different between the two formulations; whereas, we observed ~1.3-fold higher binding of the conformational antibody to NTA ICMVs, compared with ICMVs ($p < 0.01$, **Figure 3-5C**).

In vivo vaccination.

We performed vaccination studies using EBOV rGP nanoparticle formulations incorporated with a potent adjuvant molecule, MPLA [73]. The addition of MPLA improved rGP encapsulation in ICMV and NTA ICMVs (**Table 3-2**). Mice were immunized subcutaneously on day 0 and day 21, and serum samples were collected on day 35 (**Figure 3-6A**). Analysis of immune sera with ELISA indicated that mice immunized with all vaccine formulations had low levels of anti-EBOV GP IgM by day 35 (**Figure 3-6B**). On the other hand, we observed ~5-log average anti-EBOV GP IgG end point titers for both nanoparticle groups and the soluble rGP group formulated with MPLA (rGP + MPLA) (**Figure 3-6C**). Analysis of the immune sera for anti-EBOV GP IgG1 and IgG2c subclasses demonstrated similar trends, with the addition of MPLA significantly boosting antibody responses (**Figure 3-6D, E**). In particular, mice vaccinated with rGP ICMV + MPLA had the highest anti-EBOV GP IgG1 and IgG2c titers, with 6.0-fold and 7.8-fold improvement, compared with the soluble rGP + MPLA control group ($p < 0.05$ and $p < 0.01$ for IgG1 and IgG2c titers, respectively, **Figure 3-6D, E**).

Formulation	PAGE based loading efficiency (%)	rGP per batch (µg)	Mass Spec. loading efficiency (%)	Mass Spec. rGP per batch (µg)
rGP ICMV + MPLA	27.7 ± 2.9	11.1 ± 1.2	28.5	11.4
rGP NTA ICMV + MPLA	56.5 ± 3.2	22.6 ± 1.3	58.6	23.4

Table 3-2. Incorporation of rGP in nanoparticle formulations used for vaccination. Loading efficiencies and mass content of rGP ICMVs and NTA ICMVs including MPLA during synthesis, as determined by NR SDS-PAGE and confirmed by mass spectrometry. Efficiencies are reported as percent of initial rGP used for production (40 µg). Measurements reported as mean ± standard deviation.

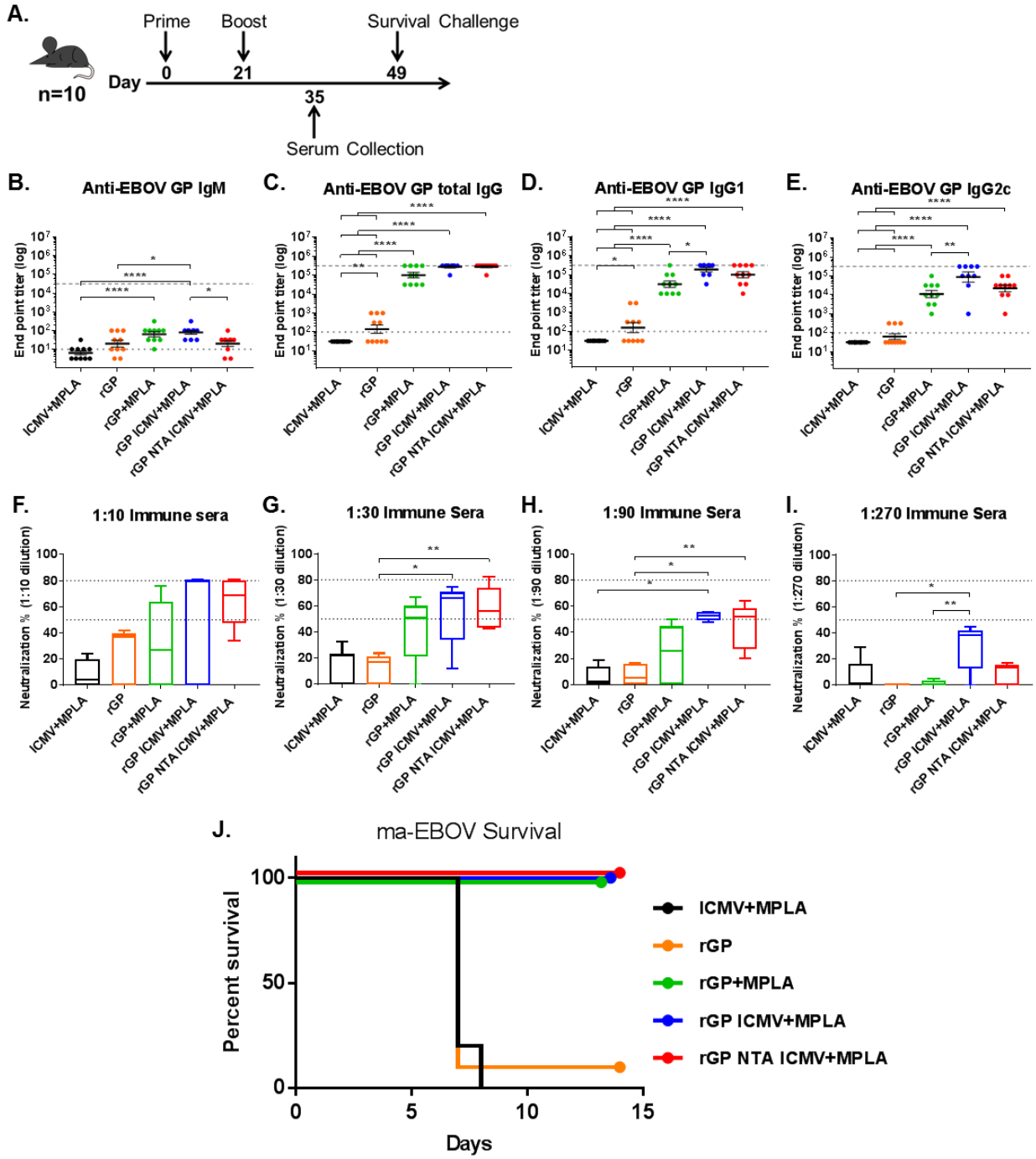
A.
Prime
Boost
Survival Challenge
n=10
Day
0
21
49
35
Serum Collection
B.
Anti-EBOV GP IgM
C.
Anti-EBOV GP total IgG
D.
Anti-EBOV GP IgG1
E.
Anti-EBOV GP IgG2c
End point titer (log)
ICMV+MPLA
rGP
rGP+MPLA
rGP ICMV+MPLA
rGP NTA ICMV+MPLA
F.
1:10 Immune sera
G.
1:30 Immune Sera
H.
1:90 Immune Sera
I.
1:270 Immune Sera
Neutralization % (1:10 dilution)
Neutralization % (1:30 dilution)
Neutralization % (1:90 dilution)
Neutralization % (1:270 dilution)
J.
ma-EBOV Survival
Percent survival
Days
ICMV+MPLA
rGP
rGP+MPLA
rGP ICMV+MPLA
rGP NTA ICMV+MPLA

Figure 3-6. Immunogenicity against rGP after *in vivo* vaccination. (A) Mice (n = 10/group) were vaccinated subcutaneously at the tail base with either Blank ICMV + MPLA, rGP, rGP + MPLA, rGP ICMV + MPLA, or rGP NTA ICMV + MPLA on day 0 and 21. Antigen and adjuvant doses were 3 μg rGP and 2.5 μg MPLA, respectively, for both injections. Serum was collected two weeks after final vaccination. (B-E) EBOV GP specific IgM, total IgG, IgG1, or IgG2c antibody responses were measured by ELISA. Dotted and dashed lines represent minimum and maximum dilutions tested, respectively. Measurements reported as geometric mean ± SEM. Non-seroconverted serum samples were assigned log-values of 0.5 (IgM) or 1.5 (IgG and subclasses) for graphical representation and statistical analysis. (F-I) Box and whisker plots of rVSV-GP neutralization by diluted serum from five randomly selected mice from each group. Percent neutralization was determined by residual infectivity of sample groups compared to naïve serum. (J) Survival curve of mice inoculated with 1000 p.f.u. of ma-EBOV on day 49. (B-I) Statistical analysis performed by one-way ANOVA followed by Tukey's multiple comparisons test. *p<0.05, **p<0.01, ***p<0.001, ****p<0.0001.

Antibody effector function was evaluated by a neutralization assay with hybrid VSV co-expressing GP and eGFP reporter protein (rVSV-GP, as described in the Supplementary Methods). Median neutralization values ranging 50-80% were observed with 10, 30, and 90-fold diluted sera from both antigen loaded ICMV formulations (**Figure 3-6F-I**). On the other hand, the median neutralization for the soluble rGP + MPLA group peaked at 51% at a 30-fold dilution and decreased to the basal level upon further dilution (**Figure 3-6F-I**). In particular, at 270-fold serum dilution, rGP + MPLA vaccine group lost the neutralizing activity; whereas, rGP ICMV + MPLA group still exhibited 38% neutralization ($p < 0.01$, **Figure 3-6I**).

Four weeks after the final vaccination, *in vivo* protection was evaluated in mice by monitoring survival after challenge with a lethal dose of murine adapted EBOV (ma-EBOV). All mice vaccinated with the vehicle control and 90% of those vaccinated with soluble antigen succumbed to infection 7-8 days after administration **(Figure 3-6J)**. In comparison, 100% survival was observed by mice immunized with either ICMV formulation, as well as the adjuvant soluble antigen group, indicating at least a month long durability in the induced immune responses.

Activation of adaptive immune cells.

To assess the cellular immune responses, mice were vaccinated as above, and secondary lymph organs were harvested 10 days after the final vaccination (**Figure 3-7A**). The frequency of EBOV GP-specific splenic B cells was quantified by an IgG ELISpot assay (**Figure 3-7B**). Significantly higher frequencies of antigen-specific B-cells were observed for the nanoparticle groups than either the soluble antigen or vehicle control groups (**Figure 3-7B**). The frequency of total and germinal center B cells in the draining lymph nodes were enumerated via flow cytometry analysis (**Figure 3-7C**). While total B cells numbers were similar between all groups (**Figure 3-7D**), the frequencies of germinal center B cells were significantly higher for both ICMV formulations, compared with the vehicle control or soluble antigen ($p < 0.05$, **Figure 3-7E**).

Though the role of T cell immune responses during EBOV infection remains elusive, cellular immunity is canonically induced during viral infections. Additionally, ICMVs have been previously reported to induce balanced Th_1/Th_2 immune responses [73, 76]. We evaluated the induction of EBOV-specific T cell responses using both ELISpot and intracellular cytokine staining (ICS)**.** ELISpot assay performed on splenocytes re-stimulated with a GP-specific peptide revealed that rGP ICMV + MPLA vaccine group generated 5.8-fold higher frequency of IFN-γ producing splenic T-cells, compared with the rGP + MPLA control group ($p < 0.05$, **Figure 3-8A**). In addition, there was a trend for an increased frequency of IFN-γ producing splenic T-cells for the rGP NTA ICMV + MPLA vaccine group, compared with the soluble rGP + MPLA control group (**Figure 3-8A**).

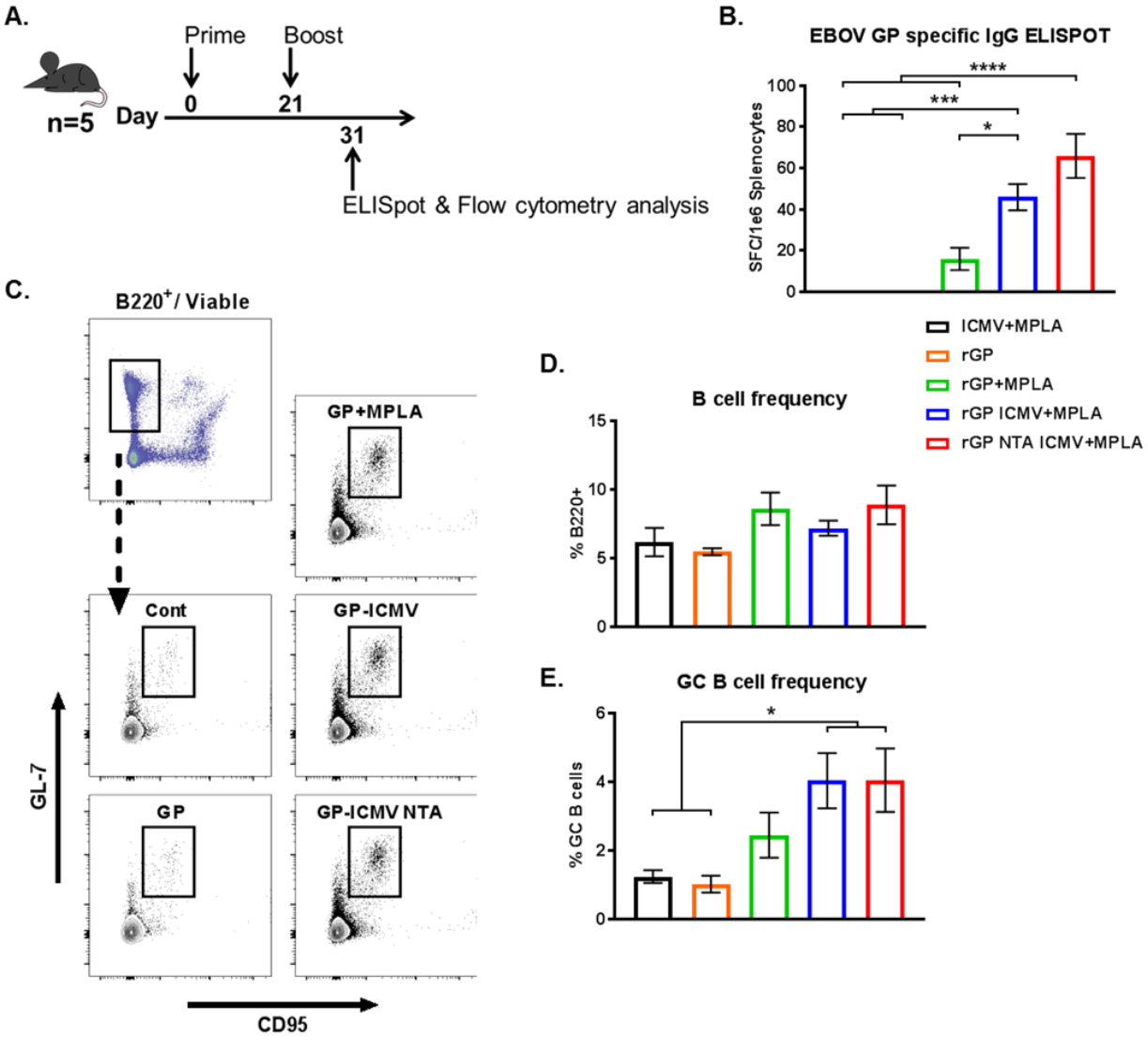

Figure 3-7. B cell activation and germinal center formation. (A) Mice (n = 5/group) were vaccinated subcutaneously at the tail base with either Blank ICMV + MPLA, rGP, rGP + MPLA, rGP ICMV + MPLA, or rGP NTA ICMV + MPLA on day 0 and 21. Antigen and adjuvant doses were 3 µg rGP and 2.5 µg MPLA, respectively, for both injections. Draining (inguinal) lymph nodes and spleens were harvested 10 days after final vaccination for ELISpot, intracellular cytokine staining (ICS), and germinal center (GC) analysis. (B) EBOV GP antigen-specific B cell frequencies from harvested spleens enumerated by ELISpot. (C) Representative flow cytometry gating of harvested B cells from draining lymph nodes of vaccinated mice. Total B cell frequencies were gated on viable/B220+ and GC B cells were additionally gated on GL-7+/CD95+. (D-E) Relative frequency of viable total B cells and GC B cells from draining lymph nodes. (B, D-E) Measurements reported as mean ± SEM. Statistical analysis performed by one-way ANOVA followed by Tukey's multiple comparisons test. *p<0.05, ***p<0.001, ****p<0.0001.

We also performed intracellular cytokine staining on splenic CD4+ and CD8+ T cells for production of IFN-γ, IL2, and TNF-α (**Figure 3-8B**). When the polyfunctional responses were parsed among the cytokine combinations, rGP ICMV + MPLA group induced the highest frequency of polyfunctional IFN-γ+/IL2+/TNF-α+ CD4+ T cells (**Figure 3-8C**), while there was a trend for increased frequencies of IFN-γ+/IL2+ and IFN-γ+/TNF-α+ CD4+ T cells for the rGP NTA ICMV + MPLA vaccine group (**Figure 3-8C**). The combined frequency of CD4+ T cells expressing at least two of the Th1-associated IFN-γ, IL2, and TNF-α cytokines were ~2-fold higher in animals vaccinated with rGP ICMV + MPLA, compared with the ICMV + MPLA control group ($p < 0.05$, **Figure 3-8D**). As for splenic CD8+ T cells, there was a trend for increased frequency of polyfunctional IFN-γ+/IL2+/TNF-α+/ CD8+ T cells for both rGP ICMV + MPLA and rGP NTA ICMV + MPLA vaccine groups (**Figure 3-8E, F**).

3.5 Discussion

Our main objective in this study was to assess the ability, feasibility, and immunogenicity of synthetic nanoparticles displaying a recombinant Ebola glycoprotein antigen. Optimization of the synthesis process included titration of ICMV components to preserve the inter-GP_1/GP_2 disulfide bond as well as the quaternary structure of rGP, which were confirmed by SDS and Blue Native PAGEs, respectively (**Figure 3-2**). Furthermore, two ICMV formulations loaded with rGP were characterized using antigen recognizing antibodies and shown to present rGP in a configurational manner with slight differences in epitope presentation. However, these differences did not substantially impact the *in vivo* immune responses of either formulation. When administered in mice, both formulations induced robust anti-EBOV GP-specific humoral

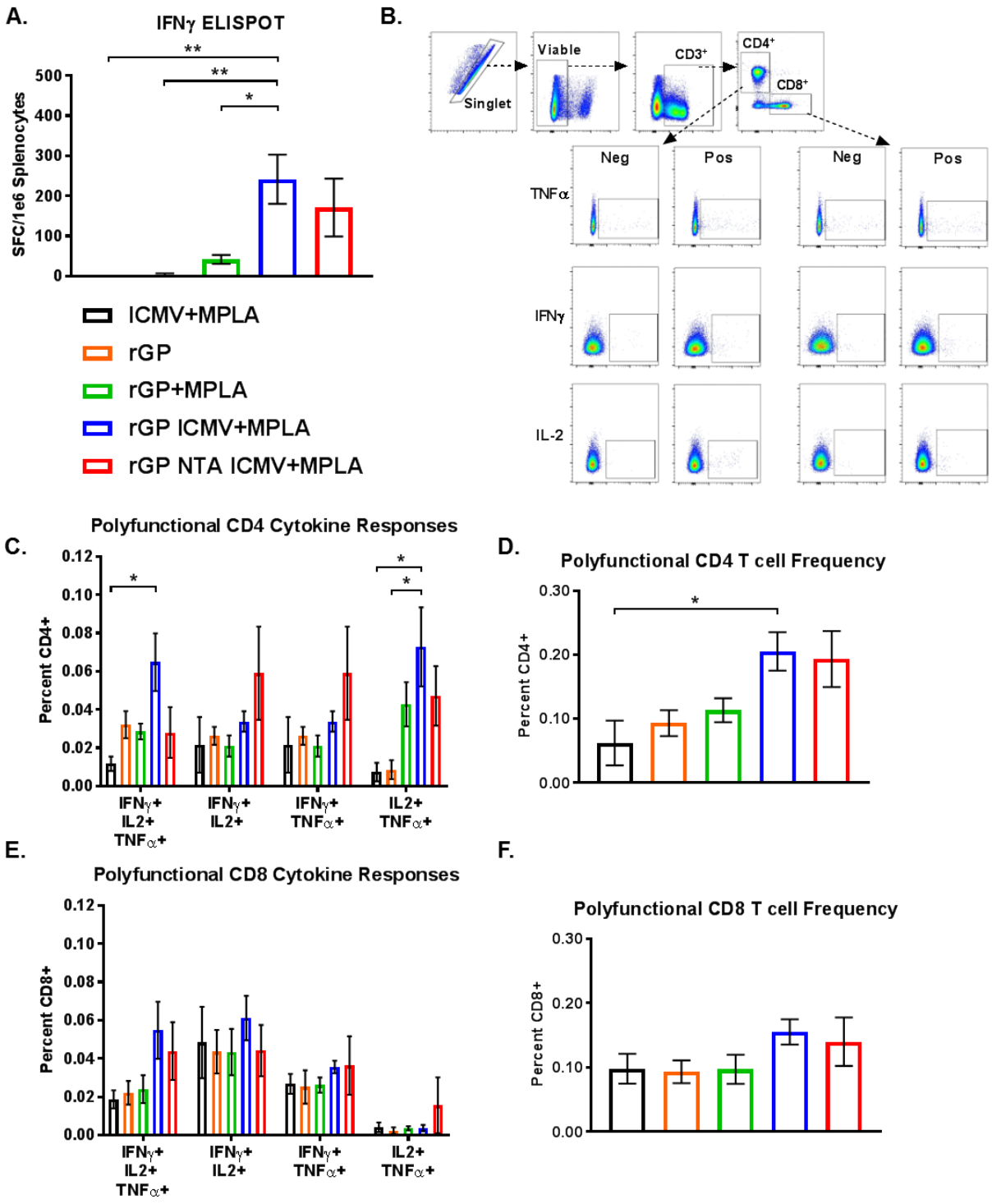

Figure 3-8. T cell immunogenicity in spleens of vaccinated mice. (A) IFN-γ producing T cell frequencies from harvested spleens enumerated by ELISpot. (B) Representative flow cytometry gating of ICS stained CD4+ and CD8+ T cells from vaccinated mice (Pos. columns) and naïve mice (Neg. columns). (C, E) Relative frequency of CD4+ and CD8+ polyfunctional T-cell subsets. (D, F) Relative frequency of combined CD4+ and CD8+ polyfunctional T-cell responses from spleens of vaccinated mice. Measurements reported as mean ± SEM. Statistical analysis performed by one-way (A, D, F) or two-way (C, E) ANOVA followed by Tukey's multiple comparisons test. *p<0.05, **p<0.01.

responses with neutralization capacity, promoted the formation of germinal center B cells, and elicited polyfunctional T cell responses.

Initial characterization of ICMV formulations revealed that the addition of DOGS-NTA phospholipids to ICMVs increased the loading efficiency of rGP via the selective interaction with the polyhistidine tag of rGP (**Table 3-1**), consistent with a previous report [123]. Additionally, we evaluated surface rGP epitopes by immunofluorescence staining and observed reverse trends for linear and conformational EBOV GP-specific antibodies to either formulation (**Figures 3-4 and 3-5**). Notably, while NTA ICMVs loaded ~2-fold more rGP than ICMVs, this trend was not observed for 6D8 or 13C6 binding. These observations may be explained in part by the high rGP density and concerted orientation on NTA ICMVs. Prior research has shown that 6D8 binds to the flexible mucin-like domain on the periphery of rGP, while 13C6 binds to the glycan cap domain at an angle in line with the rGP vertical axis [124, 125]. These data suggest that the 6D8 epitope would be more susceptible to occlusion by neighboring rGP complexes, whereas the 13C6 epitope would be less affected. However, while 13C6 epitopes are available for binding, the overall rGP density may lead to steric hindrance, limiting binding of all accessible epitopes [126].

Interestingly, we observed that after a prime-boost vaccination, mice generated potent isotype-switched antibodies against rGP for both nanoparticle groups as well as the rGP + MPLA control (**Figure 3-6B-E**). However, increased IgG1 and IgG2c titers were observed in mice immunized with rGP ICMV + MPLA, compared with other groups. When vaccination serum was tested for neutralization, immune sera from rGP ICMV + MPLA had higher neutralization capacity, compared with soluble rGP + MPLA as well as rGP NTA ICMV + MPLA (**Figure 3-6F-I**). When challenged with a lethal dose of ma-EBOV, all mice from both nanoparticle groups and the adjuvanted soluble antigen survived; whereas, 0 and 10% of mice survived from the vehicle

control and soluble antigen groups, respectively **(Figure 3-6J)**, suggesting an important role of MPLA in protective responses. However, it remains to be seen how long the protective responses are sustained, and if these results can be replicated in guinea pigs or nonhuman primates.

Further interrogation of the immune responses demonstrated increased B and T cell responses for both nanoparticle formulations, but only the rGP ICMV + MPLA group generated statistically significant increases in both B cell and polyfunctional T cell responses, compared with the control groups (**Figures 3-7 and 3-8**). This was a surprise as we expected the increased antigen density and concerted display of rGP by NTA ICMVs would enhance humoral responses. The unexpectedly low performance of rGP NTA ICMVs may be attributed to (1) the high surface antigen density, (2) nanoparticle aggregation, and/or (3) instability of NTA- polyhistidine tag interactions *in vivo*. (1) As shown in **Table 3-1**, NTA ICMVs were loaded with approximately two-fold more rGP than ICMVs; however, we did not observe a two-fold increase in antibody binding to rGP NTA ICMVs during immunostaining (**Figures 3-4 and 3-5**), indicating potential steric hindrance due to high antigen density on NTA ICMVs or masked epitopes [126]. (2) We also observed that NTA ICMVs tended to aggregate more than ICMVs *in vitro*. While the aggregates could be disrupted by bath sonication *in vitro*, this could adversely affect both particle drainage to lymph nodes and proper epitope display to B-cell receptors *in vivo*. (3) Lastly, it is possible that NTA-polyhistidine tag was not strong enough to withstand the *in vivo* condition, leading to loss of antigens, as recently demonstrated with lipid-based vaccine formulations [78]. While our proof-of-concept results presented here are encouraging, further analysis and optimization are required to address these remaining questions.

In conclusion, we have shown that rGP can be incorporated into ICMVs without adversely affecting the quaternary structure or key conformational epitopes. Two ICMV variants (standard

and NTA containing) also provided the means to control rGP loading and potentially surface orientation. Administration of rGP-loaded nanoparticles containing adjuvant in mice induced germinal center B cells, neutralizing antibody responses, and polyfunctional T cell responses. Analysis of long-term immune responses will be a main focus of future studies. Additionally, efforts are underway to optimize the nanoparticle formulation to achieve induction of cross-filovirus neutralizing immune responses.

3.6 Individual contributions

J. Bazzill, S.M. Stronsky, C.L. Cooper and J.J. Moon designed the experiments. J. Bazzill, S.M. Stronsky and L. Kalinyak performed the experiments. L.J. Ochyl contributed to the NanoFACS data. J. Steffens and S.A. van Tongeren provided technical support for *in vivo* animal studies. J. Bazzill, S.M. Stronsky, C.L. Cooper and J.J. Moon analyzed the data and wrote the manuscript. C.L. Cooper and J.J. Moon conceptualized the project and obtained funding.

Chapter 4

Development of an ICMV nanoparticle for preservation of the quaternary structure of a recombinant HIV antigen

4.1 Abstract

Thirty-five years after the discovery of human immunodeficiency virus (HIV) as the causative agent of acquired immune deficiency syndrome (AIDS) the incidence of HIV infection are declining due to the strategic use of anti-HIV medications. However, these medications are unable to cure hosts of the infection, transmission of HIV is still prevalent, and approximately 37 million people are infected worldwide. The ability of HIV to evade host immune responses coupled with its targeted infection of immune cells has made the development of HIV especially difficult and progress had all but stagnated. Recently, the discovery of rare antibodies that can protect against multiple strains of HIV have reinvigorated the search for a HIV vaccine. Here, we report the development of a lipid-based nanoparticle loaded with the recombinant human immunodeficiency virus envelope glycoprotein, BG505 SOSIP.664 (SOSIP). The nanoparticle produced is a variant of interbilayer-crosslinked multilamellar vesicles (ICMVs) modified to preserve the recombinant modifications and structural features of SOSIP. This new ICMV, called ICMV-NHS, displays ~25% loading efficiency of SOSIP and a mean diameter of ~300 nm while

preferentially bound an antibody that recognize the native HIV envelope glycoprotein compared to one that binds an aberrant form of the HIV antigen. These data indicate both the preservation ofnative antigenic sites and the preservation of the native-like conformation of SOSIP which is believed necessary to produce protective and broadly neutralizing humoral responses.

4.2 Introduction

Despite the advances in treatment of human immunodeficiency virus (HIV), it remains one of the most prevalent chronic infections worldwide. The introduction and strategic use of antiretroviral therapies have increased life expectancies, reduced transmission, and returned those infected to a relatively normal life.[127, 128] However, after three and a half decades of intense research, both a vaccine and a cure remain unseen. It is estimated that as of 2016, approximately 37 million individuals were infected with HIV worldwide, with 1.8 million new cases and 1 million acquired immunodeficiency syndrome (AIDS) related deaths that year.[41]

The high mutation rate and immune cell specificity of HIV have so far prevented anti-HIV therapeutics from curing patients.[129, 130] The rise of antiretroviral therapeutic (ART) resistant HIV strains have been observed when ARTs are administered as monotherapies or when treatment is interrupted. Treatment regimens of ARTs with two or more mechanisms of action are required to adequately control HIV replication and prevent the emergence of ART resistance.[55, 131] Additionally, early diagnosis and treatment initiation are needed to maximize ART efficacy, minimize the loss of CD4+ T-cells, and reduce transmission rates.[131] Prior to diagnosis, infected individuals can transmit HIV unknowingly and transmission is still possible during ART therapies, though the probability is dramatically reduced compared to untreated individuals.

The development of a HIV vaccine has met with similar difficulties due to the mutations that arise in HIV;[50, 132] however, the discovery of broadly neutralizing antibodies (bNAbs) has shown that protective immune responses can be generated against HIV.[133, 134] BNAbs recognize conserved regions on the HIV envelope glycoprotein (Env), the only surface displayed viral antigen that facilitates binding and viral entry into CD4+ T cells.

Conserved domains of Env are typically linked to functional domains, hence, why they are conserved between HIV strains. However, conserved domains are either masked or buried to minimize recognition and antibody production against these sites. As a result, other regions of Env are not involved in cell targeting or entry, highly antigenic, and variable (called variable domains). Antibodies are predominantly produced against these variable domains but are either non-neutralizing or strain specific.[50] Interestingly, over time uncommon characteristics like a long epitope binding domain and extensive somatic hypermutation arise in a fraction of Env-specific antibodies and are the reason bNAbs can target conserved regions of Env.[51, 135] However, these uncommon attributes are also the reason for the prolonged generation of bNAbs.[135] Additional factors such as host genetics, viral diversity, and immune tolerance limit bNAb prevalence to 20-30% of infected patients. Unfortunately, the long extensive time needed to generate bNAbs and simultaneous depletion of CD4+ T cells dramatically limit the benefit of bNAbs from clearing HIV, but they do provide a platform for vaccine candidates.

Conventional vaccines like attenuated or inactivated viruses are not viable options due to the potential for the virus to revert back to a virulent form or the risk of incomplete activation; both of which have occurred for other viral vaccines.[63, 64] To avoid these risks, Env subunit vaccines are a safer alternative, yet there are challenges with their production and efficacy that must be elucidated and overcome.[132] Early attempts to produce a recombinant Env antigen were

unsuccessful due to solubility and stability issues.[136] Simplified antigens using soluble domains of Env did not elicit protective immune responses,[137] and revealed that the native display of Env as a trimer was necessary for neutralizing antibody recognition. Recombinant alterations to Env produced a soluble and stable Env trimer retaining neutralizing epitopes. In particular, the recombinant Env antigen, BG505 SOSIP.664 (SOSIP) is a fully processed antigen produced as a trimer with a near native conformation.[138, 139] When administered as a soluble antigen, SOSIP has been shown to induce mild to moderately cross-reactive antibodies.[140] We sought to improve the immunogenicity of SOSIP by incorporating it with a lipid-based nanoparticle called interbilayer cross-linked multilamellar vesicle (ICMV), which have been previously reported to generate potent and long-lasting immune responses.[73, 76]

The production of a SOSIP ICMV was a challenging endeavor and eventually lead to the development of a new ICMV nanoparticle called ICMV-NHS. Specifically, to avoid the reduction of the introduced disulfide bond that covalently links the gp120 and gp41 subunits of SOSIP and is critical to trimer stability, the thiol-specific maleimide chemistry of ICMVs was replaced with amine specific NHS-ester (NHS) chemistry. Additionally, DTT and calcium were replaced with a polyamine containing polymer, branched polyethyleneamine (bPEI), which acted as both the cross-linking and fusion-inducing agent. Moreover, bPEI was recently reported to act as an immunostimulatory compound, eliciting balanced Th1/Th2 immune responses,[141, 142] and may serve to potentiate the induced immunological responses. Finally, we observed that a key step in ICMV production was leading to the dissociation of SOSIP trimers and upon modification of the nanoparticle synthesis method the trimer was preserved. These first trials culminated in a SOSIP nanoparticle displaying ~25% loading efficiency of SOSIP, a mean diameter of ~300 nm, and

demonstrated a preferential binding of the broadly neutralizing antibody PGV04 compared to the non-neutralizing antibody b6.

4.3 Materials and Methods

Antigen design, production and purification.

The design, production, and purification of soluble BG505 SOSIP.664 (SOSIP) and wild type (WT) antigens from HIV-1 subtype A have been described in detail previously.[138] Briefly, the recombinant alterations shared between the two antigens include a truncation at residue 664 and a point mutation (T332N) to introduce a glycan at a position commonly associated with Env immune evasion. SOSIP specific recombinant alterations include the point mutations A501C, T605C, and I559P, and modification of the cleavage sequence of gp120 from REKR to RRRRRR. To inhibit gp160 cleavage, the cleavage site of the WT antigen were altered from REKR to SEKS. The Env antigens were produced in CHO-K1 cells after stable transfection and the collected supernatants were purified by affinity chromatography with columns (GE Healthcare) loaded with either the broadly neutralizing antibody 2G12 or *Galanthus nivalis* lectin. The collected fractions were exchanged into buffer containing 10 mM Tris and 75 mM NaCl at a pH of 8.0, and size exclusion chromatography was used to specifically collect SOSIP trimers (GE Healthcare). The protein concentration of the collected trimers was determined by BCA assay (Thermo) or UV absorbance at a wavelength of 280 nm.

Nanoparticle production.

ICMV formulations were synthesized similar to those reported previously, with some modifications.[76] In brief, 1,2-dioleoyl-sn-glycero-3-phosphocholine (DOPC) and 1,2-dioleoyl-

sn-glycero-3-phosphoethanolamine-N-[4-(p-maleimidophenyl)butyramide] sodium salt (MPB), (Avanti Polar Lipids), were mixed at a 1:1 molar ratio and dried to produce thin films. Hydration buffer containing 25 μg SOSIP or WT was added to the dried films and vortexed to produce large multilamellar vesicles (MLVs), which were probe tip sonicated (QSonica) at 40% amplitude for 5 minutes to produce unilamellar vesicles (ULVs). ICMVs were formed by adding 200 mM $CaCl_2$ and 150 mM dithiothreitol (DTT), working concentrations of 33 mM and 1.24 mM, to ULV suspensions to induce nanoparticle fusion and crosslinking, respectively. The samples were incubated for one hour at 37°C to promote MPB crosslinking, then centrifuged at 14,000 r.c.f. at 4 °C to remove unloaded antigens (supernatant was used for analysis), washed with DNA grade water (Fisher), and suspended in 0.22 μm filtered PBS (Gibco).

The lipid composition of ICMV-NHSs consist of DOPC, 1,2-dioleoyl-sn-glycero-3-phospho-(1'-rac-glycerol) (sodium salt) (DOPG, Avanti Polar Lipids), and n-(Succinimidyloxy-glutaryl)-L-α-phosphatidylethanolamine, dioleoyl (DOPE-NHS, NOF America) at molar ratios of either 50:40:10, 50:30:20, or 50:0:50 (indicated in text). Immediately prior to ICMV-NHS synthesis, the antigens were buffer exchanged once into 10 mM BTP, pH ~8, via 7 kD MWCO Zeba spin desalting columns (Thermo) to remove tris buffer (amine containing) to avoid its conjugation with DOPE-NHS.

For the initial ICMV-NHS trials, 200 μL of hydration buffer containing 25 μg WT or 25 μg SOSIP antigen was added to dried lipid films and vortexed vigorously every minute for a total of 7 minutes and rested on ice. Samples were probe tip sonicated (QSonica) at 40% amplitude for 5 minutes prior to addition of the crosslinker and/or fusion inducing agent. Samples were incubated at 37 °C for one hour to promote NHS crosslinking, then centrifuged at 14,000 r.c.f. at 4 °C to

remove unloaded antigens (supernatant was used for analysis), washed with DNA grade water (Fisher), and suspended in 0.22 μm filtered PBS (Gibco).

The production of post sonication ICMV-NHSs (psICMV-NHS) proceeded similarly as ICMV-NHS with the exception that the hydration buffer volume was reduced to 100 μL (10 mM BTP, pH 7.58) without the presence of antigen to hydrate the lipid films. After probe tip sonication of the nanoparticles, 25 μg of antigen, in 100 μL of 10 mM BTP at pH ~8, was added and incubated at 37 °C for 30 minutes prior to addition of the crosslinker and/or fusion inducer. The nanoparticle mixture was incubated for another 30 minutes at 37°C then centrifuged and washed as previously described.

Extruded ICMV-NHS were produced similarly as ICMV-NHS; however, probe tip sonication was replaced with serial extrusion using a mini extruder (Avanti Polar Lipids) through 400 nm then 100 nm pore size membranes (Avanti Polar Lipids) following the manufacturer's instructions. Any residual sample retained within the extruder was collected for analysis.

To minimize sample loss and void sample dilution the extrusion method was adapted (ex2.0) where lipid films were hydrated with half the volume of antigen containing buffer (i.e. 100 μL). After each membrane extrusion, ~50 μL of pure buffer was extruded through the membrane to collect the retained residual sample and minimize sample loss. All steps after extrusion proceeded as other ICMV-NHS synthesis.

Calcium fused MLVs (Ca-MLVs) were produced by the indicated method in the text. Lipid compositions were either 50:50:0 or 50:40:10 DOPC:DOPG:DOPE-NHS, and only $CaCl_2$ was used to induce fusion.

ICMV-NHSs produced for immunostaining assays and NanoFACS analysis were produced as above, and where indicated in text particles used were produced with the addition of the lipophilic fluorophore 1,1'-Dioctadecyl-3,3,3',3'-tetramethylindodicarbocyanine, 4-chlorobenzenesulfonate salt (DiD, Thermo Scientific) at less than 0.2 molar percent.

Primary amine containing crosslinker calculations.

Branched polyethylene amine (bPEI) polymer with a molecular weight (number-based average) of 1800 Da, L-lysine, and 2,2' oxydiethylamine dihydrochloride salt (all from Sigma Aldrich), were tested as crosslinking/fusion inducing agents. Two primary amines are present on L-lysine and 2,2' oxydiethylamine, whereas for bPEI a molar ratio of 1:2:1 of 1°:2°:3° amines, respectively, was used to calculate the average number of 1° amines per polymer,[143] An average of 10.47 1° amines was calculated for 1800 Da bPEI.

Nanoparticle size.

Particle diameter and zeta potential were measured by dynamic light scattering (DLS) of nanoparticles dilutes in 0.22 μm filtered PBS using a Malvern ZetaSizer Nano ZSP.

Antigen loading and quaternary structure.

Antigen loading was assessed by poly-acrylamide gel electrophoresis under non-reducing conditions (NR PAGE). Samples were prepared following manufacturer's instructions, loaded into gradient (4-12%) or 8% Bis-Tris Plus gels (Invitrogen) for ICMVs and ICMV-NHSs, respectively. Gels of ICMVs ran for 35 minutes at 165 V, whereas, ICMV-NHS loaded gels ran for 45-60 minutes at ~180 V to maximize the separation of bPEI from the antigens. Protein content was assessed by Silver Stain (Thermo), imaged with FluorChem M (Protein Simple) digital imager, and quantified using ImageJ software.

The preservation of quaternary structures after formulation was evaluated by Blue Native (BN) PAGE analysis via NativePAGE™ Novex® Bis-Tris gel system (Life Technologies) following manufacturer's protocols with some minor modifications. Specifically, the samples were incubated in either n-Dodecyl β-D-maltoside (DDM, Invitrogen), Triton X-100 (Fisher) or octyl β-D-glucopyranoside (ODBG, Sigma) and various concentrations prior to loading and running BN PAGE gels. Any samples that were not detergent incubated were prepared in sample buffer and remained on ice until loaded. BN PAGEs of loaded ICMVs or antigens alone were run at room temperature using light or dark blue cathode buffer (contains Coomassie Stain) for approximately 100 minutes. The analysis of the BN PAGEs was carried out following manufacturer's instructions. For ICMV-NHS loaded gels, dark blue cathode buffer was used for migration followed by destaining according to manufacturer's instructions and protein migration was assessed by silver stain (Thermo Fisher). All gels were imaged using a FluorChem M (Protein Simple) digital imager.

Antigen conformation analysis.

Immunofluorescence stained nanoparticles were prepared by incubating equal volumes of nanoparticles with 4 °C in 0.04 mg/mL antigen specific primary monoclonal antibodies PGV04 or b6 (kind gifts from the International AIDS Vaccine Initiative), or human IgG_1 kappa isotype (EMD Millipore) in FACS buffer (1% BSA in PBS), or in FACS buffer alone. Samples were washed by centrifuging at 20,817 r.c.f. for 30-60 minutes at 4 °C, and the pellets suspended in FACS buffer. The wash step was repeated prior to incubation in 100 μL phycoerythrin (PE) conjugated α-human IgG (Fcγ) secondary antibody (ebioscience) for one hour at room temperature. Unbound secondary antibody was removed by washing and the particles were plated, and fluorescence signal was measured at 488/578 for PE and 644/670 nm for DiD (select samples). For NanoFACS analysis

the samples were transferred to FACS tubes after the plate-based measurements, and analyzed on a Beckman Coulter MoFlo Astrios with M1 and M2 masks. NanoFACS data was analyzed via FloJo software.

Statistical Analysis.

Determination of statistical significance was performed using Prism 7.0.3. One-way ANOVA significance tests with Tukey's post-hoc multiple comparison test was used for group-wise analysis as indicated in the figure legends.

4.4 Results

SOSIP ICMV trial formulations.

Initial ICMV trials utilized both the fully cleaved SOSIP antigen along with an un-cleaved control Env antigen (WT) that does not form a native like trimer and is prone to binding non-neutralizing antibodies (**Figure 4-1**). The introduced disulfide bond of SOSIP is critical for the

Figure 4-1. Illustrations of HIV envelope glycoprotein antigens. Both SOSIP and wild type (WT) antigens are truncated at residue 664, removing the membrane proximal region (MPER), transmembrane domain (TM), and cytosolic tail (CT). Asterisk (*) indicates the site of the introduced glycan at the T332N point mutation. "X" indicates the approximate site of the I559P point mutation on SOSIP. Point mutations (A501C and T605C) are indicated for the introduced SOSIP disulfide bond. Diagram of the SOSIP trimer consisting of gp120 (dark blue), truncated gp41 (light blue), and the introduced disulfide bond (red line).

stability of the recombinant antigen. The placement and function of this disulfide bond is reminiscent of the endogenous GP_1/GP_2 disulfide bond of rGP (**Figure 3-1**) which was disrupted by DTT during ICMV production. To avoid a similar effect, WT and SOSIP loaded ICMVs were produced by the modified method for rGP loading where the DTT content was reduced by half for a 1:1 mole ratio of thiol to maleimide. Analysis of antigen loading by non-reducing SDS PAGE (NR PAGE) indicated ~80% loading efficiency of WT in ICMVs relative to the supernatant (unloaded antigen, **Figure 4-2A**). In comparison, SOSIP loading was comparable between the particles and supernatants, indicating ~50% loading efficiency, **Figure 4-2B**).

SOSIP from the ICMV and supernatant samples showed no signs of reduction of the introduced disulfide bond (absence of lower molecular weight bands, **Figure 4-2B**). To assess if WT and SOSIP trimers were preserved, both samples were analyzed by non-denaturing and non-reducing Blue Native PAGE. Due to the lipid composition of the nanoparticles, detergents were required to effectively disrupt and migrate the nanoparticle components. However, detergents may disrupt the weak hydrophobic interactions that contribute to the trimeric configuration. To account for this possibility, stock antigens were incubated with detergent at the same concentration as the samples, and no effect was observed on either trimer (**Figure 4-2C, D**). The antigen from WT ICMV samples appeared unaffected by ICMV synthesis and migrated similarly to the standards (~720 kD) and no visible lower molecular weight bands were observed (**Figure 4-2C**). In stark contrast, the SOSIP containing samples appeared at molecular weights of ~720 kD, ~480 kD, and ~242 kD, indicating the presence of trimers, dimers, and gp140 monomers, respectively (**Figure 4-2D**).

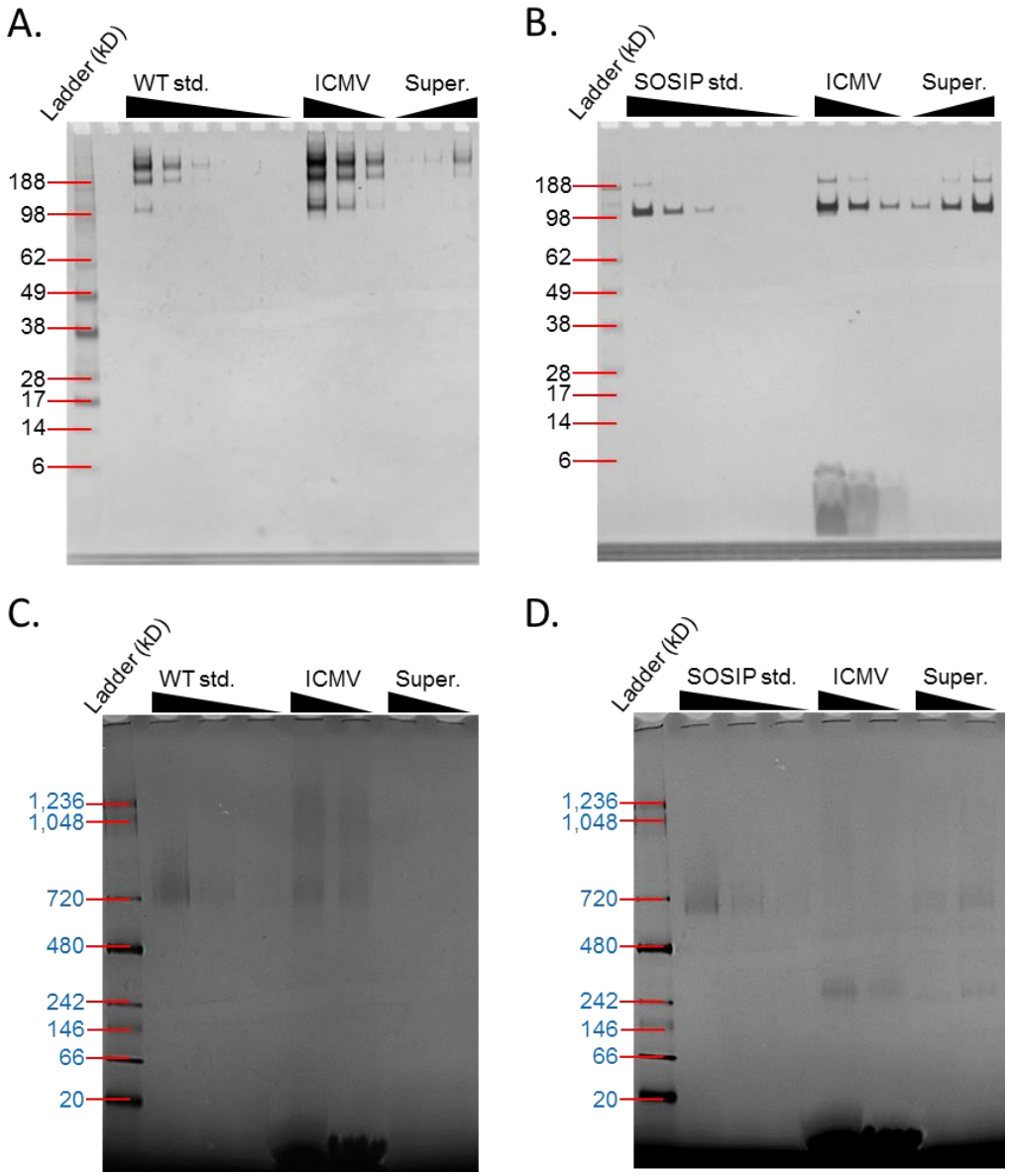

Figure 4-2. WT and SOSIP ICMV characterization. Loaded antigens (ICMV) were compared to supernatant (Super.) containing unloaded antigen, and antigen standards (std.). Evaluation of WT (A) and SOSIP (B) ICMV loading by non-reducing SDS PAGE. Blue Native PAGEs of WT (C) and SOSIP (D) ICMVs and supernatants to assess preservation of trimers.

Probe tip sonication disrupts SOSIP trimers.

Though the recombinant disulfide bond of SOSIP was retained after ICMV synthesis, the potential of DTT to reduce disulfides was observed previously (**Chapter 3**). To eliminate this potentially deleterious effect, a new nanoparticle using amine-reactive NHS chemistry was

selected to replace the thiol-reactive maleimide chemistry of standard ICMVs. The maleimide-functionalized phospholipid MPB was replaced with the NHS-functionalized phospholipid DOPE-NHS. In conjunction, DTT and calcium were replaced with branched polyethylene amine (bPEI). Initial production of SOSIP ICMV-NHS consisted of the same production method as standard ICMVs, depicted in **Figure 4-3A**. When the supernatant of SOSIP loaded ICMV-NHS was evaluated by BN PAGE the trimer was again dissociated (**Figure 4-3B**). In addition, bPEI migrated poorly and produced a large smear throughout the lane, making clear identification of the antigen difficult and potentially affecting antigen migration. To aid in migrating bPEI, additional detergent and charge shift molecules were added for BN PAGE analysis, though, the amphiphilic properties of these components may have contributed to the disruption of SOSIP trimers (**Figure 4-3B**).

To elucidate if SOSIP trimer dissociation was a result of BN PAGE preparation or the nanoparticle synthesis process, simplified nanoparticles were produced using DOPG (anionic phospholipid) in place of DOPE-NHS and calcium in place of bPEI as the fusion inducer. The changes in lipid composition served two purposes: one, removing NHS and bPEI as variables for the analysis; and two, non-crosslinked MLVs are more easily disrupted by detergents, thus requiring less detergent and charge shift molecules for BN PAGE analysis. The calcium-fused MLVs (Ca-MLVs) were produced by the same method as ICMV-NHSs (**Figure 4-3C**), and a stepwise analysis was conducted to evaluate trimers at each stage of production. The pellets and respective supernatants from each step were analyzed by BN PAGE, and gp140 monomers appeared after the probe tip sonication step (**Figure 4-3D**). These results conflicted with prior data showing trimer retention after SOSIP (in buffer) sonicated across multiple settings (**Figure 4-3E**), including those used for ICMV-NHS and Ca-MLV production (5 minutes at 40% intensity).

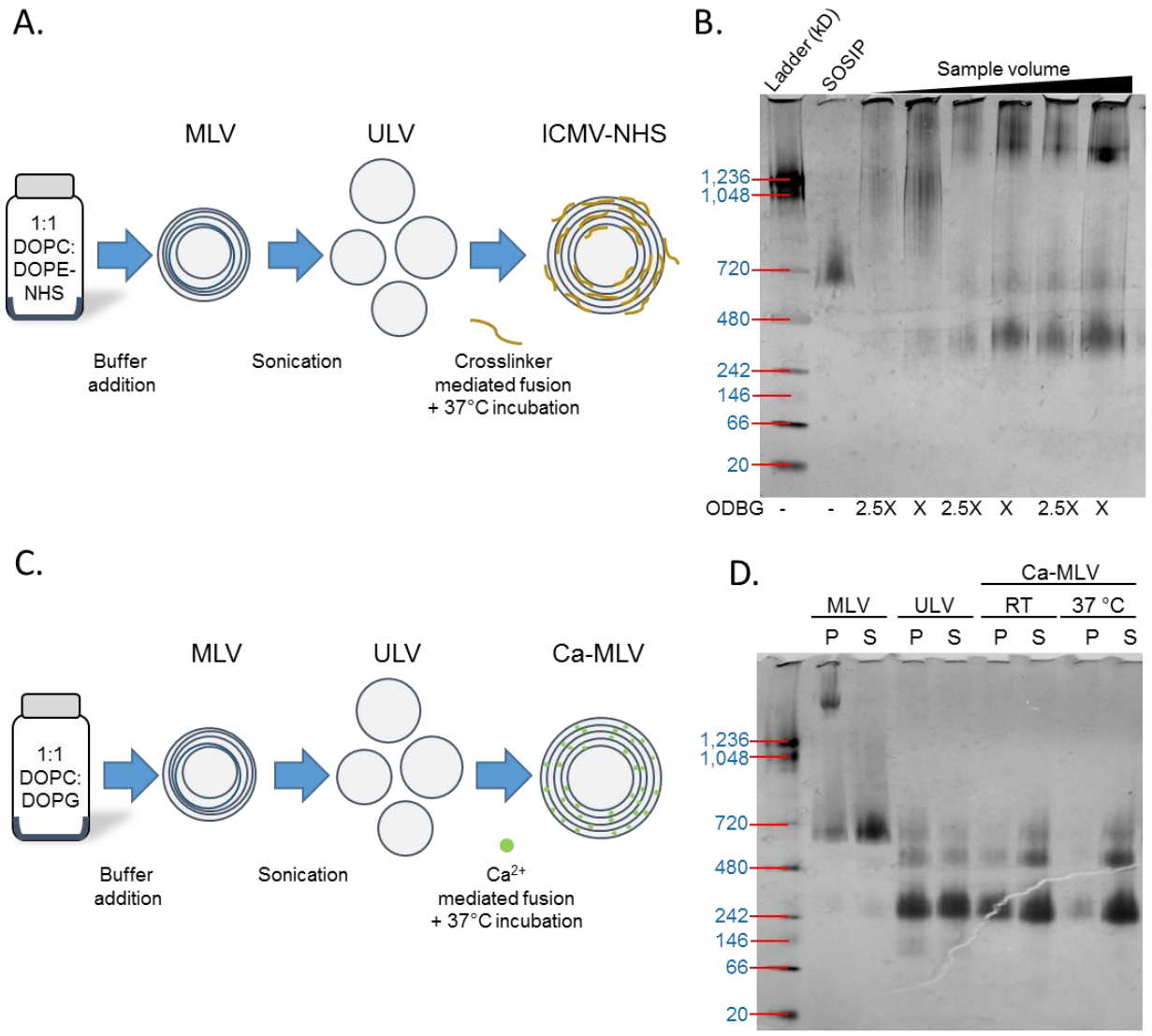

Figure 4-3. ICMV-NHS design and trials. (A) Schematic of each step of ICMV-NHS production. (B) Blue Native PAGE of SOSIP ICMV-NHS supernatant in increasing volumes. The relative amount of detergent, ODBG, is indicated below the gel (a "-" indicates no ODBG). (C) Schematic of calcium fused MLV (Ca-MLV) production. (D) Blue Native PAGE of samples removed at each step of SOSIP loaded Ca-MLV production. P = particle/pellet, S = supernatant. (E) Blue Native PAGE of stock SOSIP after 2 or 5 minutes of sonication at 20 and 40% amplitude.

To confirm if probe tip sonication was leading to SOSIP trimer dissociation, Ca-MLVs were produced using extrusion in place of sonication and again evaluated by BN PAGE at each step of production (**Figure 4-4A**). All stages of extruded Ca-MLV synthesis displayed SOSIP trimers and confirmed that the dissociation of SOSIP trimers was occurring during the probe tip sonication. While gp140 monomers were observed, the majority of SOSIP was retained as trimers (**Figure 4-4A**). Additionally, gp140 monomer bands were present in all samples incubated with detergent, indicating some contribution of the detergent to trimer dissociation (**Figure 4-4A**, far right lanes). Unfortunately, SOSIP loading was much lower in extruded Ca-MLVs compared to sonicated Ca-MLVs (**Figures 4-3D vs. 4-4A**). When the extruded Ca-MLVs method was evaluated, it was determined that after each extrusion a portion of sample was retained in the extruder chamber. The residual sample was collected after each extrusion step, and assessed along with the final produced and was shown to contain large amounts of SOSIP trimers (**Figure 4-4A**,

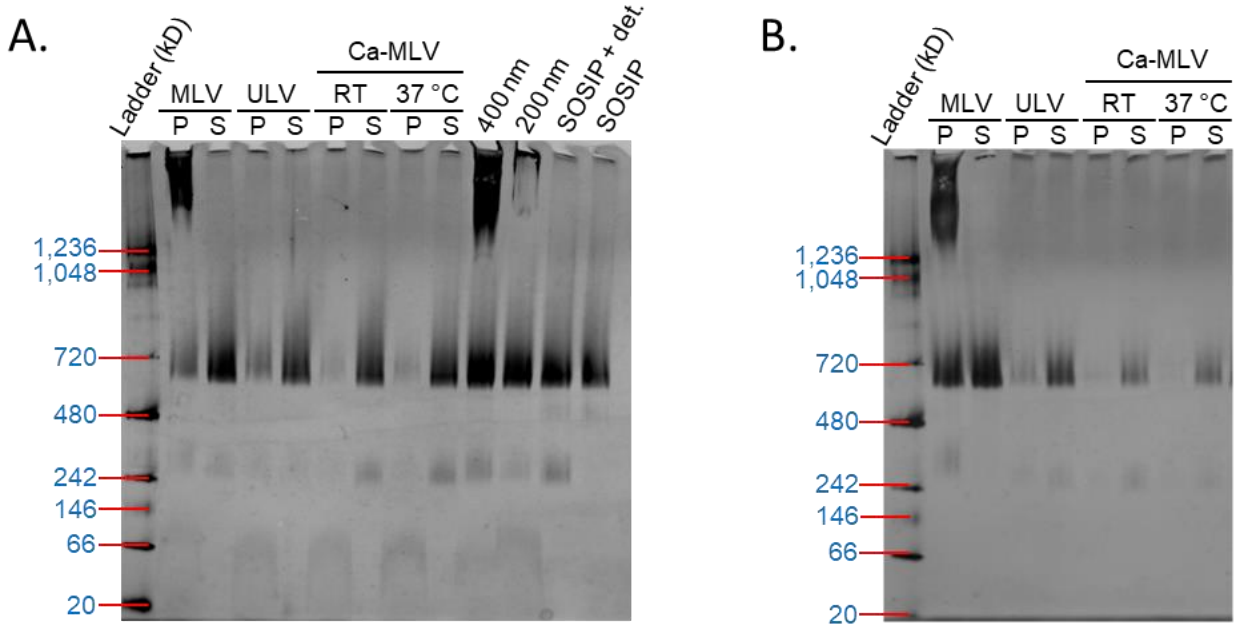

Figure 4-4. Extrusion Ca-MLV trials. Blue Native PAGE of extruded SOSIP Ca-MLVs (A) Ca-MLVs containing 10% DOPE-NHS (B) from each stage of production. P = particle/pellet, S = supernatant. (A) Residual samples (400 nm and 200 nm) from the extrusion chamber and SOSIP +/- detergent (det.) controls.

400 and 200 nm lanes). To increase the loading of SOSIP DOPE-NHS was reincorporated at 10% (mol/mol) into the lipid films, and calcium was again used in place of bPEI to allow for optimal DOPE-NHS conjugation to SOSIP. Unfortunately, SOSIP loaded remained low even in the presence of DOPE-NHS when calcium was used as a fusion inducing agent (**Figure 4-4B**).

Extruded ICMV-NHSs preserve SOSIP trimers and conformational epitopes.

The use of a cationic polymer as a fusion inducer may enhance antigen loading by electrostatically interacting with anionic residues on the antigen or phospholipids to reduce the electrostatic repulsion and promote loading of the antigen. While a similar effect can occur with calcium ions, a cationic polymer with multiple ionized residues could bind with more avidity and would be less easily displaced. The bPEI polymer used in this study has on average ≥ 10 ionized amines per polymer (only tertiary amines calculated) at pH 8. In addition to acting as a buffer between the antigen and ULVs, bPEI can react with DOPE-NHS via unionized primary and, less-favorably, secondary amines.

Trial productions of ICMV-NHSs were conducted using formulations containing 10% or 20% molar DOPE-NHS. Since bPEI can compete with SOSIP for DOPE-NHS conjugation, the bPEI content (based on primary amines) was not added in extreme excess like calcium ions but added at either an equimolar or 1.5-fold excess of primary amines to the DOPE-NHS present in the specific formulation. Additionally, a final formulation was included where equimolar bPEI was supplemented with $CaCl_2$ to observe any impact on antigen loading or nanoparticle formation or size. A trend emerged in which nanoparticle diameters and size homogeneity, measured as polydispersity indices (PDI), increased as the bPEI content increased (**Figure 4-5A, B**) to a point

A.

WT ICMV-NHS trials	Z-Avg (nm)	PDI	ZP (mV)
△ 10% NHS, (1:1)	274	0.22	-20
△ 10% NHS, (1.5:1)	336	0.26	-21
△ 10% NHS, (1:1) + Ca^{2+}	210	0.19	-24
△ 20% NHS, (1:1)	346	0.27	-22
△ 20% NHS, (1.5:1)	5594	0.62	-18

B.

SOSIP ICMV-NHS trials	Z-Avg (nm)	PDI	ZP (mV)
○ 10% NHS, (1:1)	233	0.20	-22
○ 10% NHS, (1.5:1)	238	0.17	-22
○ 10% NHS, (1:1) + Ca^{2+}	198	0.30	-27
○ 20% NHS, (1:1)	339	0.28	-24
○ 20% NHS, (1.5:1)	1873	0.76	-20

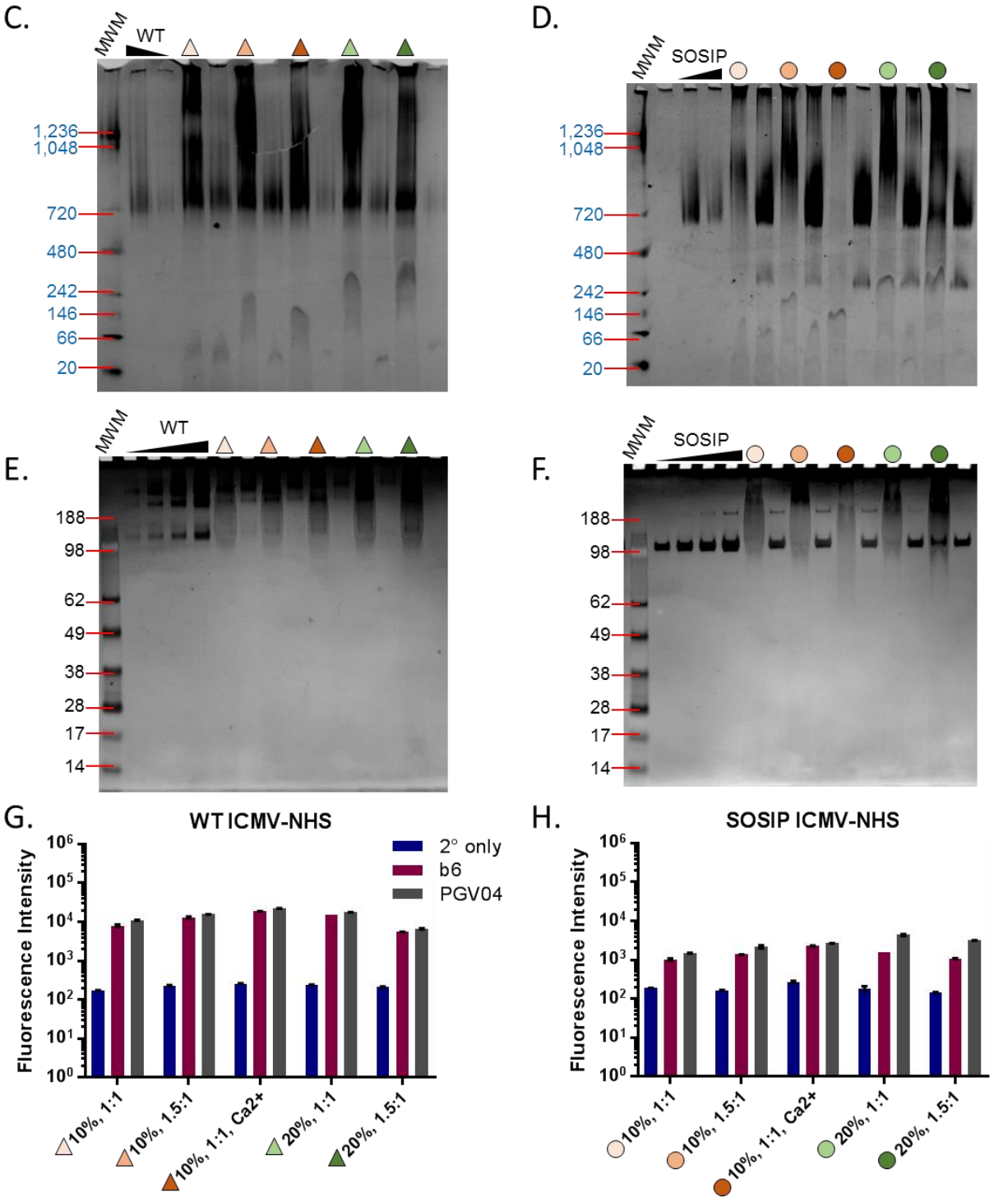

Figure 4-5. Characterization of extruded WT and SOSIP ICMV-NHSs. (A, B) Tables of Z-Avg diameters, polydispersity indices (PDI) and zeta potentials (ZP) of WT and SOSIP ICMV-NHSs containing 10 or 20% DOPE-NHS. Molar ratios of bPEI primary amine:NHS are indicated in parentheses. (C, D) BN PAGEs of WT and SOSIP ICMV-NHSs, with the respective supernatants next to particle lanes. (E, F) NR PAGEs of WT and SOSIP ICMV-NHSs, with the respective supernatants next to particle lanes. (G, H) Average secondary antibody signals from immunofluorescence stained WT or SOSIP ICMV-NHSs. Particles are color and shape matched.

where large aggregates formed. In contrast, ICMV-NHSs produced with both bPEI and $CaCl_2$ displayed the lowest average diameters and PDIs of 0.19 and 0.30 for WT and SOSIP particles, respectively. Interestingly, despite the increasing content of bPEI or the presence of $CaCl_2$, the zeta potential (measured in PBS) of the nanoparticles remained relatively unchanged, ranging from -18 to -24 mV and -20 to -27 mV for WT and SOSIP nanoparticle formulations, respectively. Analysis of the trial formulations by Blue Native PAGE revealed that increasing bPEI adversely affected the migration of the components (**Figure 4-5C, D**). Some apparent bands of WT trimer were visible in the particle fractions (indicated by triangles), but were difficult to discern (**Figure 4-5C**). Similar results were obtained with SOSIP where the particle lanes (indicated by circles) migrated poorly with no distinct evidence of SOSIP trimers (**Figure 4-5D**). Conversely, antigen bands from the supernatant fractions (unloaded antigen) migrated as trimers for both WT and SOSIP, albeit some monomer bands were observed in the SOSIP samples (**Figure 4-5C, D**), suggesting the antigens were mainly retained as trimers throughout ICMV-NHS synthesis.

Quantification of the protein content of the particle and supernatant fraction was attempted by non-reducing (NR) PAGE. While WT and SOSIP bands easily appeared in lanes loaded with the supernatants (**Figure 4-5E, F**), interference by bPEI was again observed in the particle fraction samples and interfered with protein content quantification. However, WT bands were clearly evident in the particle lanes, whereas, SOSIP bands were faint except for one formulation (**Figure**

4-5F, far right lanes). Nevertheless, the majority of SOSIP antigen was contained within the supernatant fractions, indicating low antigen loading.

Lastly, the presence WT and SOSIP on ICMV-NHS surfaces was evaluated using the previously described indirect immunofluorescence staining assay[73] with the antigen-specific primary antibodies b6 and PGV04 (non-neutralizing and broadly neutralizing antibodies, respectively). Fluorescence signals of the fluorophore-conjugated secondary antibody revealed much greater levels of primary antibody binding to WT particles than SOSIP particles (**Figure 4-5G, H**), aligning with the enhanced loading of WT that was observed compared to SOSIP (**Figure 4-5E, F**). Notably, both SOSIP formulations containing 20% DOPE-NHS demonstrated approximately 2.8-fold increased binding of PGV04 compared to b6; whereas, PGV04 binding was only 1.2-1.6 fold higher for the 10% DOPE-NHS containing SOSIP formulations. Preferential binding of the broadly neutralizing antibody PGV04 over the non-neutralizing b6 is a desired trait for a HIV vaccine candidate. To evaluate if this trend was directly related to the DOPE-NHS content, ICMV-NHS formulations with further increased amounts of DOPE-NHS were produced and assessed for a greater selectivity of PGV04 binding.

Modified ICMV-NHS method improves SOSIP loading but not nanoparticle size.

SOSIP ICMV-NHSs containing 50% DOPE-NHS were produced by two methods. The first, termed post sonication (psICMV-NHSs), added SOSIP after the sonication step and the mixtures was incubated at 37°C prior to addition of the crosslinking agent. The second method utilized extrusion with a wash of the chamber between each extrusion step to aid with sample recovery. Additionally, both methods used half the initial volume of buffer for hydration, to prevent excessive dilution of the formulations during synthesis.

For these experiments the bPEI content was reduced to 0.6:1 and 0.7:1 (primary amine:NHS), resulting in total bPEI concentrations similar to that used for the 20% ICMV-NHSs. The rational for this alteration was that if the bPEI amount is lowered then then more DOPE-NHS would be available to bind to the antigen and unreacted bPEI would be less present, which may limit aggregation of the nanoparticles. Conversely, the observed interference of bPEI in the PAGE based quantification methods may be related to the poor migration of bPEI conjugated to DOPE-NHS. Therefore, formulations using the small molecule crosslinkers, l-lysine and 2,2' oxydiethylamine (22O) were produced to see if bPEI could be replace by a suitable small molecule crosslinker. L-lysine and 22O are diamine containing compounds and were added at primary amine:NHS molar ratios of 4:1 and 1:1. At these low concentrations $CaCl_2$ was used to supplement fusion of the ULVs.

When measured by DLS, psICMV-NHSs fused with 0.6:1 and 0.7:1 bPEI displayed diameters of ~500 and ~4000 nm, respectively, indicating aggregation of the nanoparticles (**Figure 4-6A**). Similar results were measured for ICMV-NHSs produced by the modified extrusion method, with diameters of ~1850 and ~7300 nm. Interestingly, as the bPEI concentration increased for these samples, the zeta potential of the nanoparticles became less negative, a trend not observed previously. Conversely, all ICMVs produced with l-lysine or 22O ranged in size from 120-218 nm and displayed zeta potentials of approximately -24 mV (**Figure 4-6A**). Though the small molecule crosslinkers improved nanoparticle size and zeta potential, antigen loading was highest for psICMV-NHS produced with bPEI. (**Figure 4-6B**). These data suggest a beneficial effect of increasing bPEI on antigen loading but a deleterious effect on the nanoparticle size.

A.

Post sonication	Z-Avg. (nm)	PDI	ZP (mV)
ULV	76	0.21	-18
ICMV-NHS, bPEI (0.5:1)	518	0.33	-18
ICMV-NHS, bPEI (0.7:1)	4134	0.54	-11
ICMV-NHS, L-lysine (4:1) + Ca^{2+}	136	0.34	-24
ICMV-NHS, 22O (1:1) + Ca^{2+}	123	0.32	-26

Modified extrusion	Z Avg. (nm)	PDI	ZP (mV)
100 nm liposomes	149	0.20	-15
ICMV-NHS, bPEI (0.5:1)	1849	0.68	-17
ICMV-NHS, bPEI (0.7:1)	7290	0.87	-7.0
ICMV-NHS, L-lysine (4:1) + Ca^{2+}	120	0.18	-24
ICMV-NHS, 22O (1:1) + Ca^{2+}	218	0.29	-23

B.

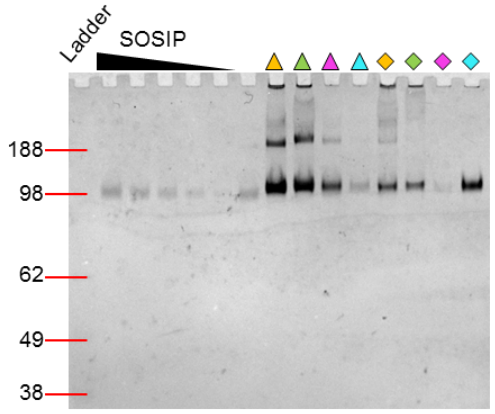

Figure 4-6. Characterization of post sonication (ps) and modified extrusion SOSIP ICMV-NHS trials. (A) Tables of Z-Avg diameters, PDI, and ZP of SOSIP ICMV-NHSs synthesized via p.s. (top) or modified extrusion (bottom) method using various crosslinker/fusion inducer compounds. Indicated in parentheses are the molar ratios of primary amine:NHS ester. (B) Silver stained NR PAGE of SOSIP content of the above nanoparticles, loaded in equal volumes. Samples are shape and color matched.

Optimization of SOSIP psICMV-NHSs.

To optimize the bPEI content for ICMV-NHSs production, the polymer concentration was incrementally lowered to produce approximately ideal nanoparticle sizes without significantly reducing antigen loading. For this, SOSIP psICMV-NHSs were produced using bPEI at 0.3:1, 0.35:1, and 0.4:1 1° amine:NHS ratios, and particle diameters were measured as 328, 314, and 381 nm, respectively, with PDIs of 0.27, 0.28, and 0.36 and zeta potentials around -19 mV for all particles (**Figure 4-7A**). Though the sample intensities were outside the range of the standards, the

loading efficiencies for the nanoparticles were calculated to be at least 26% (**Figure 4-7A**). The observed migration of SOSIP from the ICMV-NHS samples appeared at higher molecular weights than the standards or unloaded SOSIP, indicating conjugation of DOPE-NHS to the antigens (**Figure 4-7B**). From these formulations, the particle produced with 0.35:1 bPEI primary amine:NHS was selected to evaluate the surface antigen display, due to the balance of antigen loading, nanoparticle diameter and low PDI. SOSIP psICMV-NHSs were produced with the addition of the lipophilic fluorophore DiD, and the particles were analyzed by immunofluorescence assay and NanoFACS, a method adapted from others to evaluate antigen display on individual nanoparticles. [99-103]

A.

	LE%	Size (d.nm)	PDI	ZP (mV)
SOSIP psICMV-NHS, bPEI (0.3:1)	26	328	0.27	-19
SOSIP psICMV-NHS, bPEI (0.35:1)	32	314	0.27	-20
SOSIP psICMV-NHS, bPEI (0.4:1)	≥40*	381	0.36	-18

B.

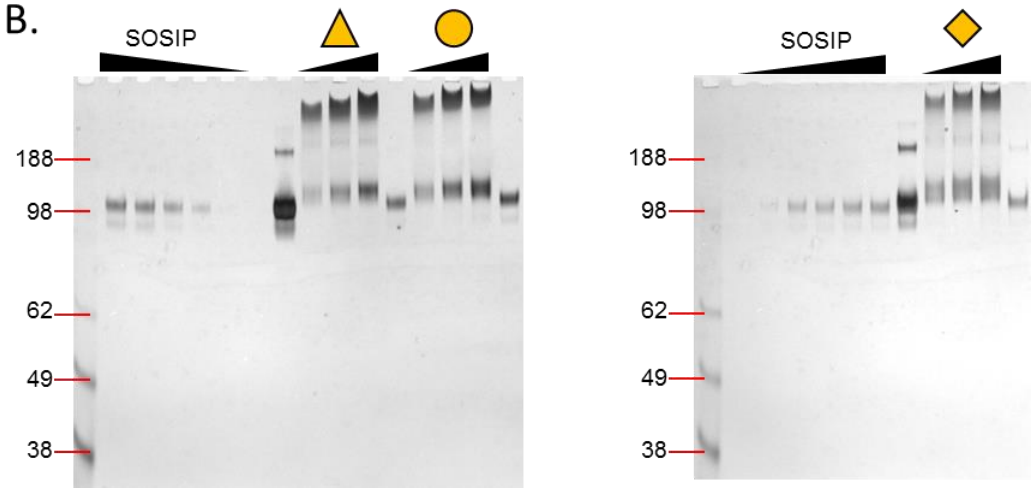

Figure 4-7. Optimization of SOSIP psICMV-NHS production. (A) Table of Z-Avg diameters, PDI, and ZP of SOSIP psICMV-NHS using increasing amounts of bPEI crosslinker (molar ratio of primary amines:NHS ester indicated in parentheses). ((B) Silver stained NR PAGE of SOSIP content of the above nanoparticles, loaded in increasing volumes. Samples are matched by shape.

The retention of DiD in the immunofluorescence stained nanoparticles were not significantly different when measured in bulk, though ~75% of particles were lost during the

processing (Figure 4-8A). Binding of the broadly neutralizing primary antibody (PGV04) was significantly higher than any other primary antibody ($p<0.0001$), whereas, the non-neutralizing primary antibody (b6) bound at similar levels as the isotype control, indicating it may be non-specifically bound to the nanoparticles (Figure 4-8B). Individual analysis of the nanoparticles via NanoFACS measured comparable DiD signals between sample groups, and a similar trend of selective PGV04 binding compared to control groups (Figure 4-8C, D).

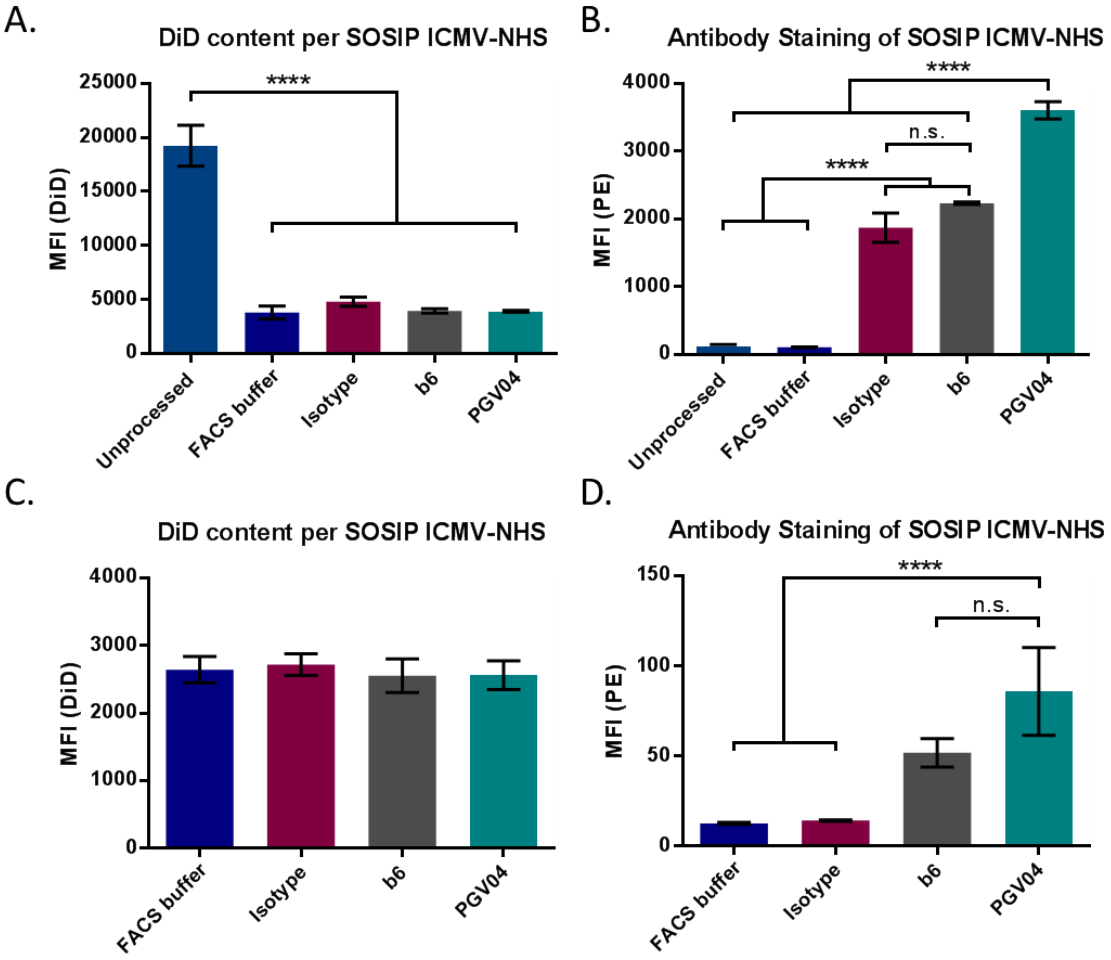

Figure 4-8. Surface antigen display on SOSIP psICMV-NHS. (A) DiD (left) and secondary antibody binding (right) signals of immunofluorescence stained nanoparticles as measured by plate reader. (B) DiD and secondary antibody signals of individual nanoparticles as measured by NanoFACS analysis. Measurements are reported as means ± s.d. Statistical analysis was conducted by one-way ANOVA followed by Tukey's multiple comparison test. (n.s.) $p > 0.05$, (****) $p < 0.0001$.

4.5 Discussion

The development of a new ICMV nanoparticle utilizing primary amine chemistry via NHS-ester chemistry was prompted by the reduction sensitive recombinant SOSIP antigen (**Figure 4-1**). Early in the development of NHS containing ICMVs (ICMV-NHS), dissociation of the SOSIP trimer was observed and determined to be caused by the probe tip sonication step during ICMV synthesis (**Figure 4-3**). Extrusion-based production methods were used to confirm that this was indeed the case (**Figures 4-4**); however, extruded ICMV-NHSs demonstrated poor recovery of the sample, which contributed to low antigen loading (**Figure 4-4 and 4-5**). It was determined that modification to the original method where SOSIP would be added after probe tip sonication yielded the highest amount of antigen recovery and loading (**Figure 4-6**).

However, optimizing ICMV-NHS loading and size proved challenging when using the polycationic polymer bPEI. Initially, 1800 Da bPEI was a suitable choice for ICMV-NHS production since it could serve as both the crosslinking agent and fusion inducer, and low molecular weight bPEI are less cytotoxic.[144-146] Additionally, recent research has demonstrated bPEI as an immunostimulatory compound,[141, 142] which would be of added benefit for vaccine nanoparticles.

Unfortunately, an unfavorable trend was discovered between antigen loading and particle size in relation to the bPEI amounts used, where increasing bPEI resulted in increased antigen loading but particle size also increased to the point of large aggregate formations (**Figures 4-5A, B, 4-6A, and 4-7A**). As a possible replacement for bPEI, diamine containing small molecules were also tested as crosslinking agents (reminiscent to DTT) along with $CaCl_{2\,as}$ the fusion inducer, and observed sub-200 nm ICMV-NHSs, but the loading of SOSIP was poor compared to bPEI (**Figure 4-6A, B**). Potentially, factors such as the salt form of the small molecules used or additional

negatively charged residues may have impacted the efficacy of the small molecule crosslinkers. Regardless, bPEI containing nanoparticles displayed the highest antigen loading and were further tuned for a more ideal nanoparticle diameter.

Optimization of bPEI fused ICMV-NHSs using the post sonication method (psICMV-NHSs) produced particles with approximately 20-30% loading efficiencies and diameters between 310-330 nm (**Figure 4-7A**). One formulation in particular, bPEI content of 0.35:1 molar primary amine:NHS, was tested for Env-specific antibody binding via immunofluorescence staining. Bulk sample analysis revealed significantly higher binding of the broadly neutralizing antibody PGV04 compared to the non-neutralizing antibody b6 and control groups (**Figure 4-8A**). Individual particle analysis displayed similar results, but statistical significance not observed between PGV04 and b6 (**Figure 4-8D**).

These efforts demonstrate the first steps in producing SOSIP loaded ICMV-NHSs, but further optimization is required. Specifically, NHS-esters are less stable than maleimides and subject to hydrolysis,[144-146] which is accelerated by increasing pH, water content, and temperature. These factors were accounted during production to mitigate hydrolysis prior to the addition of antigen and crosslinker, yet inconsistencies were still observed. Additionally, bPEI polymers are not uniform in size but range around the average molecular weight of 1800 Da. Refinement of the polymer size may lead to more consistent production of ICMV-NHSs. Furthermore, the negative zeta potentials of ICMV-NHSs indicate that bPEI is not extensively bound to the surfaces; however, it may still may bind to SOSIP antigens, effecting recognition by ENV-specific antibodies or impacting antibody generation. As an alternative to bPEI, the small molecules spermidine and spermine have well defined masses (145.25 and 202.34 Da, respectively), contain amines suitable for NHS-ester conjugation, and ionized amines that may

induce fusion of ULVs. While these data demonstrate a role for ICMV-NHSs in specific applications, further work is needed to develop and characterize the crucial components for the stable and consistent production of this new type of nanoparticle.

4.6 Individual contributions

J. Bazzill and J.J. Moon designed the experiments. J. Bazzill performed the experiments. L.J. Ochyl contributed to the NanoFACS data. J. Bazzill and J.J. Moon analyzed the data. J. Bazzill wrote this report.

Chapter 5

Conclusions and Future Directions

In this body of work three distinct viral sources have been tried and evaluated for incorporation with ICMVs. Two of the projects (HCV and EBOV) progressed to animal studies with no or minor alterations to ICMV composition, respectively. The third project (HIV) required extensive alterations to produce a viable nanoparticle, and are currently being optimized and validated. Even after applying lessons learned from the EBOV project in which the antigen, rGP, is structurally reminiscent to the HIV SOSIP antigen, modifications to the point of producing a new variant of ICMV were required. While this highlights the ability to modify ICMVs as needed, it also underscores how drastically antigens and antigen variants are incorporated into ICMVs, and that extensive characterization and validation are required for even the most minor alterations.

While the projects summarized here focused on the immunogenicity aspect of vaccine formulation, in depth analysis of each formulation will likely yield valuable information as to how the antigens are altered, affected, or modified by the many processes and reactions involved in producing ICMVs and ICMV-NHSs. Notably, determining the extent and location of MPB or DOPE-NHS conjugation to antigens may provide insight into if important epitopes on the antigen are being masked by the bound lipids and help to select the suitable nanoparticle format or optimize

the formulation parameters. The location and extent of functionalized phospholipid binding can be evaluated by LC-MS after proteolytic digestion antigens from produced nanoparticles. When compared to stock antigen this data can yield the extent of conjugation (in terms or potential vs. bound residue), relative positions of the conjugated sites, and if specific residues are more prone to conjugation than others. In addition, analysis by LC-MS can provide data on where and to what extent DTT may reduce antigens and thus affecting their immunogenic properties. This method can provide greater resolution and less background compared to simpler colorimetric methods such as Ellman's reagent.

Another general facet of the ICMVs that was not elucidated was where the antigens were being loaded during ICMV formation. The two most likely sites are the inner-most core and the outer-most exterior of the nanoparticles. The inter-bilayer space, 5 nm distance, does not provide much room for most protein antigens. However, determining if antigens reside in this space is exceedingly difficult. Currently, a method is under development to determine the fraction of antigen on the exterior of ICMVs by using membrane impermeable, functionalized molecules to bind to externally bound antigens and the resulting shift in molecular weight can be used to resolve the internal versus external antigens. Specifically, NHS-functionalized polyethylene glycol (5 kD MW) is incubated in excess with ICMVs overnight to bind with lysine residues and analyzed by PAGE. PEGylated antigens (external) migrate at higher molecular weights than non-PEGylated antigens (internal). The resulting difference in band intensities between treated and untreated samples are used to calculate the internal and external antigen fractions. This method requires further optimization due to poor resolution using standard PAGE-based quantification methods. The use of functionalized fluorophores or dual fluorophore-tagged and NHS-functionalized PEG may yield better results.

Improvements to the immunofluorescence assay would help to move this form a qualitative to a quantitative technique. As it stands, the use of whole antibodies limits the quantification of presented epitopes due to steric hindrance as a result of the bulky antibody size and shape as well as uncertainties in whether one or both F(Ab)s are bound to an epitope. Furthermore, while indirect immunostaining methods greatly enhance the resolution of signals, the potential for disproportionate binding between samples detracts from accurate quantification by this method. Switching to direct immunofluorescence using F(Ab) fragments in place of whole antibodies could allow for greater binding to all or a higher fraction of antigens as well as providing a direct measurement of the epitope presence. However, some hurdles that may need troubleshooting would be to determine an output method that produces a strong signal from direct F(Ab) staining and optimizing the assays to avoid F(Ab) dissociation from the antigens. Additionally, this method does not capture the *in vivo* conditions of antibody binding to the nanoparticles, so may be best used as a supplementary method to the indirect immunofluorescence assay.

Future directions for the HCV project include validating the display of E2.661 and E2c.661 on the surface of ICMVs to evaluate if the C652 or basic residues of the back layer contribute to the display of the antigen on ICMV surfaces. Use of alanine mutagenesis of the sites along with immunofluorescence staining or electron microscopy may provide insight into the specific orientation of the antigens.[147] Additionally, further evaluation of the generated antibody responses are also needed to investigate vaccine efficacy and develop future vaccination schemes. The current work evaluated antibodies produced against two linear epitopes. Obviously, other epitopes contributed to the immune response, but to what extent and impact they had have yet to be analyzed. Lastly, enhancing the breadth of the generated neutralizing antibodies is the focus of future experiments, but without evaluating the factors above, this will be based on trial and error.

Rational design of vaccines will require feedback of the generated immune responses to then adapt the antigen to lead the immune response in the direction desired and in a timely manner. Taking lessons from chronic hepatitis C, researchers are utilizing antigenic diversity to induce broadly neutralizing antibodies (bNAbs) including altered glycosylation patterns.[148] The difficulty will lie in determining what factors are most important to bNAb generation and how to efficiently reproduce these factors within individuals.

The next stages for the EBOV project include dose optimization including analysis of antigen density, display, and particle count on antibody generation, systemic delivery, and *in vivo* efficacy. Additionally, the current studies demonstrated protection in mice one month after vaccination; future studies will need to evaluate long-term protection, including memory B-cell responses, antigen-specific antibody titers, protection after challenge, and the impact or changes viral challenge may induce on the antibody repertoire. Specifically, secreted GP is believed to be an antigenic decoy, and its presence during viral challenge may induce a subversive antibody response.[29] Lastly, the positive results seen in mice warrant investigation of ICMV protection of higher order animals, particularly guinea pigs, which are the next step for EBOV vaccine candidate prior to non-human primates.

Many of the near future experiments for the HIV project pertain to evaluating and characterizing SOSIP ICMV-NHSs and were highlighted above, but further in the future vaccination of mice will be used to assess general immunogenic responses and stability of the nanoparticles after administration. Once determined as safe and viable animal studies will utilize rabbits which have been shown to generate bNAbs with similar modifications as human bNAbs, unlike mice.[149-151] However, similar to the HCV vaccinations, rational antigen design will likely be needed to steer immune responses towards bNAbs. Previous research has demonstrated that

autologous neutralizing antibodies can be induced with the SOSIP antigen,[152, 153] but neutralization breadth was absent. Other reports utilizing sequential alterations in SOSIP to lead immune responses towards bNAbs.[154-156] Additionally, the importance of SOSIP glycans has been reported for induction of bNAbs to buried epitopes[157] as well as specifically against the glycans.[158, 159] These factors will need to be taken into account for a successful SOSIP ICMV vaccine, and may require additional analysis of individual animals to determine if a "one vaccine fits all" scheme is a viable option.

Finally, the overarching and continuing goal for these projects is to produce protective immune responses while avoiding non-neutralizing responses. Given the unconventional progression and evasion mechanisms of these pathogens along with the trends of current research, it is possible that a new strategy will be required for effective vaccines against HCV, HIV, and EBOV. So far this has been alluded to in the literature given the difficulties of inducing broadly protective immune responses with static subunit vaccines. A recurring and growing trend is the use of dynamic antigens to steer immune responses towards specific fates. Whether or not this can occur using small or drastic alterations is uncertain and likely. In concert with the modulation of the vaccines is the response of the recipient. Virulent pathogens like those presented here will necessitate highly effective vaccines, and given the variability observed in bred animals the diversity in response by humans will likely be greater. In essence, our and others research appear to be pointing to a future of personalized vaccines where patients are monitored for efficacy, possibly resulting in tailored booster vaccines to re-orientate or reinforce the generated immune response. Obviously, this is a far cry from the desired one-shot fully-protective model, but an unconventional problem may dictate an unconventional answer.

Bibliography

1. *Global Health Estimates 2016: Deaths by Cause, Age, Sex, by Country and by Region, 2000-2016*. 2018, World Health Organization: Geneva.

2. Morens, D.M., G.K. Folkers, and A.S. Fauci, *The challenge of emerging and re-emerging infectious diseases.* Nature, 2004. **430**(6996): p. 242-9.

3. Morens, D.M., et al., *The 1918 influenza pandemic: lessons for 2009 and the future.* Crit Care Med, 2010. **38**(4 Suppl): p. e10-20.

4. Stenseth, N.C., et al., *Plague: past, present, and future.* PLoS Med, 2008. **5**(1): p. e3.

5. Ross, A.G., S.M. Crowe, and M.W. Tyndall, *Planning for the Next Global Pandemic.* Int J Infect Dis, 2015. **38**: p. 89-94.

6. Wolfe, N.D., C.P. Dunavan, and J. Diamond, *Origins of major human infectious diseases.* Nature, 2007. **447**(7142): p. 279-83.

7. Choo, Q.L., et al., *Isolation of a cDNA clone derived from a blood-borne non-A, non-B viral hepatitis genome.* Science, 1989. **244**(4902): p. 359-62.

8. *Global Hepatits Report 2017*. 2017, World Health Organization: Geneva.

9. *Hepatitis C*. October 2nd, 2017 [cited 2018 June 21st]; Available from: http://www.who.int/news-room/fact-sheets/detail/hepatitis-c.

10. Forner, A., M. Reig, and J. Bruix, *Hepatocellular carcinoma.* Lancet, 2018. **391**(10127): p. 1301-1314.

11. *Guidelines for the screening, care and treatment of persons with chronic hpeatits C infection.* 2016, World Health Organization: Geneva, Switzerland.

12. Messina, J.P., et al., *Global distribution and prevalence of hepatitis C virus genotypes.* Hepatology, 2015. **61**(1): p. 77-87.

13. Krey, T., et al., *Structural basis of HCV neutralization by human monoclonal antibodies resistant to viral neutralization escape.* PLoS Pathog, 2013. **9**(5): p. e1003364.

14. Kong, L., et al., *Structural basis of hepatitis C virus neutralization by broadly neutralizing antibody HCV1*. Proc Natl Acad Sci U S A, 2012. **109**(24): p. 9499-504.

15. Giang, E., et al., *Human broadly neutralizing antibodies to the envelope glycoprotein complex of hepatitis C virus.* Proc Natl Acad Sci U S A, 2012. **109**(16): p. 6205-10.

16. Puchades Renau, L. and M. Berenguer, *Introduction to hepatitis C virus infection: Overview and history of hepatitis C virus therapies.* Hemodial Int, 2018. **22 Suppl 1**: p. S8-S21.

17. Di Bisceglie, A.M., et al., *Recombinant interferon alfa therapy for chronic hepatitis C. A randomized, double-blind, placebo-controlled trial.* N Engl J Med, 1989. **321**(22): p. 1506-10.

18. *Ebola virus disease*. 2018 February 12, 2018 [cited 2018 May 7, 2018]; Available from: http://www.who.int/en/news-room/fact-sheets/detail/ebola-virus-disease.19. Khan, M.A., et al., *Epitope-based peptide vaccine design and target site depiction against Ebola viruses: an immunoinformatics study.* Scand J Immunol, 2015. **82**(1): p. 25-34.

20. Khan, F.N., et al., *A review on the antagonist Ebola: A prophylactic approach.* Biomed Pharmacother, 2017. **96**: p. 1513-1526.

21. Perry, D.L., et al., *Ebola Virus Localization in the Macaque Reproductive Tract during Acute Ebola Virus Disease.* Am J Pathol, 2018. **188**(3): p. 550-558.

22. Messaoudi, I. and C.F. Basler, *Immunological features underlying viral hemorrhagic fevers.* Curr Opin Immunol, 2015. **36**: p. 38-46.

23. Cooper, C.L. and S. Bavari, *A race for an Ebola vaccine: promises and obstacles.* Trends Microbiol, 2015. **23**(2): p. 65-6.

24. Qiu, X., et al., *Sustained protection against Ebola virus infection following treatment of infected nonhuman primates with ZMAb.* Sci Rep, 2013. **3**: p. 3365.

25. Qiu, X., et al., *Successful treatment of ebola virus-infected cynomolgus macaques with monoclonal antibodies.* Sci Transl Med, 2012. **4**(138): p. 138ra81.

26. Shedlock, D.J., et al., *Antibody-mediated neutralization of Ebola virus can occur by two distinct mechanisms.* Virology, 2010. **401**(2): p. 228-35.

27. Wilson, J.A., et al., *Epitopes involved in antibody-mediated protection from Ebola virus.* Science, 2000. **287**(5458): p. 1664-6.

28. Lee, J.E. and E.O. Saphire, *Ebolavirus glycoprotein structure and mechanism of entry.* Future Virol, 2009. **4**(6): p. 621-635.

29. de La Vega, M.A., et al., *The multiple roles of sGP in Ebola pathogenesis.* Viral Immunol, 2015. **28**(1): p. 3-9.

30. Mohan, G.S., et al., *Antigenic subversion: a novel mechanism of host immune evasion by Ebola virus.* PLoS Pathog, 2012. **8**(12): p. e1003065.

31. Olal, D., et al., *Structure of an antibody in complex with its mucin domain linear epitope that is protective against Ebola virus.* J Virol, 2012. **86**(5): p. 2809-16.

32. Coller, B.G., et al., *Clinical development of a recombinant Ebola vaccine in the midst of an unprecedented epidemic.* Vaccine, 2017. **35**(35 Pt A): p. 4465-4469.

33. Agnandji, S.T., et al., *Phase 1 Trials of rVSV Ebola Vaccine in Africa and Europe.* N Engl J Med, 2016. **374**(17): p. 1647-60.

34. Regules, J.A., et al., *A Recombinant Vesicular Stomatitis Virus Ebola Vaccine.* N Engl J Med, 2017. **376**(4): p. 330-341.

35. Geisbert, T.W., et al., *Recombinant adenovirus serotype 26 (Ad26) and Ad35 vaccine vectors bypass immunity to Ad5 and protect nonhuman primates against ebolavirus challenge.* J Virol, 2011. **85**(9): p. 4222-33.

36. Stanley, D.A., et al., *Chimpanzee adenovirus vaccine generates acute and durable protective immunity against ebolavirus challenge.* Nat Med, 2014. **20**(10): p. 1126-9.

37. Sridhar, S., *Clinical development of Ebola vaccines.* Ther Adv Vaccines, 2015. **3**(5-6): p. 125-38.

38. Fischer, W.A., et al., *Ebola virus disease: an update on post-exposure prophylaxis.* The Lancet Infectious Diseases, 2018. **18**(6): p. e183-e192.

39. BarreSinoussi, F., *HIV as the cause of AIDS.* Lancet, 1996. **348**(9019): p. 31-35.

40. Barresinoussi, F., et al., *Isolation of a T-Lymphotropic Retrovirus from a Patient at Risk for Acquired Immune-Deficiency Syndrome (Aids).* Science, 1983. **220**(4599): p. 868-871.

41. *UNAIDS Data 2017*. 2017, Joint United Nations Programme on HIV/AIDS (UNAIDS).

42. Heeney, J.L., A.G. Dalgleish, and R.A. Weiss, *Origins of HIV and the evolution of resistance to AIDS.* Science, 2006. **313**(5786): p. 462-466.

43. Bush, S. and D.M. Tebit, *HIV-1 Group O Origin, Evolution, Pathogenesis, and Treatment: Unraveling the Complexity of an Outlier 25 Years Later.* AIDS Rev, 2015. **17**(3): p. 147-58.

44. Sharp, P.M. and B.H. Hahn, *Origins of HIV and the AIDS pandemic.* Cold Spring Harb Perspect Med, 2011. **1**(1): p. a006841.

45. Gao, F., et al., *Origin of HIV-1 in the chimpanzee Pan troglodytes troglodytes.* Nature, 1999. **397**(6718): p. 436-41.

46. *HIV Transmission*. March 16, 2018 [cited 2018 June 21]; Available from: https://www.cdc.gov/hiv/basics/transmission.html.

47. McMichael, A.J., et al., *The immune response during acute HIV-1 infection: clues for vaccine development.* Nat Rev Immunol, 2010. **10**(1): p. 11-23.

48. Bomsel, M. and V. David, *Mucosal gatekeepers: selecting HIV viruses for early infection.* Nat Med, 2002. **8**(2): p. 114-6.

49. Fletcher, C.V., et al., *Persistent HIV-1 replication is associated with lower antiretroviral drug concentrations in lymphatic tissues.* Proc Natl Acad Sci U S A, 2014. **111**(6): p. 2307-12.

50. Kong, L. and Q.J. Sattentau, *Antigenicity and Immunogenicity in HIV-1 Antibody-Based Vaccine Design.* J AIDS Clin Res, 2012. **S8**: p. 3.

51. Kwong, P.D., J.R. Mascola, and G.J. Nabel, *Broadly neutralizing antibodies and the search for an HIV-1 vaccine: the end of the beginning.* Nat Rev Immunol, 2013. **13**(9): p. 693-701.

52. Sather, D.N., et al., *Factors associated with the development of cross-reactive neutralizing antibodies during human immunodeficiency virus type 1 infection.* J Virol, 2009. **83**(2): p. 757-69.

53. van Gils, M.J., et al., *Prevalence of cross-reactive HIV-1-neutralizing activity in HIV-1-infected patients with rapid or slow disease progression.* AIDS, 2009. **23**(18): p. 2405-14.

54. Thompson, M.A., et al., *Antiretroviral treatment of adult HIV infection: 2012 recommendations of the International Antiviral Society-USA panel.* JAMA, 2012. **308**(4): p. 387-402.

55. Marsden, M.D. and J.A. Zack, *HIV/AIDS eradication.* Bioorg Med Chem Lett, 2013. **23**(14): p. 4003-10.

56. Al-Dakkak, I., et al., *The impact of specific HIV treatment-related adverse events on adherence to antiretroviral therapy: a systematic review and meta-analysis.* AIDS Care, 2013. **25**(4): p. 400-14.

57. Katlama, C., et al., *Barriers to a cure for HIV: new ways to target and eradicate HIV-1 reservoirs.* The Lancet, 2013. **381**(9883): p. 2109-2117.

58. Kovochich, M., M.D. Marsden, and J.A. Zack, *Activation of latent HIV using drug-loaded nanoparticles.* PLoS One, 2011. **6**(4): p. e18270.

59. Margolis, D.M., *How Might We Cure HIV?* Curr Infect Dis Rep, 2014. **16**(3): p. 392.

60. Bazin, H., *A brief history of the prevention of infectious diseases by immunisations.* Comparative Immunology, Microbiology and Infectious Diseases, 2003. **26**(5-6): p. 293-308.

61. Riedel, S., *Edward Jenner and the history of smallpox and vaccination.* Proc (Bayl Univ Med Cent), 2005. **18**(1): p. 21-5.

62. Murphy, K.P., *Janeway's Immunobiology, 8th edition*. 8th ed. 2012, United States of America: Garland Science, Taylor & Francis Group, LLC.

63. Gnanashanmugam, D., et al., *Shedding and reversion of oral polio vaccine type 3 in Mexican vaccinees: comparison of mutant analysis by PCR and enzyme cleavage to a real-time PCR assay.* J Clin Microbiol, 2007. **45**(8): p. 2419-25.

64. Whitney, J.B. and R.M. Ruprecht, *Live attenuated HIV vaccines: pitfalls and prospects.* Curr Opin Infect Dis, 2004. **17**(1): p. 17-26.

65. Zhao, Q., et al., *Virus-like particle-based human vaccines: quality assessment based on structural and functional properties.* Trends Biotechnol, 2013. **31**(11): p. 654-63.

66. Tan, M. and X. Jiang, *Subviral particle as vaccine and vaccine platform.* Curr Opin Virol, 2014. **6**: p. 24-33.

67. Ewer, K.J., et al., *Viral vectors as vaccine platforms: from immunogenicity to impact.* Curr Opin Immunol, 2016. **41**: p. 47-54.

68. Lundstrom, K., *RNA-based drugs and vaccines.* Expert Rev Vaccines, 2015. **14**(2): p. 253-63.

69. Tregoning, J.S. and E. Kinnear, *Using Plasmids as DNA Vaccines for Infectious Diseases.* Microbiol Spectr, 2014. **2**(6).

70. O'Hagan, D.T. and C.B. Fox, *New generation adjuvants--from empiricism to rational design.* Vaccine, 2015. **33 Suppl 2**: p. B14-20.

71. Guven, E., et al., *Aluminum hydroxide adjuvant differentially activates the three complement pathways with major involvement of the alternative pathway.* PLoS One, 2013. **8**(9): p. e74445.

72. Moyle, P.M. and I. Toth, *Modern subunit vaccines: development, components, and research opportunities.* ChemMedChem, 2013. **8**(3): p. 360-76.

73. Moon, J.J., et al., *Enhancing humoral responses to a malaria antigen with nanoparticle vaccines that expand Tfh cells and promote germinal center induction.* Proc Natl Acad Sci U S A, 2012. **109**(4): p. 1080-5.

74. Morelli, A.B., et al., *ISCOMATRIX: a novel adjuvant for use in prophylactic and therapeutic vaccines against infectious diseases.* J Med Microbiol, 2012. **61**(Pt 7): p. 935-43.

75. Demento, S.L., et al., *Role of sustained antigen release from nanoparticle vaccines in shaping the T cell memory phenotype.* Biomaterials, 2012. **33**(19): p. 4957-64.

76. Moon, J.J., et al., *Interbilayer-crosslinked multilamellar vesicles as synthetic vaccines for potent humoral and cellular immune responses.* Nat Mater, 2011. **10**(3): p. 243-51.

77. Pejawar-Gaddy, S., et al., *Design of lipid nanocapsule delivery vehicles for multivalent display of recombinant Env trimers in HIV vaccination.* Bioconjug Chem, 2014. **25**(8): p. 1470-8.

78. Watson, D.S., et al., *Antibody response to polyhistidine-tagged peptide and protein antigens attached to liposomes via lipid-linked nitrilotriacetic acid in mice.* Clin Vaccine Immunol, 2011. **18**(2): p. 289-97.

79. Ghouri, Y.A., I. Mian, and J.H. Rowe, *Review of hepatocellular carcinoma: Epidemiology, etiology, and carcinogenesis.* J Carcinog, 2017. **16**: p. 1.

80. Liang, T.J. and J.W. Ward, *Hepatitis C in Injection-Drug Users - A Hidden Danger of the Opioid Epidemic.* N Engl J Med, 2018. **378**(13): p. 1169-1171.

81. Keck, Z.Y., et al., *Definition of a conserved immunodominant domain on hepatitis C virus E2 glycoprotein by neutralizing human monoclonal antibodies.* J Virol, 2008. **82**(12): p. 6061-6.

82. Kong, L., et al., *Structure of hepatitis C virus envelope glycoprotein E2 antigenic site 412 to 423 in complex with antibody AP33.* J Virol, 2012. **86**(23): p. 13085-8.

83. Law, M., et al., *Broadly neutralizing antibodies protect against hepatitis C virus quasispecies challenge.* Nat Med, 2008. **14**(1): p. 25-7.

84. Schofield, D.J., et al., *Human monoclonal antibodies that react with the E2 glycoprotein of hepatitis C virus and possess neutralizing activity.* Hepatology, 2005. **42**(5): p. 1055-62.

85. de Jong, Y.P., et al., *Broadly neutralizing antibodies abrogate established hepatitis C virus infection.* Sci Transl Med, 2014. **6**(254): p. 254ra129.

86. Broering, T.J., et al., *Identification and characterization of broadly neutralizing human monoclonal antibodies directed against the E2 envelope glycoprotein of hepatitis C virus.* J Virol, 2009. **83**(23): p. 12473-82.

87. Dowd, K.A., et al., *Selection pressure from neutralizing antibodies drives sequence evolution during acute infection with hepatitis C virus.* Gastroenterology, 2009. **136**(7): p. 2377-86.

88. Keck, Z.Y., et al., *Antibody Response to Hypervariable Region 1 Interferes with Broadly Neutralizing Antibodies to Hepatitis C Virus.* J Virol, 2016. **90**(6): p. 3112-22.

89. von Hahn, T., et al., *Hepatitis C virus continuously escapes from neutralizing antibody and T-cell responses during chronic infection in vivo.* Gastroenterology, 2007. **132**(2): p. 667-78.

90. Spaete, R.R., et al., *Characterization of the hepatitis C virus E2/NS1 gene product expressed in mammalian cells.* Virology, 1992. **188**(2): p. 819-30.

91. Selby, M.J., et al., *Complex processing and protein:protein interactions in the E2:NS2 region of HCV.* Virology, 1994. **204**(1): p. 114-22.

92. Michalak, J.P., et al., *Characterization of truncated forms of hepatitis C virus glycoproteins.* J Gen Virol, 1997. **78 (Pt 9)**: p. 2299-306.

93. Flint, M., et al., *Functional analysis of cell surface-expressed hepatitis C virus E2 glycoprotein.* J Virol, 1999. **73**(8): p. 6782-90.

94. Kong, L., et al., *Hepatitis C virus E2 envelope glycoprotein core structure.* Science, 2013. **342**(6162): p. 1090-4.

95. Tzarum, N., I.A. Wilson, and M. Law, *The Neutralizing Face of Hepatitis C Virus E2 Envelope Glycoprotein.* Front Immunol, 2018. **9**: p. 1315.

96. Ruwona, T.B., et al., *Fine mapping of murine antibody responses to immunization with a novel soluble form of hepatitis C virus envelope glycoprotein complex.* J Virol, 2014. **88**(18): p. 10459-71.

97. Dao Thi, V.L., M. Dreux, and F.L. Cosset, *Scavenger receptor class B type I and the hypervariable region-1 of hepatitis C virus in cell entry and neutralisation.* Expert Rev Mol Med, 2011. **13**: p. e13.

98. Farci, P., et al., *The outcome of acute hepatitis C predicted by the evolution of the viral quasispecies.* Science, 2000. **288**(5464): p. 339-44.

99. Danielson, K.M., et al., *Diurnal Variations of Circulating Extracellular Vesicles Measured by Nano Flow Cytometry.* PLoS One, 2016. **11**(1): p. e0144678.

100. Nolte-'t Hoen, E.N., et al., *Quantitative and qualitative flow cytometric analysis of nanosized cell-derived membrane vesicles.* Nanomedicine, 2012. **8**(5): p. 712-20.

101. Pasalic, L., et al., *Enumeration of extracellular vesicles by a new improved flow cytometric method is comparable to fluorescence mode nanoparticle tracking analysis.* Nanomedicine, 2016. **12**(4): p. 977-986.

102. van der Pol, E., et al., *Particle size distribution of exosomes and microvesicles determined by transmission electron microscopy, flow cytometry, nanoparticle tracking analysis, and resistive pulse sensing.* J Thromb Haemost, 2014. **12**(7): p. 1182-92.

103. van der Vlist, E.J., et al., *Fluorescent labeling of nano-sized vesicles released by cells and subsequent quantitative and qualitative analysis by high-resolution flow cytometry.* Nat Protoc, 2012. **7**(7): p. 1311-26.

104. Krey, T., et al., *The disulfide bonds in glycoprotein E2 of hepatitis C virus reveal the tertiary organization of the molecule.* PLoS Pathog, 2010. **6**(2): p. e1000762.

105. Kong, L., et al., *Structural flexibility at a major conserved antibody target on hepatitis C virus E2 antigen.* Proc Natl Acad Sci U S A, 2016.

106. Khan, A.G., et al., *Structure of the core ectodomain of the hepatitis C virus envelope glycoprotein 2.* Nature, 2014. **509**(7500): p. 381-4.

107. Fenouillet, E., et al., *Contribution of redox status to hepatitis C virus E2 envelope protein function and antigenicity.* J Biol Chem, 2008. **283**(39): p. 26340-8.

108. WHO. *Ebola virus disease*. 2018 February 12, 2018 [cited 2018 May 7, 2018]; Available from: http://www.who.int/en/news-room/fact-sheets/detail/ebola-virus-disease.

109. Hood, C.L., et al., *Biochemical and structural characterization of cathepsin L-processed Ebola virus glycoprotein: implications for viral entry and immunogenicity.* J Virol, 2010. **84**(6): p. 2972-82.

110. Lee, J.E., et al., *Structure of the Ebola virus glycoprotein bound to an antibody from a human survivor.* Nature, 2008. **454**(7201): p. 177-82.

111. Ji, Y., et al., *Design of Fusion Proteins for Efficient and Soluble Production of Immunogenic Ebola Virus Glycoprotein in Escherichia coli.* Biotechnol J, 2018: p. e1700627.

112. Konduru, K., et al., *Ebolavirus Glycoprotein Fc Fusion Protein Protects Guinea Pigs against Lethal Challenge.* PLoS One, 2016. **11**(9): p. e0162446.

113. Lehrer, A.T., et al., *Recombinant proteins of Zaire ebolavirus induce potent humoral and cellular immune responses and protect against live virus infection in mice.* Vaccine, 2017.

114. Rios-Huerta, R., et al., *Expression of an immunogenic LTB-based chimeric protein targeting Zaire ebolavirus epitopes from GP1 in plant cells.* Plant Cell Rep, 2017. **36**(2): p. 355-365.

115. Konduru, K., et al., *Ebola virus glycoprotein Fc fusion protein confers protection against lethal challenge in vaccinated mice.* Vaccine, 2011. **29**(16): p. 2968-77.

116. Bengtsson, K.L., et al., *Matrix-M adjuvant enhances antibody, cellular and protective immune responses of a Zaire Ebola/Makona virus glycoprotein (GP) nanoparticle vaccine in mice.* Vaccine, 2016. **34**(16): p. 1927-35.

117. Rao, M., et al., *Cytotoxic T lymphocytes to Ebola Zaire virus are induced in mice by immunization with liposomes containing lipid A.* Vaccine, 1999. **17**(23-24): p. 2991-8.

118. Rao, M., et al., *Induction of Immune Responses in Mice and Monkeys to Ebola Virus after Immunization with Liposome-Encapsulated Irradiated Ebola Virus: Protection in Mice Requires CD4+ T Cells.* Journal of Virology, 2002. **76**(18): p. 9176-9185.

119. Fan, Y. and J.J. Moon, *Particulate delivery systems for vaccination against bioterrorism agents and emerging infectious pathogens.* Wiley Interdiscip Rev Nanomed Nanobiotechnol, 2016.

120. Chahal, J.S., et al., *Dendrimer-RNA nanoparticles generate protective immunity against lethal Ebola, H1N1 influenza, and Toxoplasma gondii challenges with a single dose.* Proc Natl Acad Sci U S A, 2016. **113**(29): p. E4133-42.

121. Li, A.V., et al., *Generation of effector memory T cell-based mucosal and systemic immunity with pulmonary nanoparticle vaccination.* Sci Transl Med, 2013. **5**(204): p. 204ra130.

122. Cazares, L.H., et al., *Development of a liquid chromatography high resolution mass spectrometry method for the quantitation of viral envelope glycoprotein in Ebola virus-like particle vaccine preparations.* Clin Proteomics, 2016. **13**(1): p. 18.

123. Ingale, J., et al., *High-Density Array of Well-Ordered HIV-1 Spikes on Synthetic Liposomal Nanoparticles Efficiently Activate B Cells.* Cell Rep, 2016. **15**(9): p. 1986-99.

124. Davidson, E., et al., *Mechanism of Binding to Ebola Virus Glycoprotein by the ZMapp, ZMAb, and MB-003 Cocktail Antibodies.* J Virol, 2015. **89**(21): p. 10982-92.

125. Murin, C.D., et al., *Structures of protective antibodies reveal sites of vulnerability on Ebola virus.* Proc Natl Acad Sci U S A, 2014. **111**(48): p. 17182-7.

126. Cheng, W., *The Density Code for the Development of a Vaccine?* J Pharm Sci, 2016. **105**(11): p. 3223-3232.

127. Nsanzimana, S., et al., *Life expectancy among HIV-positive patients in Rwanda: a retrospective observational cohort study.* The Lancet Global Health, 2015. **3**(3): p. e169-e177.

128. Collaboration, T.A.T.C., *Life expectancy of individuals on combination antiretroviral therapy in high-income countries: a collaborative analysis of 14 cohort studies.* The Lancet, 2008. **372**(9635): p. 293-299.

129. Moir, S., T.W. Chun, and A.S. Fauci, *Pathogenic mechanisms of HIV disease.* Annu Rev Pathol, 2011. **6**: p. 223-48.

130. Korber, B., et al., *Evolutionary and immunological implications of contemporary HIV-1 variation.* Br Med Bull, 2001. **58**: p. 19-42.

131. Gunthard, H.F., et al., *Antiretroviral treatment of adult HIV infection: 2014 recommendations of the International Antiviral Society-USA Panel.* JAMA, 2014. **312**(4): p. 410-25.

132. Mascola, J.R. and B.F. Haynes, *HIV-1 neutralizing antibodies: understanding nature's pathways.* Immunol Rev, 2013. **254**(1): p. 225-44.

133. Corti, D. and A. Lanzavecchia, *Broadly neutralizing antiviral antibodies.* Annu Rev Immunol, 2013. **31**: p. 705-42.

134. van Gils, M.J. and R.W. Sanders, *Broadly neutralizing antibodies against HIV-1: templates for a vaccine.* Virology, 2013. **435**(1): p. 46-56.

135. Kwong, P.D. and J.R. Mascola, *Human antibodies that neutralize HIV-1: identification, structures, and B cell ontogenies.* Immunity, 2012. **37**(3): p. 412-25.

136. Earl, P.L., et al., *Native oligomeric human immunodeficiency virus type 1 envelope glycoprotein elicits diverse monoclonal antibody reactivities.* J Virol, 1994. **68**(5): p. 3015-26.

137. Graham, B.S. and J.R. Mascola, *Lessons from failure--preparing for future HIV-1 vaccine efficacy trials.* J Infect Dis, 2005. **191**(5): p. 647-9.

138. Sanders, R.W., et al., *A next-generation cleaved, soluble HIV-1 Env trimer, BG505 SOSIP.664 gp140, expresses multiple epitopes for broadly neutralizing but not non-neutralizing antibodies.* PLoS Pathog, 2013. **9**(9): p. e1003618.

139. Sanders, R.W., et al., *Stabilization of the Soluble, Cleaved, Trimeric Form of the Envelope Glycoprotein Complex of Human Immunodeficiency Virus Type 1.* Journal of Virology, 2002. **76**(17): p. 8875-8889.

140. Beddows, S., et al., *A comparative immunogenicity study in rabbits of disulfide-stabilized, proteolytically cleaved, soluble trimeric human immunodeficiency virus type 1 gp140, trimeric cleavage-defective gp140 and monomeric gp120.* Virology, 2007. **360**(2): p. 329-40.

141. Sheppard, N.C., et al., *Polyethyleneimine is a potent systemic adjuvant for glycoprotein antigens.* Int Immunol, 2014. **26**(10): p. 531-8.

142. Wegmann, F., et al., *Polyethyleneimine is a potent mucosal adjuvant for viral glycoprotein antigens.* Nat Biotechnol, 2012. **30**(9): p. 883-8.

143. Willner, I., et al., *Photoinduced Electron-Transfer Processes Using Organized Redox-Functionalized Bipyridinium Polyethylenimine Tio2 Colloids and Particulate Assemblies.* Journal of Physical Chemistry, 1993. **97**(28): p. 7264-7271.

144. Cuatrecasas, P. and I. Parikh, *Adsorbents for affinity chromatography. Use of N-hydroxysuccinimide esters of agarose.* Biochemistry, 1972. **11**(12): p. 2291-9.

145. Lomant, A.J. and G. Fairbanks, *Chemical probes of extended biological structures: synthesis and properties of the cleavable protein cross-linking reagent [35S]dithiobis(succinimidyl propionate).* J Mol Biol, 1976. **104**(1): p. 243-61.

146. Staros, J.V., R.W. Wright, and D.M. Swingle, *Enhancement by N-hydroxysulfosuccinimide of water-soluble carbodiimide-mediated coupling reactions.* Anal Biochem, 1986. **156**(1): p. 220-2.

147. Gopal, R., et al., *Probing the antigenicity of hepatitis C virus envelope glycoprotein complex by high-throughput mutagenesis.* PLoS Pathog, 2017. **13**(12): p. e1006735.

148. Li, D., et al., *Altered Glycosylation Patterns Increase Immunogenicity of a Subunit Hepatitis C Virus Vaccine, Inducing Neutralizing Antibodies Which Confer Protection in Mice.* J Virol, 2016. **90**(23): p. 10486-10498.

149. Hu, J.K., et al., *Murine Antibody Responses to Cleaved Soluble HIV-1 Envelope Trimers Are Highly Restricted in Specificity.* J Virol, 2015. **89**(20): p. 10383-98.

150. Chen, Y., et al., *A novel rabbit monoclonal antibody platform to dissect the diverse repertoire of antibody epitopes for HIV-1 Env immunogen design.* J Virol, 2013. **87**(18): p. 10232-43.

151. Forsell, M.N., et al., *Biochemical and immunogenic characterization of soluble human immunodeficiency virus type 1 envelope glycoprotein trimers expressed by semliki forest virus.* J Virol, 2005. **79**(17): p. 10902-14.

152. Sanders, R.W., et al., *HIV-1 VACCINES. HIV-1 neutralizing antibodies induced by native-like envelope trimers.* Science, 2015. **349**(6244): p. aac4223.

153. Havenar-Daughton, C., et al., *Direct Probing of Germinal Center Responses Reveals Immunological Features and Bottlenecks for Neutralizing Antibody Responses to HIV Env Trimer.* Cell Rep, 2016. **17**(9): p. 2195-2209.

154. Escolano, A., et al., *Sequential Immunization Elicits Broadly Neutralizing Anti-HIV-1 Antibodies in Ig Knockin Mice.* Cell, 2016. **166**(6): p. 1445-1458 e12.

155. He, L., et al., *Presenting native-like trimeric HIV-1 antigens with self-assembling nanoparticles.* Nat Commun, 2016. **7**: p. 12041.

156. Pissani, F., et al., *Motif-optimized subtype A HIV envelope-based DNA vaccines rapidly elicit neutralizing antibodies when delivered sequentially.* Vaccine, 2012. **30**(37): p. 5519-26.

157. Langedijk, J.P. and H. Schuitemaker, *A sweet surprise for HIV broadly neutralizing antibodies.* Nat Med, 2012. **18**(11): p. 1616-7.

158. Coss, K.P., et al., *HIV-1 Glycan Density Drives the Persistence of the Mannose Patch within an Infected Individual.* J Virol, 2016. **90**(24): p. 11132-11144.

159. Go, E.P., et al., *Comparative Analysis of the Glycosylation Profiles of Membrane-Anchored HIV-1 Envelope Glycoprotein Trimers and Soluble gp140.* J Virol, 2015. **89**(16): p. 8245-57.